PRODERNA

Programa de Pós-Graduação em Engenharia de Recursos Naturais da Amazônia

Evaluating variable-speed operation for improved hydropower plant operation

Tiago Machado Wanzeler

Doctorate Thesis presented to Postgraduate Program in Natural Resources Engineering of the Amazon, ITEC, of Federal University of Pará, as a partial fulfillment of the requirements for the degree of Doctor of Science in Natural Resource Engineering.

Advisor: André Luiz Amarante Mesquita

Tucuruí, PA

Dez 2025

Universidade Federal do Pará

PRODERNA
Programa de Pós-Graduação em Engenharia de Recursos Naturais da Amazônia

ITEC INSTITUTO DE TECNOLOGIA UFPA

"AVALIAÇÃO DA OPERAÇÃO EM VELOCIDADE VARIÁVEL PARA MELHORAR A OPERAÇÃO DE USINAS HIDRELÉTRICAS"

Tiago Machado Wanzeler

TESE SUBMETIDA AO CORPO DOCENTE DO PROGRAMA DE PÓS-GRADUAÇÃO EM ENGENHARIA DE RECURSOS NATURAIS DA AMAZÔNIA - PRODERNA/ITEC/UFPA COMO PARTE DOS REQUISITOS NECESSÁRIOS PARA OBTENÇÃO DO GRAU DE DOUTOR EM ENGENHARIA DE RECURSOS NATURAIS.

Aprovada por:

gov.br Documento assinado digitalmente
ANDRE LUIZ AMARANTE MESQUITA
Data: 18/12/2025 17:26:34-0300
Verifique em https://validar.iti.gov.br

Prof. Dr. André Luiz Amarante Mesquita (Presidente)

gov.br Documento assinado digitalmente
CLAUDIO JOSE CAVALCANTE BLANCO
Data: 26/12/2025 10:09:15-0300
Verifique em https://validar.iti.gov.br

Prof. Dr. Claudio José Cavalcante Blanco (Membro Interno)

gov.br Documento assinado digitalmente
MARCO VALERIO DE ALBUQUERQUE VINAGRE
Data: 18/12/2025 22:34:14-0300
Verifique em https://validar.iti.gov.br

Prof. Dr. Marco Valério de Albuquerque Vinagre (Membro Externo)

gov.br Documento assinado digitalmente
IVAN MARQUES DE TOLEDO CAMARGO
Data: 18/12/2025 20:44:06-0300
Verifique em https://validar.iti.gov.br

Prof. Dr. Ivan Marques de Toledo Camargo (Membro Externo)

gov.br Documento assinado digitalmente
CARLOS BARREIRA MARTINEZ
Data: 18/12/2025 17:32:49-0300
Verifique em https://validar.iti.gov.br

Prof. Dr. Carlos Barreira Martinez (Membro Externo)

gov.br Documento assinado digitalmente
GILTON CARLOS DE ANDRADE FURTADO
Data: 22/12/2025 11:03:02-0300
Verifique em https://validar.iti.gov.br

Prof. Dr. Gilton Carlos Andrade Furtado (Membro Externo)

Belém, PA - Brasil
Dezembro de 2025

ACKNOWLEDGMENTS

First and foremost, I express my deepest gratitude to God, who has blessed me with life, strength, and health to undertake and complete this work. Without His guidance and grace, this journey would not have been possible.

I extend my sincere appreciation to my advisor, Professor Dr. André Luiz Amarante Mesquista, a mentor whom I deeply admire. His vast knowledge, unwavering pursuit of excellence, and continuous encouragement were fundamental in shaping this research. His guidance provided me with the confidence and structure needed to achieve meaningful results, and without his support, this work would not have been accomplished.

A special thank you to my friend Rodolfo Ramalho, whose support and encouragement came at crucial moments, reminding me that perseverance and determination are key elements in any challenging endeavor.

I am profoundly grateful to my family, especially my parents, Rozilene Machado, and Elizeu Wanzeler, for their unconditional love and unwavering support throughout my academic journey. They have always stood by my side, encouraging me to pursue my goals with dedication and resilience. Their belief in my potential has been a driving force in my life.

My heartfelt thanks go to Suzany Alves for her companionship, motivation, and encouragement, which played a vital role in keeping me focused and determined to complete this significant milestone. This work is also dedicated to my son, Taylor Silveira Wanzeler, who is my greatest motivation. He gives me the strength to keep learning, growing, and striving for new knowledge and opportunities.

I also extend my gratitude to the Federal University of Pará (UFPA) for providing me with the opportunity and resources to conduct this research. The institution's support has been invaluable in enabling me to develop this work and make a contribution to the field.

To all who supported me, inspired me, and cheered for me.

Thank you!

Resumo da Tese apresentada ao PRODERNA/UFPA como parte dos requisitos necessários para a obtenção do grau de Doutor em Ciências (D.Sc.)

AVALIAÇÃO DA OPERAÇÃO EM VELOCIDADE VARIÁVEL PARA MELHORAR O FUNCIONAMENTO DE USINAS HIDRELÉTRICAS

Tiago Machado Wanzeler

Orientador: Prof. Dr. André Luiz Amarante Mesquita

Área de Concentração: Uso e Transformação de Recursos Naturais

A transição acelerada em direção às fontes renováveis de energia exige soluções inovadoras para garantir estabilidade e confiabilidade ao sistema elétrico. Este trabalho investiga a conversão parcial ou total de usinas hidrelétricas existentes para operação em VSO como meio de melhorar a operação. Entre as tecnologias disponíveis, o MMC se destaca por seu caráter modular e escalável e por sua adequação a elevados níveis de tensão e potência, possibilitando o retrofit para VSO sem a necessidade de substituição das máquinas síncronas existentes. Propõe-se uma metodologia geral que combina diagramas de colina universais, leis de similaridade e um algoritmos de redespacho sob VSO. Simulações baseadas em dados históricos de operação comparam os modos FSO e VSO para diversos cenários de conversão parcial e total. Os resultados mostram uma redução no número de partidas e paradas, variando de cerca de 19% com apenas três unidades convertidas para VSO até 32% para a conversão integral da usina. Ao mesmo tempo, a VSO combinada ao despacho otimizado aumenta sistematicamente a energia anual gerada: o ganho é da ordem de 2,5% em relação ao caso histórico em FS. O redespacho otimizado também indica que a maior parte desses benefícios de flexibilidade e ganho de energia pode ser capturada com conversão parcial, delineando um caminho de modernização mais econômico do que a conversão de todas as unidades. Em outra análise, o mesmo arcabouço é estendido para a mitigação de cavitação, empregando um critério σ–N_s e estratégias de ajuste em vazão e velocidade baseadas em VSO. Para uma faixa modesta de tolerância de potência, que pode ser compensada por outras unidades, cerca de 75% das horas de operação inicialmente cavitantes são transferidas para uma região segura. Em suma, o estudo mostra que a conversão de usinas hidrelétricas existentes para VSO é tecnicamente viável e altamente vantajosa, oferecendo uma estratégia integrada para reduzir ciclos de partidas e paradas, aumentar a produção de energia e a energia firme e mitigar cavitação, apoiando assim a integração confiável de altas participações de geração renovável variável.

Palavras-chave: Conversão de Usinas, Velocidade Variável, Partidas e Paradas, Redistribuição de Potência, Integração de Fontes Renováveis.

Abstract of Thesis presented to PRODERNA/UFPA as a partial fulfillment of the requirements for the degree of Doctor of Science (D.Sc.)

EVALUATING VARIABLE-SPEED OPERATION FOR IMPROVED HYDROPOWER PLANT OPERATION

Tiago Machado Wanzeler

Advisor: André Luiz Amarante Mesquita

Research Area: Use and Transformation of Natural Resources

The accelerating transition toward renewable energy demands innovative solutions for grid stability and reliability. This work investigates partial and total conversion of existing large hydropower plants to VSO as a means to increase operational flexibility, reduce start–stop cycles, improve efficiency and enhance energy production. Among available technologies, the MMC stands out for its modular, scalable design and suitability for high voltage and power ratings, enabling VSO retrofits without replacing existing synchronous machines. A general methodology is proposed that combines universal hill charts, similarity laws and a power-redispatch algorithm to exploit the extended H–Q–N operating domain under VSO. Simulations using historical operating data compare FSO and VSO for several partial- and full-conversion scenarios. The results show a consistent reduction in machine starts and stops, from about 19% with only three units converted to VSO up to 32% for full-plant conversion. At the same time, VSO combined with optimized dispatch systematically increases annual energy production: for the representative hydrological year, the gain is of the order of 2.5% relative to the historical fixed-speed baseline, whereas optimization alone (without VSO) yields negligible additional energy. The optimized redispatch further indicates that most of these flexibility and energy-gain benefits can be captured with partial conversion, outlining a more cost-effective modernization path than converting all units. In a second step, the same framework is extended to cavitation mitigation using a σ–N_s criterion and VSO-based adjustment strategies in discharge and speed. For a modest power-tolerance band that can be compensated by other units, up to approximately 75% of initially cavitating operating hours are transferred to a safe region with limited deviation from the original dispatch. Overall, the study shows that VSO conversion of existing hydropower plants is technically feasible and highly beneficial, offering an integrated strategy to reduce start–stop cycles, increase energy production and firm energy, and mitigate cavitation, thereby supporting the reliable integration of high shares of variable renewable generation.

Keywords: Variable-Speed Operation, Start–Stop Cycle Reduction, Hydropower Scheduling, Cavitation Mitigation, Retrofitting Hydropower Plants.

CONTENTS

LIST OF FIGURES

LIST OF TABLES

LIST OF NOMENCLATURE

AC	Alternating Current
AG	Auxiliary Generator
BESS	Battery Energy Storage Systems
CAPES	Coordination for the Improvement of Higher Education Personnel
CFI	Powerhouse I
CFII	Powerhouse II
CFSM	Converter Fed Synchronous Machine
DC	Direct Current
DCO	Shutdowns Due to Operational Convenience
DFIG	Doubly Fed Induction Generator
DFIM	Doubly Fed Induction Machine
FAPC	Fast Active Power Control
FS	Fixed Speed
FSC	Full-Size Converter
FSFC	Full-Size Frequency Converter
FSO	Fixed Speed Operation
FSU	Fixed Speed Unit
GU	Generanting Unit
IEEE	Institute of Electrical and Electronic Engineers
IGCT	Integrated-Commutated Thyristors
kV	kilo Volts
M3C	Modular Multilevel Matrix Converter
MMC	Modular Multilevel Converter
MVA	Mega Volt-Ampére
MW	Mega Watts
ONS	National System Operator
OPR	Operating Under Normal Conditions
PHES	Pumped Hydro Energy Storage
PWM	Pulse Width Modulation

RES	Renewable Energy Sources
SciELO	Scientific Electronic Library Online
SFC	Static Frequency Converters
SIN	National Interconnected System
SM	Synchronous Machines
THD	Total Harmonic Distortion
THP	Tucuruí Hydropower Plant
VS	Variable Speed
VSI	Voltage Source Inverter
VSO	Variable Speed Operation
VSU	Variable Speed Unit
VSPSP	Variable Speed Pumped Storage Plants
VS-PSU	Variable Speed Pumped Storage Units

LIST OF SYMBOLS

Q_{ED}	Discharge Factor
n_{ED}	Speed Factor
P_{ED}	Power Factor
Q	Flow Rate
D	Turbine Diameter
H_G	Gross Head
H_N	Net Head
N	Speed
P	Power
$\boldsymbol{\eta}$	Efficiency
g	Gravitational acceleration
ρ	Water Density
k	Loss Coefficient
N_1	Speed 1
N_2	Speed 2
Q_1	Flow at Speed 1
Q_2	Flow at Speed 2
P_{t1}	Turbine Power at Speed 1
P_{t2}	Turbine Power at Speed 2
η_1	Efficiency at Speed 1
η_2	Efficiency at Speed 2
N_s	Synchronous Speed
H_r	Required Net Head
P_r	Required Power
N_r	Required Speed
Q_h	Homologous Flow
H_h	Homologous Net Head
P_h	Homologous Power

1. INTRODUCTION

1.1. GENERAL CONSIDERATIONS

The transition to renewable energy sources (RESs) at the global level has fundamentally changed energy systems, creating unprecedented challenges for grid stability and reliability [1]. The management of variability associated with RESs becomes particularly demanding. Innovations such as virtual inertia and rapid frequency response are necessary to address these challenges [2].

Hydroelectric reservoirs are essential assets for balancing an electrical grid due to the variable and intermittent nature of various renewable energy sources, such as solar and wind. These reservoirs have the unusual capacity to store energy and release it when it is needed. Hydropower facilities that operate in tandem with renewable energy sources not only reduce volatility but also increase system flexibility and efficiency, especially when they implement variable speed operation (VSO) [3]. This feature makes hydropower a crucial component in maintaining the stability and dependability of the system. In addition, frequent operation increases wear and tear on turbines and generators, hence reducing their useful life and increasing preventive and corrective maintenance costs.

The retrofitting of existing hydroelectric plants to VSO has emerged as a promising solution to these challenges [4,5]. The conversion of large hydroelectric plants to VSO can deliver numerous benefits that address the challenges faced within today's power systems concerning the critical contributions that VSO makes in enhancing grid efficiency and stability, as identified in [6] and [7] as transformative improvements in renewable energy integration.

Therefore, VSO can increase hydraulic efficiency and optimize water use in large-scale hydropower systems [8,9]. Additionally, recent integration evaluations have emphasized the strategic importance of hydropower in stabilizing hybrid renewable systems [10,11]. Shi [12] emphasized the role of VSO in improving peak regulation for power grids with increasing intermittent sources such as wind energy, whereas Yang [13] highlighted the efficiency of VSO in controlling fluctuations associated with wind generation.

One of the most remarkable benefits of VSO is the greater flexibility in frequency control. The accelerated response of VSO units to changes in frequency, cited by [14], ensures proper grid stabilization. Such a feature becomes increasingly important for systems that are becoming increasingly reliant on variable renewable sources, such as solar and wind energy. Furthermore, VSO is compatible with renewable energy. As noted by the authors in [13], variable-speed systems can balance out the intermittent output of renewables, effectively raising the share of renewable energy that the grid can accommodate. This function assumes added importance as the world's energy mix shifts increasingly toward green energy.

By decoupling turbine speed from grid frequency, VSO improves frequency control through rapid responses to fluctuations and improved fault ride-through capabilities [14,15], increases resource productivity by reducing energy losses via water use optimization [16–18], and increases operational flexibility via dynamic adjustment to renewable intermittency [12,13]. Studies on hydropower plants integrated into DC transmission systems have shown that VSO improves grid stabilization by minimizing energy losses during transient events [17]. This capability is critical for modern grids with high solar and wind penetration because the rapid frequency modulation of VSO mitigates instability risks while supporting fault recovery [14,15].

In addition to these operational advantages, VSO offers critical ancillary services support. VSO units provide superior frequency, power, and voltage/reactive power control [7]. All this adds up to improved reliability for the grid as a whole. This also creates a provision for new revenue streams through the various ancillary service markets that are in place [19]. Another important benefit is the decrease in machine downtime. The flexible operation of VSO units reduces the frequency and duration of outages, improving operational continuity and equipment reliability [20]. In terms of the lifespan of turbines and bearings, mechanical stress and wear are also reduced because of optimized operating conditions [14].

Building on these operational improvements, the implementation of VSO in large hydropower plants also offers a significant enhancement in the operational area and active power control [21]. This would increase the operating window, even at low loads, after retrofitting and moving into variable-speed operations. This extension of the operational domain becomes particularly important for accommodating variable grid demand,

especially in systems with high penetration of renewable energy sources. Better capabilities in active power control enable the absolute power to be controlled with high accuracy, primarily in pump mode, which helps stabilize grid frequency and thus supports primary control. In a power station as large as Tucurui, this implies not only an increase in its overall efficiency but essentially guarantees that the power plant works as a reliable contributor to grid stability while optimally producing energy under very flexible operating conditions. This is indeed a crucial aspect of CFSM-based retrofitting when it comes to modernizing a hydroelectric plant.

Furthermore, the economic benefits of adopting variable-speed operation in large hydropower plants, such as Tucuruí, are both substantial and multifaceted, as highlighted in[18]. Higher operational efficiency is achieved by VSO, which optimizes energy conversion, thereby providing long-term decreases in operational expenditures. The VSO system's flexibility enables easy management of demand fluctuations, maximizing the utilization of water resources in an economically beneficial manner. Moreover, the VSO system can be easily integrated into wind and solar renewable energy sources, requiring minimal infrastructure investments to enhance grid compatibility. It also increases the energy generation capacity of the hydropower plant, hence increasing electricity production and corresponding revenue growth. All these economic benefits position VSO as part of a game-changing technological solution for the modernization and long-term financial and operational sustainability of hydropower plants.

Such features represent VSO as one of the key retrofits for modern hydropower plants in adapting to the changes occurring in the energy sector, where an increasing number of energy sources are renewable. The ability of VSO to offer increased operational flexibility, enhanced stability to the grid, and decreased mechanical stress is very significant for retrofitting existing large-scale hydropower infrastructure. This research demonstrates how the implementation of VSO can lead to a significant improvement in operations, characterized by a reduced number of start-stop cycles, an extended equipment lifespan, and optimized energy dispatch. This highlights how the research results demonstrate the practicality and enormous benefits of deploying VSO in a similar kind of plant worldwide when two significant and strategically important challenges are simultaneously tackled.

Implementing VSO in hydropower plants requires advanced technologies that can handle new operational demands. Therefore, among the most widely used options for these conversions are the doubly fed induction machine (DFIM) and the converter-fed synchronous machine (CFSM), as highlighted in [6,22,23]. The modular multilevel converter (MMC) [24] is also among the current solutions for VSO implementation. This technology features a modular and scalable structure, making it suitable for extensive plant retrofits. It enables conventional synchronous machines to achieve variable speed operation capability without requiring the replacement of the existing generation system [7]. Each has its own set of advantages and has been applied in retrofitting projects worldwide, providing valuable insights into its use in large-scale plants, such as the Tucuruí Hydropower Plant (THP).

This doctoral qualifying examines three critical aspects of VSO implementation: reducing start-stop cycles, minimizing operational exposure to cavitation-prone conditions, and enhancing firm energy output. FSO often forces generating units into hydraulic conditions that can lead to cavitation, a damaging phenomenon that erodes turbine components and decreases long-term efficiency. By allowing finer control over rotational speed, VSO can help shift operations away from cavitation-prone regions, thereby reducing mechanical stress and extending the equipment's lifespan. Additionally, the flexibility offered by VSO enables more efficient water use during periods of low inflow, thereby increasing firm energy, a metric directly related to a plant's guaranteed energy delivery and revenue potential. These aspects will be further examined in this research as part of a comprehensive evaluation of the technical and economic impacts of VSO on large hydroelectric systems.

Building on these considerations, this doctoral qualifying evaluates the total or partial conversion of traditional hydro plants to VSO and proposes a structured methodology for assessing its feasibility. A new operational region under VSO is defined using similarity theory and turbine performance curves. Additionally, a short-term dispatch algorithm has been developed to minimize start-stop cycles and enhance operational efficiency. By integrating these components, the study provides a comprehensive framework that supports the technical implementation of VSO while emphasizing its broader operational and economic benefits.

1.2. MOTIVATIONS

The motivation for this research stems from the need to address increasingly critical operational challenges faced by large hydroelectric power plants in Brazil, especially in light of the growing penetration of intermittent renewable energy sources such as solar and wind. The variability and unpredictability of these energy sources have introduced new demands for operational flexibility and grid stability, positioning hydroelectric plants as pivotal to balancing strategies. In this context, traditional fixed-speed systems have demonstrated limitations in adapting to these evolving dynamics, resulting in operational inefficiencies and increased mechanical wear.

Previous dissertations and theses developed in partnership with this research group have systematically explored issues affecting large-scale hydro plants, including the rise in the number of start-stop cycles, the occurrence of cavitation under suboptimal hydraulic conditions, and the reduced efficiency of dispatch under rigid operational constraints. These studies have highlighted that traditional fixed-speed configurations, although robust, are no longer fully adequate to meet the evolving demands of modern power systems.

Furthermore, the THP, one of the largest in Brazil, is entering a natural phase of technological renewal after decades of operation. This context of planned modernization presents a unique opportunity to investigate advanced solutions such as VSO. Unlike traditional fixed-speed units, VSO allows dynamic adjustment of turbine speed, offering multiple technical and economic advantages. Among them are the potential reduction in start-stop cycles, the minimization of exposure to cavitation-prone operating points, and improved turbine efficiency through better alignment with hydraulic conditions.

One particularly relevant aspect for plant operators is the potential impact of VSO on firm energy calculations. By increasing the plant's operational range to accommodate a wider variety of hydraulic conditions, especially during periods of reduced inflow, VSO may contribute to an increase in firm energy. Since firm energy defines the guaranteed amount of energy that a plant can supply, directly influencing its contractual commitments and financial returns, this improvement represents a strong economic driver for considering such conversion.

In summary, this research is motivated by the confluence of academic advances, operational challenges, and strategic opportunities. The convergence of modern renewable energy integration demands, the need to reduce mechanical stress and cavitation, and the economic opportunity presented by increasing firm energy reinforce the relevance of exploring the feasibility and benefits of implementing VSO in large-scale hydroelectric plants, using THP as a case study.

1.3. OBJECTIVES

1.3.1. General Objective

Evaluate the technical and operational feasibility of converting existing large hydropower plants from fixed-speed to variable-speed operation (VSO), through partial and total conversion scenarios, by developing and applying a unified methodological availability risks framework that:

- extends the admissible operating range via similarity laws and hill charts,
- reduces machine start–stop cycles through optimized power redispatch, and
- mitigates cavitation-prone operation, while providing first indications of the impact on energy gains and firm-energy potential under current market frameworks.

1.3.2. Specific Objectives

i. *Literature and technology review:* Survey and critically review the state of the art on variable-speed operation in hydropower, with emphasis on large-plant retrofits, power-electronic interface solutions (particularly modular multilevel converters) and existing experiences, identifying technological trends, limitations and open research gaps.

ii. *Definition of the VSO operating range:* Derive the extended operating domain for VSO using universal hill charts and similarity equations, redefining the H–Q–N limits for the case-study plant and quantifying how the admissible region expands relative to conventional fixed-speed operation.

iii. *Development of a dispatch and redispatch algorithm:* Design, implement and validate a power-redispatch algorithm capable of simulating partial and total VSO conversion scenarios, minimizing the number of start–stop cycles of the generating units while respecting hydraulic and operational constraints.

iv. *Assessment of energy gains and partial vs. full conversion:* Quantify the gains in annual energy production obtained with VSO, both without and with optimized flow allocation, comparing different partial- and full-conversion configurations and identifying to what extent most of the benefits can be captured with partial conversion.

v. *Cavitation mitigation analysis under VSO:* Extend the methodological framework to cavitation mitigation by:
   a. detecting cavitation-prone operating points via a σ–N_s criterion;
   b. applying VSO-based adjustment strategies in discharge and speed; and
   c. quantifying the reduction in cavitating operating hours for different power-tolerance levels that can be compensated by other units.

1.4. THESIS CONTRIBUTIONS

This thesis provides a set of technical and methodological contributions to support the feasibility analysis and implementation of VSO in large hydroelectric power plants. The main contributions are summarized as follows:

i. *Development of an operational simulation algorithm:* A Python-based dispatch algorithm was created to simulate the real-time distribution of generation across units operating under both fixed-speed and variable-speed modes. The algorithm enables hourly simulation of various conversion scenarios and quantifies the reduction in start-stop cycles resulting from VSO implementation.

ii. *Implementation of a hill curve interpolation framework:* An interpolation tool was developed using SciPy's griddata function to generate 2D and 3D efficiency surfaces from scattered operational data. This contribution enabled the application of hill curves in an automated and scalable manner, which is essential for real-time simulation and dispatch evaluation.

iii. *Iterative net head calculation engine:* A numerical method was implemented to estimate net head from gross head and power values using an iterative algorithm based on turbine efficiency. This process ensures accurate hydraulic modeling and supports dispatch decision-making under both FSO and VSO conditions.

iv. *Quantitative assessment of cavitation mitigation and increasing of the energy impacts:* The thesis extends the VSO framework to explicitly address cavitation, combining a σ–N_s criterion with VSO-based adjustment strategies in discharge and speed. For a representative Francis unit, the proposed strategies mitigate up to approximately 75% of the historically cavitating operating hours within a modest power-tolerance band that can be compensated by other units. In parallel, the energy-gain analysis under VSO with optimized redispatch provides a first indication of the positive impact on annual production and, consequently, on firm-energy potential, establishing a solid basis for more detailed regulatory and economic assessments in future work..

1.5. WORK STRUCTURE

This thesis is structured to provide a logical and comprehensive analysis of the technical and operational feasibility of converting hydroelectric power plants to VSO, following a clear progression from foundational concepts to applied methodologies and results.

The document is organized as follows: **Chapter 1** introduces the research, outlines the general context, the motivations that led to its development, the general and specific objectives, and the primary contributions generated by the study. **Chapter 2** presents a comprehensive review of key topics related to this research. **Chapter 3** discusses the theoretical and analytical bases that support the implementation of VSO. It covers hydropower control principles, including the use of hill curves, the application of similarity laws to expand the operational range, the utilization of universal diagrams for visual analysis, and the expected performance effects resulting from variations in speed. **Chapter 4** outlines the step-by-step approach developed to assess the feasibility and

benefits of converting hydropower plants to VSO. This includes determining key operational parameters under variable speed, developing a dispatch strategy to minimize machine starts and stops, and establishing procedures for analyzing cavitation exposure and estimating the potential impact on firm energy delivery. **Chapter 5** applies the proposed methodology to the case studies, detailing the modelling steps, conversion scenarios (partial and total VSO) and the configuration of the dispatch and redispatch simulations. **Chapter 6** presents the main technical results obtained so far, including: (i) the expanded operational range achieved with VSO; (ii) the reduction in start–stop cycles for different conversion configurations; (iii) the gains in annual energy production with and without optimized flow allocation; and (iv) the performance of VSO-based cavitation mitigation strategies for different power-tolerance levels. **Chapter 7** consolidates the main conclusions drawn from the case study, validating the methodological framework for assessing VSO conversion in large hydropower plants and highlighting the benefits in terms of operational flexibility, reduced mechanical stress, increased energy output and mitigation of cavitation-prone operation. Finally, the **References** chapter compiles all sources cited throughout the work.

2. LITERATURE REVIEW

This chapter discusses various studies focusing on the operation of hydroelectric power plants at variable speeds. In addition to exploring the benefits and technological enablers of VSO, particular attention is given to the operational challenges associated with many start-stop cycles, including their mechanical, economic, and efficiency-related impacts. The analysis of previous research reveals the potential and technical limitations involved in converting existing hydroelectric plants, providing a comprehensive understanding of the topic and identifying knowledge gaps to which this study can contribute. These investigations encompass technical aspects, including operational efficiency and water resource management, as well as financial factors and environmental and sustainability concerns. The relevance of this topic to the energy sector is emphasized, highlighting the importance of such studies for the evolution of hydroelectric generation practices and the strengthening of the renewable energy matrix. The information-gathering process was conducted using academic research platforms, including SciELO, IEEE, CAPES Journal Portal, Google Scholar, and ScienceDirect.

2.1. VARIABLE SPEED OPERATION (VSO)

Given the current energy transition scenario, the efficiency and adaptability of energy systems are crucial for balancing generation and consumption in power grids. In this context, variable speed operation systems emerge as a promising solution, offering not only more effective energy management but also improved stability and reliability of the electrical system. This section examines various studies that investigate the applicability, benefits, and challenges associated with large-scale systems utilizing variable-speed technology.

The review begins with an analysis of technical advancements and innovations in variable speed systems, highlighting how these technologies contribute to a more dynamic response to energy demand and supply fluctuations. Following this, key studies discussing the primary benefits of these systems are presented, including energy efficiency optimization, loss reduction, and improved response to peak demand. Additionally, real-world cases of hydropower plants that have been successfully

converted to operate under variable speed conditions are presented, illustrating the practical feasibility and benefits of such implementations.

Several studies have significantly contributed to the understanding and improvement of variable speed systems. Krishnakumar et al. [26] presented a detailed analysis of pumped storage plants, focusing on electrical machines (generators/motors), operational optimization techniques, and management of power generation and water pumping systems for energy storage. Mesquita et al. [27] proposed a solution to reduce energy consumption in water supply systems by utilizing variable-speed centrifugal pumps. Ciocan et al. [28] discussed the importance of developing variable-speed pump-turbine technologies in the hydroelectric market, emphasizing the need for grid stability and peak energy availability. The study highlighted that new hydroelectric plants based on variable speed pump turbines represent a promising direction for the sector.

Deng et al. [29] analyzed the dynamic behavior and performance regulation of variable speed pumped storage plants, aiming to mitigate fluctuations caused by wind power plants and pump mode operations. Muljadi et al. [30] addressed the dynamic modeling of a variable-speed hydroelectric power plant, detailing a dynamic generator/converter energy model focused on turbine control optimization. The study also mentioned the replacement of a synchronous generator with a Doubly Fed Induction Generator (DFIG) in a pumped-storage plant, enabling variable-speed operation. Iliev et al. [14] presented key advancements in variable speed Francis turbine technology, including control and monitoring systems, performance modeling and simulation, and the challenges associated with installation and maintenance.

Mohanpurkar et al. [7] examined the modeling and analysis of a variable speed pumped storage hydroelectric plant for transient stability in power systems, highlighting the importance of active power and frequency control. The study emphasized the need for real-time simulations to evaluate interactions between hydraulic and electrical energy systems.

VSO represents a significant advancement in efficiency and adaptability. The final part of this section examines various studies that compare these systems with Fixed Speed (FS) alternatives, highlighting the advantages of operational flexibility. Selected studies discuss how the ability to adjust operational speed enhances load management and demand response, reduces mechanical wear, and optimizes energy consumption.

Bidgoli et al. [6] provided a comparative analysis of the technical characteristics and operational performance of two electrical machine technologies used in variable-speed pumped storage hydroelectric plants: Synchronous Machines (SM) and DFIG. The results indicated that DFIG offers several technical advantages over conventional synchronous machines, such as higher energy efficiency at low speeds, improved torque control, and lower maintenance costs. However, synchronous machines still hold advantages in terms of dynamic response and high-speed performance.

Yang et al. [13,16] discussed the use of variable-speed Pumped Hydro Energy Storage (PHES) plants to mitigate fluctuations caused by renewable energy systems. Their results demonstrated that variable-speed PHES units effectively smooth wind power generation fluctuations and improve grid stability, thereby enhancing system reliability. Padoan et al. [31] compared the dynamic behavior of variable-speed and fixed-speed units in a pumped storage hydro plant with two 320 MW units. The study demonstrated that variable speed (VS) architecture enhances power system stability characteristics, particularly for local and inter-area oscillation modes, while also discussing the challenges and opportunities associated with implementing variable-speed units in pumped storage plants.

Li et al. [32] presented a new excitation control method for variable-speed units, comparing its performance with traditional current-source-based VSPSP excitation control. The proposed VSPSP excitation control model accurately reflected the characteristics of a controllable voltage source, yielding more precise voltage and reactive power simulation results for transient stability analysis.

Wegiel et al. [33] analyzed the efficiency of a variable speed conversion system in a small-scale hydroelectric plant, concluding that the use of VSO significantly increases efficiency and allows for more adaptable operation under varying demand conditions. Pannatier [34] conducted a detailed analysis of the dynamic behavior of a variable speed 2×320 MW pump-turbine hydroelectric plant, including hydraulic and electrical component modeling.

Bidgoli et al. [35] developed a model and controller for a DFIG-based pumped storage system, comparing both fixed and variable speed configurations. Their results showed that variable speed DFIG operation not only eliminates oscillation modes but also

significantly enhances rotor angle and transient voltage stability in interconnected power grids.

In a similar direction, Nicolet et al. [36] conducted a detailed analysis of the dynamic behavior of an energy network comprising thermal, wind, and hydroelectric plants, focusing on the advantages of variable speed pumped storage units during transient operation. The study demonstrated that these units enhance power system efficiency and reliability, facilitate better integration of diverse energy sources, and provide key benefits such as active power control in pump mode, improved efficiency in generation mode, and enhanced grid stability through reactive power control.

Shi et al. [12] proposed strategies for coordinating the operation of Variable Speed Pumped Storage Units (VS-PSU) and wind power plants, reducing wind farm output fluctuations and contributing to the safe, economic, and stable operation of power systems. The study further emphasized key benefits such as peak regulation and frequency modulation.

Acosta et al. [37] evaluated the optimal frequency support of variable-speed hydroelectric plants combined with Battery Energy Storage Systems (BESS) equipped with Fast Active Power Control (FAPC) technology. The study concluded that integrating variable speed hydro units with BESS significantly improves frequency response, even in low-inertia scenarios, while also increasing machine lifespan and reducing generator start-stop cycles.

Huang et al. [38] presented a simulation model for a variable-speed pumped hydro storage system, analyzing its performance across different operational scenarios, including pumping mode, generation mode, and transition phases. The results showed that variable-speed operation enhances energy efficiency and reduces mechanical wear compared to fixed-speed systems.

Zuo et al. [39] and Feng et al. [40] explored the characteristics of the S-shaped region in pump-turbine performance curves under turbine mode, analyzing the advantages of variable speed pumped storage units in renewable energy grids, which often experience stability issues during transient processes. Their studies concluded that, despite ongoing technical challenges, variable-speed pumped storage remains a highly promising solution for improving the stability and efficiency of renewable energy grids.

Polster [21] discusses the retrofit of pumped storage plants for operation with CFSM and presents the results of the conversion of two VS plants commissioned by Verbund Hydro Power: Malta Oberstufe and Kaprun Oberstufe. Sivakumar [41] mentions that conventional synchronous machines can be converted into variable-speed machines by adopting Static Frequency Converters (SFC) between the stator and the grid connection. This study focuses on a conversion case at Kadamparai Hydroelectric Plant in India, detailing both the benefits and challenges of the transition, particularly in terms of operational efficiency. Bortoni et al. [23] explore different strategies for converting fixed-speed hydro plants to VSO, highlighting its benefits for existing hydropower stations (such as Furnas), especially when operating under sub-nominal water pressure.

Valavi [4] presents the two main configurations for enabling VSO in existing hydroelectric plants: DFIM and CFSM. The study also discusses how the motivations, services, values, and technology of variable-speed hydro plants have evolved over time. The author concludes that with advancements in power electronics, converters capable of handling large power capacities (above 500 MW) will become more feasible, reinforcing that CFSM technology offers several advantages over DFIM.

Similarly, H. Ye et al. [22] examine the system configurations and operational characteristics of two variable speed pumped storage solutions: DFIM and CFSM. Basić et al. [42] also discuss these technologies and provide insights into power electronics innovations for variable-speed hydro plants, emphasizing their role in supporting grid stability in high-penetration renewable energy environments. Tiwari et al. [43] present the advantages of CFSM technology for pumped storage plants, outlining steady-state control strategies for efficient operation in both turbine and pump modes. Torres [44] investigates the partial conversion of generating units to reversible turbines (RT) operating in hydraulic short-circuit mode for active power stabilization in hydroelectric plants, reducing the frequency of generator start-stop cycles.

A noteworthy case of a successful conversion is described in Schlunegger [45], which details the partial conversion of a synchronous generator to a variable speed system using a frequency converter at Grimsel 2 Hydroelectric Plant in 2013. This frequency converter enabled the 100 MW machine to operate at VS, allowing optimal adaptation of the power output to grid scheduling requirements, as well as facilitating primary and secondary control power generation. Nicolet et al. [46] present the benefits of using a

Full-Size Frequency Converter (FSFC) solution for rapid mode transitions in Francis pump-turbines at existing pumped-storage plants. The study evaluates the feasibility of quick mode transitions and their implications for safe grid operation under variable speed conditions.

Following a recent trend in power plant conversion technologies, Modular Multilevel Converters stand out as an innovative and efficient solution. The final part of this section examines academic research that details the application and advantages of MMCs in enabling variable-speed operations. The studies reviewed here examine how MMCs, with their precise and dynamic control over voltage and current, are well-suited for managing load variations and enhancing energy efficiency.

MMC technology is highly valued for its modularity, scalability, and seamless integration with existing infrastructure. It facilitates both partial and complete conversions of traditional power plants into more adaptable and sustainable models, even for high-power applications. Through this review, we seek to understand the relevance and impact of MMCs in the current landscape of hydroelectric plant conversions.

In this regard, Steimer et al. [47] describe how MMC converters achieve total energy conversion efficiency exceeding 98.5%, utilizing advanced Integrated-Commutated Thyristors (IGCTs) and supporting power ratings from 50 MVA to 500 MVA. Dekka [48] presents the development of MMC circuit topologies, mathematical models, and control diagrams, discussing their evolution and technical challenges over time. The study highlights that MMC technology is among the most promising for medium-to-high voltage and power applications, given its fault-tolerant operation, transformer-less design, and high-quality output waveforms.

Holzer [49] discusses established concepts in conventional hydroelectric power plants, explaining power converter functionality and synchronous machine operations. The study concludes by strongly recommending MMC technology for large-scale hydro plants, identifying it as a superior alternative to Full-Size Converters (FSC). Tiwari et al. [50] further elaborate on the use of MMC technology for variable-speed hydro plants, analyzing factors such as torque availability at rest and how variable-speed operation enhances efficiency and energy regulation in pump mode. In another study, Tiwari et al. [20] compare three MMC topologies for variable-speed operation in pumped-storage plants using Full-Size Converters (FSC).

A notable industrial application is described in [51], which introduces the MM7 Modular Multilevel Converter by GE Power Conversion, a scalable solution up to 300 MVA and 36 kV, designed with standardized modular power cells. The study highlights MM7's key benefits, including modularity, transformer-less design, enhanced power quality, and improved grid compliance.

Polster [19] discusses the modernization project of the Malta Oberstufe Hydroelectric Plant in Austria, which underwent a major retrofit after over 40 years of operation. This project included the replacement of existing generator and hydraulic systems with new variable-speed solutions utilizing CFSM and MMC technology. Despite the converted machines in Malta being rated at 80 MW, the study confirms that MMC technology is scalable for machines exceeding 300 MW. The findings demonstrate MMC's advanced benefits and practical application for hydroelectric energy storage in commercial-scale plants.

Gontijo [52] presents a recent detailed study on new MMC-based solutions for high-power, medium-voltage electric machine drives, focusing on two MMC topologies: one designed for low-frequency applications and another for modern medium-voltage, high-power wind turbines. Similarly, Basić et al. [24] highlight the massive potential of MMC-based retrofits for large-scale pumped-storage plants, enhancing grid flexibility and meeting future energy system demands. The study identifies MMC's scalability and redundancy as critical advantages for large hydroelectric units.

Christe et al. [2] introduce the first direct AC/AC Modular Multilevel Converter (MMC) for hydroelectric plants, successfully deployed in a variable-speed pumped-storage facility. The study emphasizes how this converter completely decouples machine dynamics from grid dynamics, enabling simpler and more efficient variable-speed operation with high torque across the entire speed range.

Lastly, [53] provides up-to-date insights into pumped-storage hydro plants (PHSPs) and outlines the different PHSP configurations, including fixed-speed and variable-speed turbines. The study introduces the Modular Multilevel Matrix Converter (M3C) for direct AC/AC conversion, along with upgrade pathways that do not require replacing synchronous machines or pump turbines. The report concludes that MMC technology is the best choice for modernizing existing hydro plants.

The research discussed in this section underscores the transformative potential of variable speed plants in modern power systems. These systems offer significant advantages, including enhanced operational flexibility, improved efficiency, better frequency regulation, and reduced mechanical wear, making them a crucial solution for integrating renewable energy sources into global power grids. The studies presented demonstrate that variable speed technology represents a viable and highly beneficial retrofit for existing hydroelectric plants, paving the way for future advancements in sustainable and adaptive energy generation.

2.2. TECHNICAL SOLUTIONS FOR VARIABLE SPEED OPERATION

VSO implementation in hydro plants depends on state-of-the-art technologies that can meet the requirements of modern energy systems. Such technologies include increased operational flexibility, grid stability, and compatibility with renewable sources. DFIM, CFSM, and MMC are among the most popular solutions for VSO implementation. Each of these has its own set of advantages and has been applied in retrofitting projects around the world, giving valuable insight into its use in large-scale plants such as Tucuruí.

Many studies and case experiences have proven that it is possible and beneficial to retrofit hydropower plants into VSO, showing that these technologies are indeed very versatile in many different situations. For instance, in [45], a 100 MW machine installed for the Grimsel 2 hydropower plant allowed for a successful partial conversion of a synchronous generator towards the end of 2013, therefore proving that frequency converters can make variable speed operation achievable. Retrofitted with a frequency converter, this 100 MW machine then made real optimized adaptation to load scheduling possible as it enabled primary and secondary control energy generation, showing real significant operational improvements.

Similarly, explores the possibility of converting existing synchronous machines to variable speed operation at the Kadamparai hydropower plant in India [41]. In this work, the application of SFC between the stator and grid supply is put forward as one of the workable methods to realize VSO. It also considers efficiency enhancements and operationally difficult aspects following such a change, with a focus brought to bear on

how traditional synchronous machines can be made workable with modern energy requirements through advanced technology.

It has been noted that the plant was built within the context of the comprehensive modernization project of the Malta and Kaprun pumped storage hydropower plant in Austria [21]. The replacement of the existing generation and hydraulic systems with variable speed solutions formed part of the retrofit for a plant that was located at almost 2,000 meters above sea level. CFSM using state-of-the-art MMCs were brought to market as part of the Malta retrofit. The studies were conducted with converted machines rated at 80 MW. Therefore, they have confirmed the scalability of MMC technology for machinery well above 300 MW.

Apart from retrofits, other new installations, such as Frades 2 in Portugal, highlight the increasing attention that VSO technology has been garnering. According to [54], the Frades 2 pumped storage hydropower plant has a capacity of 780 MW, equipped with two 390 MW DFIM units, which to date are the largest and most powerful units installed anywhere in Europe. This was commissioned in 2017 and demonstrated that DFIM technology can achieve high levels of power while also providing the adaptability that modern grid operations require.

These examples demonstrate that VSO technologies are versatile and proven effective in various settings, right from the retrofit of old infrastructures to the provision of new installations. Learning from such experiences, this paper aims to draw lessons from the global implementations of VSO and assess the potential and impacts of converting the Tucuruí hydropower plant to variable speed operation. The actual benefits observed in these projects support the viability of the proposed solutions that aim to address the operational and economic challenges of large hydropower plants.

2.2.1. Double Fed Induction Machine (DFIM)

The doubly fed induction machine is one of the most common technologies applied in variable-speed operation hydropower plants due to its efficiency, capability, and low operating expenses. A leading solution refers to a technology that represents a wound-rotor induction machine, where both the stator and rotor windings are interconnected with separate power sources. This means that the stator will be directly connected to the grid,

while a bidirectional converter will supply power to the rotor. With this, the rotor will turn with excellent efficiency over a wide range of speeds, ensuring smooth acceleration and proper magnetic field build-up, even at speeds below synchronous.

In practical applications, the DFIM stands out as a widely used solution for enabling variable speed operation in large hydroelectric power plants. It enables the use of more cost-effective converters, as well as the already proven DFIM reliability in large systems. However, the adaptation of DFIM for retrofitting existing hydropower plants makes its adoption much more difficult and expensive. This is because, in practice, it would require replacing the synchronous machines currently used with new induction machines, resulting in significantly increased capital expenditure. In principle, this makes DFIM less attractive than other technologies, such as CFSM, for use in older plants with limited budgets, as CFSM allows for the use of existing synchronous generators.

Nonetheless, for new installations or specific retrofitting scenarios where replacing the generator is feasible, the DFIM remains a competitive option. As stated by [18], improvements in technology within power electronics have led to cost reductions alongside higher ratings for converters, thereby further solidifying the DFIM drive as a low-cost option for greenfield projects. Its dynamic speed adjustment capacity also better integrates with sources of renewable energy. While DFIM offers cost-effective solutions for greenfield projects, its limitations in retrofits pave the way for more adaptable technologies, such as CFSM, discussed in the next section.

To better illustrate the typical configuration of a DFIM in variable-speed hydropower applications, Figure 1 presents the schematic layout of the excitation system. This diagram highlights the main components involved, including the direct grid connection of the stator and the bidirectional converter that supplies the rotor via a DC link.

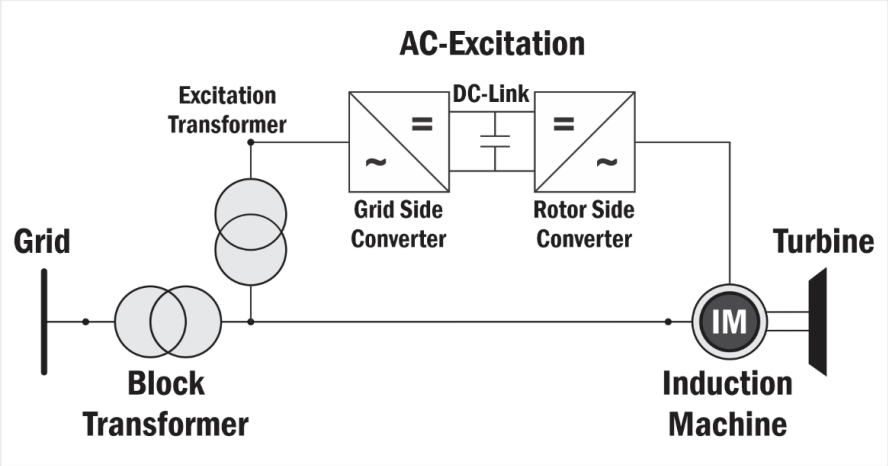

Figure 1 - Schematic of a Doubly Fed Induction Machine (DFIM) excitation system.

2.2.2. Converter Fed Synchronous Machine (CFSM)

The converter-fed synchronous machine offers a flexible and dependable alternative for implementing VSO in large hydropower plants. It involves a synchronous machine directly coupled to the grid through a full-scale power converter. In this way, the CFSM achieves very accurate control of both speed and torque, allowing the machine to operate independently of the grid frequency. This feature places the CFSM at the heart of what is considered an innovative technology for upgrading existing hydropower installations.

Compared to the DFIM, the CFSM offers significant technological advancements, as noted by [52]. This arises from the fact that while the DFIM has half-converters at its rotor input, the CFSM utilizes full-fledged power electronic inverters at its rotor input, along with a synchronous motor, to achieve precise speed control. This system gives an excellent level of flexibility in operations and guarantees relatively higher efficiency under any operating condition. This makes it an attractive option, whether for retrofitting or new constructions.

The main components of the CFSM system are a synchronous generator, grid-side converter, and machine-side converter, interconnected via a DC link. Such a design enables the separate control of active and reactive power, performing optimally even under variable-speed conditions. Additionally, the converter controls the machine so that it continues to run at the grid frequency, regardless of the rotor speed. This decoupling

from the rotor speed, on which the conventional frequency is dependent, means that CFSM plants will be able to operate with maximum efficiency over a wide range of speeds- thus making them more flexible and reliable.

Historically, the adoption of power electronic converters at high voltage levels was constrained by the limited power ratings of semiconductor devices. Only in recent years have significant technological advances overcome such limitations, allowing the implementation of high-capacity CFSMs on a large scale [52]. Key advances responsible for opening up such possibilities regarding the repowering of existing fixed-speed plants are CFSM-based VSO technology.

Examples would be the Grimsel 2 in Switzerland [45] and Kaprun in Austria [21] power plants, where applied CFSM retrofits high-capacity systems, then these latter retrofits will stand as milestone measures in applied CFSMs. The success of these implementations proves that CFSM technology can sufficiently modernize hydropower plants and meet increased demands regarding renewable energy integration. As [24] has argued, the market for repowering already installed fixed-speed plants with CFSM-based solutions is big, and such solutions would bring about better operational performance together with improved flexibility toward the grid requirements.

To illustrate the configuration and operational principles of the Converter-Fed Synchronous Machine (CFSM) system, Figure 2 depicts the typical arrangement used in hydropower retrofitting for variable speed operation. The diagram illustrates the integration of a full-scale frequency converter between the grid and the synchronous machine, comprising a grid-side converter, a stator-side converter, and a DC link. This setup enables complete decoupling between the machine speed and the grid frequency, allowing flexible and efficient operation across a broad range of hydraulic conditions.

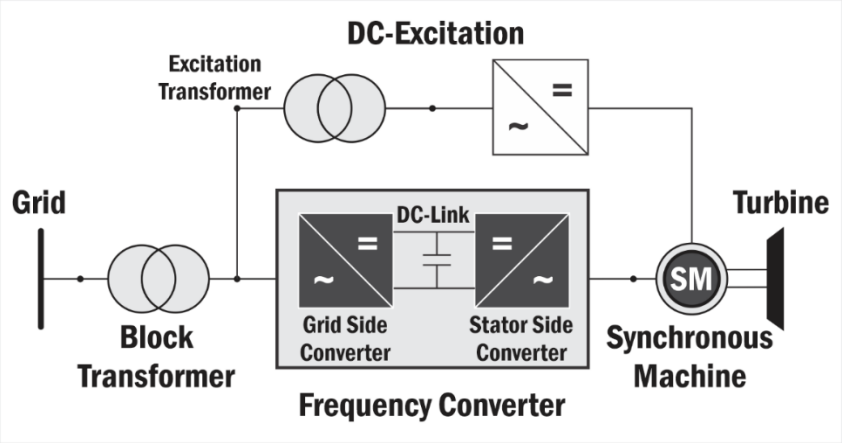

Figure 2 - Schematic of a Converter Fed Synchronous Machine (CFSM).

Moreover, the variable speed operation for hydropower plants can be achieved with effectiveness through technologies based on CFSM or DFIM. While technology based on DFIM offers a cheaper solution for new installations [18], it also implies rather big problems for the existing fleet since salient-pole synchronous machines are to be replaced by doubly fed technology. Technology based on CFSM, especially if combined with MMC, provides much more flexibility, efficiency, and scalability compared to CFSM, and this should make it the technology of choice for retrofitting large hydropower plants like Tucuruí.

The following Table I presents a summary of the main differences between constant speed units, DFIM units, and CFSM units, adapted from [22].

Table 1 – Summary of Constant – Speed, DFIM and CFSM Units

Criteria	***Variable-Speed Unit***	
	DFIM	***CFSM***
Frequency converter	*15–30% of Smachine* *Strong grid code → Large converter size*	*100% of SMachine*
Electrical machine	*Asynchronous machine* *Unit designed for full apparent power*	*Synchronous machine* *Unit designed for active power only (cos phi 1) – around 10-15% smaller than conventional unit*
Speed variation range	*Limited (typical around ±7%, max ±10%)* *Limited by rotor power capability*	*Larger (theoretically 100%)*

		But limited by the hydraulic (typical ±10-15%, max ±20%)
Operating efficiency	*Increase by 3% compared to constant-speed*	*increase by 1-3% compared to constant-speed*
System complexity	*The high number of components Breakers, phase shift disconnector, etc*	*Conventional unit incl. frequency converter Breaker on HV level*
Cost of Implementation	*Medium*	*High*

2.2.3 Modular Multilevel Converter (MMC)

The modular multilevel converter is a cutting-edge power electronics technology that plays a pivotal role in enabling VSO in modern hydropower plants. Among the advanced converter topologies, the MMC is unique in that it is modular and scalable in design, thereby making it possible to achieve high voltage and power levels with high efficiency and reliability [52]. A schematic of the retrofit of an existing plant with MMC for conversion is shown in Figure 3.

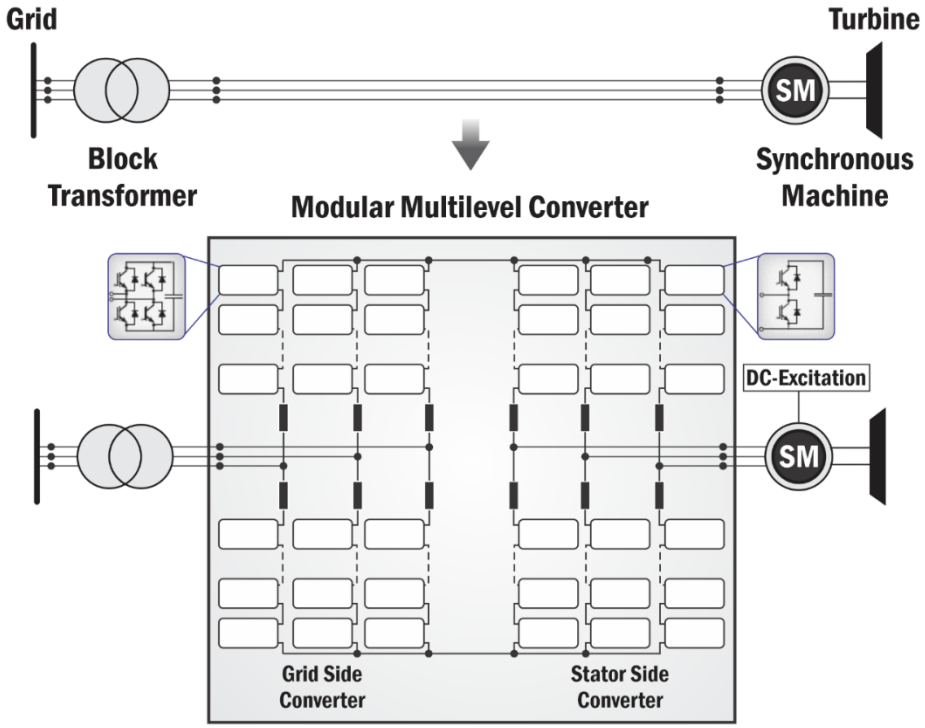

Figure 3 - Retrofit of an existing plant with I-MMC for conversion adapted from [24].

The MMC consists of submodules that can be connected in series and parallel to form the overall converter structure. Each submodule includes power switches and capacitors to provide control at the required voltage and current waveforms. Since it is modular, harmonic distortion is low [52]. The MMC acts as a converter and an interface between the machine and the grid, allowing the synchronous machine to be operated in a variable-speed drive system without the need for additional equipment for this purpose.

Gontijo [52] investigates these new converter solutions with a modular multilevel for high-power medium-voltage electrical machine drive applications. Since the MMC is inherently modular, high-voltage procedures could be implemented by scaling up and steadying the system. This is a very significant step forward for the electrical engineering industry. These characteristics make the MMC a very good solution for large hydropower plants to be retrofitted for VSO, with this providing both technical and economic benefits.

Another added advantage resulting from the adoption of MMC-based solutions is the realization of additional operational benefits. Near-sinusoidal voltage waveforms at relatively low Total Harmonic Distortion (THD) achievable with MMCs were presented in reference to conventional Pulse Width Modulation (PWM) modulated Voltage Source Inverters (VSIs) [53]. This advantage proved the applicability of MMC even in high-capacity applications. This will ensure reliable and efficient plants with significant power demands. In addition, the performance of the CFSM in comparison with the conventional DFIM is detailed by [47], bringing out its superiority both in terms of efficiency and flexibility for variable speed applications.

The MMC has found application in large-scale retrofits like that of the Kaprun plant in Austria [21], where its ability to handle power levels greater than 300 MW is possible, for plants of Tucuruí's kind, where high capacity and operational reliability are of paramount importance, scalability and fault tolerance offered by MMC set new benchmarks. Unlike DFIM, which would require the replacement of already installed synchronous machines to allow the system to run at variable speeds, MMC can easily be retrofitted with the current infrastructure without having to replace the synchronous machines. This feature drastically reduces the cost and is suitable for most large machinery.

2.3. START–STOP PROBLEM IN HYDROPOWER PLANTS

Hydropower plants have increasingly been demanded to provide fast-response ancillary services in frequency regulation and the balance of systems [2,15], sometimes through stopping and starting operations. When frequent, start–stop cycles cause several mechanical, thermal, and hydraulic stresses on major components of hydropower generating units. These transients significantly contribute to the phenomenon of high-cycle fatigue in turbine runners, accelerating material degradation and the cracking process, especially in Francis and Pelton turbines [55]. These transients are not confined only to hydraulic boundaries but also extend even to electrical components. The stator insulation of generators ages much more rapidly because of temperature cycling, and the lifespan of the equipment is also drastically reduced [56,57]. Pressure and velocity measurements in a Francis turbine model have shown that startup and shutdown events result in severe flow instabilities and unsteady pressure loads, especially in the draft tube [58].

From a cost perspective, start–stop events translate directly into increased operation and maintenance (O&M) expenditures. A methodology for calculating both direct and indirect costs associated with each start–stop cycle, including a wear-induced reduction in service life and earlier rehabilitation requirements, has been proposed [59]. Additionally, models have been developed to evaluate the trade-off between keeping units running at low loads or shutting them down, incorporating equipment degradation and water loss [60]. A critical literature review conducted by Savin et al. [61] consolidates and compares multiple methodologies for estimating start–stop costs in hydropower plants, highlighting the lack of standardized approaches and the variability in cost estimates depending on plant size, technology, and operational regime.

Institutional research conducted by the U.S. Department of the Interior (USDI) has also advanced this discussion. Their report introduced a bottom-up cost model incorporating maintenance, component replacement, lost generation, and water usage, estimating start–stop costs between $274 and $411 per cycle [62]. A follow-up study [63] extended this methodology through a standardized model for calculating cycling costs, highlighting the significance of metal fatigue in generator components, such as rotor poles and stator windings, due to start–stop operations.

In addition to maintenance and repair implications, frequent start–stop operations have broader economic consequences. Cycling results in a higher equivalent forced outage rate (EFOR) and reduced long-term plant availability [64]. The cumulative effect of these cycles not only increases the immediate costs but also undermines the strategic role of hydropower as a reliable and efficient grid balancer. Therefore, the subsequent sections of this paper explore how VSO emerges as a feasible solution to mitigate these challenges by increasing dispatch flexibility and the operating range of generating units.

2.4. VARIABLE SPEED AND CAVITATION

Cavitation is a critical concern in hydraulic turbines due to its deleterious effects on efficiency, structural integrity, and operational lifespan. It manifests through the formation and collapse of vapor bubbles in low-pressure regions, leading to material erosion, noise, vibrations, and even mechanical failure [65,66]. Traditional fixed-speed hydro turbines are often constrained to operate within predefined stable zones to mitigate cavitation risks. However, the adoption of VSO offers new opportunities to optimize turbine performance while minimizing cavitation exposure.

The physical fundamentals and mechanisms of cavitation in hydraulic machines have been comprehensively reviewed in classical and modern works. Arndt [65] provided foundational insights into cavitation behavior in fluid machinery, identifying how operational conditions such as pressure drop, surface roughness, and flow velocity govern bubble formation and collapse. Avellan [66] extended this understanding by categorizing cavitation types across various turbine components, highlighting how operating point deviations influence cavity development and damage severity.

Recent reviews highlight the complexity of cavitating turbulent flows and emphasize the importance of advanced simulation techniques for their accurate prediction. Luo et al. [67] summarized advances in computational modeling and the persistent challenge of reconciling numerical and experimental results, particularly in unsteady multiphase regimes inside hydro turbines. Similarly, Kumar and Saini [68] and Brijkishore and Khamparia [69] reinforced the relevance of modern cavitation modeling and diagnostics in hydropower applications.

In the context of variable speed, Trivedi et al. [70] provided a key contribution by investigating cavitation behavior during speed variations in a Francis turbine. Their findings revealed that specific speed transitions can intensify pressure fluctuations and cavitation inception, especially under ramping conditions. Nevertheless, careful adjustment of runner speed and guide vane opening enabled operation away from critical cavitation-prone zones, demonstrating a potential strategy for mitigating the issue.

Numerical studies, such as those by Celebioglu et al. [71] and Ayli [72], have shown that VSO can shift the operating point to regions of the turbine hill chart where cavitation indices are lower, thereby reducing the severity and frequency of cavitation phenomena.

Moreover, Presas et al. [8] presented recent insights into the use of variable speed as a water-saving and cavitation-reducing strategy in hydropower plants. By operating turbines at non-synchronous speeds, the system can avoid operation near critical conditions typically associated with part-load or overload cavitation, thereby contributing to a prolonged equipment lifespan and lower maintenance needs.

In summary, while VSO introduces operational flexibility and potential efficiency gains, it also poses new challenges in cavitation control. Nonetheless, the literature demonstrates that with accurate modeling, real-time monitoring, and strategic dispatch, it is possible to minimize operational exposure to cavitation-prone conditions through VSO. These findings reinforce the importance of integrating cavitation risk assessment in the early stages of turbine control strategy development under VSO.

2.5. INCREASING POWER GENERATION AND FIRM ENERGY BY VSO

Firm energy plays a central role in the Brazilian electricity market, serving as the foundation for the contractual guarantees between generators and market agents. According to the National Power System Operator (ONS), firm energy of a hydropower system is defined as the highest amount of energy that can be continuously supplied by the system without deficit, under constant system configuration and repeating the historical inflow sequence. For individual hydropower plants, it corresponds to the plant's average energy production during the critical hydrological period, which is the most extended interval where the system reservoirs are depleted without total intermediate refills.

The article by Westin et al. [72] reinforces the importance of accurate flow measurement for accurate firm energy estimation, demonstrating how errors in streamflow rating curves and inflow data can lead to miscalculations that directly impact the contractually assured energy of a plant.

In the context of VSO, expanding the operational range of hydro turbines enables more flexible dispatch strategies. This flexibility not only improves operational efficiency and reduces start-stop operations but also increases the adequate availability of generating units across various hydraulic conditions. Consequently, this expanded availability can contribute to increasing the firm energy of the plant, as more consistent and prolonged energy output becomes possible even under varying inflow regimes.

2.6. ECONOMIC ASPECTS

As we advance in understanding the technical implications of these systems, it becomes equally crucial to examine the economic dimensions associated with these technologies. This final section of the theoretical framework chapter focuses on economic analyses that investigate the operational and maintenance costs associated with these systems, with particular attention to the expenses incurred by the frequent start-stop cycles of machines in large hydroelectric plants. The studies discussed here assess how storage strategies and operational methodologies can mitigate the financial impacts of these occurrences, optimizing resource utilization and extending the lifespan of power plant equipment. Additionally, this review explores the economic models proposed to quantify the savings achieved through the implementation of VSO systems, which enable more efficient and cost-effective plant operation. By highlighting these studies, we aim to provide an integrated perspective that combines both technical and economic aspects, which are crucial for the long-term sustainability of hydroelectric plants.

In this context, Vieira et al. [73] present a methodology for determining the costs related to the start-stop processes of hydroelectric generating units, as well as the costs associated with their operation as synchronous compensators. In a later study, Vieira et al. [74] developed an economic valuation methodology to estimate the financial cost of start-stop cycles and synchronous compensator operation, providing a techno-economic strategy for optimizing short-term operational planning. This study also serves as a

decision-support tool for determining whether to shut down a generating unit or maintain it in synchronous compensator mode, in accordance with prevailing market regulations.

Osburn [62] identifies the most critical factors affecting the costs of starting and stopping a generating unit in hydroelectric power plants and proposes a methodology for calculating these costs. Similarly, Engevik [18] presents a detailed study investigating the design and operational considerations of large synchronous machines powered by converters in hydroelectric applications. This study includes a series of calculations on different types of losses in hydrogenerator designs and explores how the choice of optimal nominal frequency in CFSMs can reduce overall project costs.

Savin et al. [61] provide a critical review of the literature on the costs associated with generator start-stop cycles in hydroelectric plants. They categorize the different approaches used to estimate these costs into two main classes economic and techno-economic and discuss the advantages and limitations of each approach. James DeHann [63] develops a methodology to estimate the costs of hydroelectric generator start-stop cycles, ramping, synchronous compensation, and operation in rough zones. Additionally, he presents an Excel-based model designed to apply the methodology and provide an initial cost estimation range.

Building on this research, Savin et al. [75] conducted a study focused on modeling the degradation of hydroelectric equipment and estimating the costs associated with generator start-stop cycles. In a related study, Savin et al. [55] propose a strategy for estimating the additional costs resulting from frequent turbine start-stop operations due to high-frequency fatigue. In another study by the same authors [56], the aging of hydroelectric generator stators due to thermal cycles during start-stop processes is examined through an accelerated life model and an empirical approach, assessing the impact of these cycles on stator lifespan. The article also discusses the practical implications of these findings for the hydroelectric power industry.

Finally, in [57] it delves into equipment deterioration modeling in hydroelectric power plants, aiming to evaluate the total cost of generator start-stop cycles. Given the wide variety of equipment present in a hydroelectric plant, this study requires a multidisciplinary approach that integrates multiple fields, including mechanical and electrical engineering, hydraulics, data processing, reliability analysis, safety, and maintenance strategies. The study also details the methods used to estimate equipment

degradation and how these costs can be minimized through preventive maintenance and technological upgrades.

3. VARIABLE SPEED HYDROPOWER CONTROL

3.1. HYDROPOWER CONTROL AND THE HILL CURVE

Accurate modeling of turbine performance under various hydraulic and mechanical circumstances is essential for operating hydropower plants. According to Vieira et al. [76], hill curves are crucial modeling tools in hydroelectric generation optimization because they provide precise efficiency estimations under various operational circumstances. These curves, which show turbine efficiency (η_t) as a function of the net head (H_N) and turbine power (P_t), are among the basic tools for comprehending turbine efficiency. These charts help control systems that optimize energy production and operational reliability and guide optimal operating points. To apply these curves in simulation and dispatch optimization under VSO, H_N must be precisely computed, which requires reconstructing flow conditions from measurable variables such as the gross head (H_G) and P_t.

Hence, H_N can be determined through an iterative process based on the relationship between H_G (the difference between the upstream level and the downstream level) and operational losses as shown equation (3). In this equation, k is a constant that depends on the hydraulic and mechanical characteristics of each generating unit, such as penstock geometry, friction factors, and head losses. The equations used for each iteration are detailed below:

$$\eta_t = f_{hill,N_s}(P_t, H_N) \quad (1)$$

$$Q = \frac{P_t}{\rho g H_N \eta_t} \quad (2)$$

$$H_N = H_G - k.Q^2 \quad (3)$$

To determine H_N for each generating unit, an iterative algorithm was developed on the basis of equations (1), (2) and (3). The process starts with H_G and P_t as inputs. An initial estimate of H_N is assumed, typically $H_N \approx H_G$, which is then used to interpolate the turbine efficiency (η_t) from the hill curve data equation (1). Given η_t and H_N, the discharge (Q) is calculated using equation (2). This Q value is then used to update H_N via equation (3). The process iterates until the variation in H_N between iterations is within a

predefined tolerance. Figure 4 shows the iterative procedure implemented to calculate H_N.

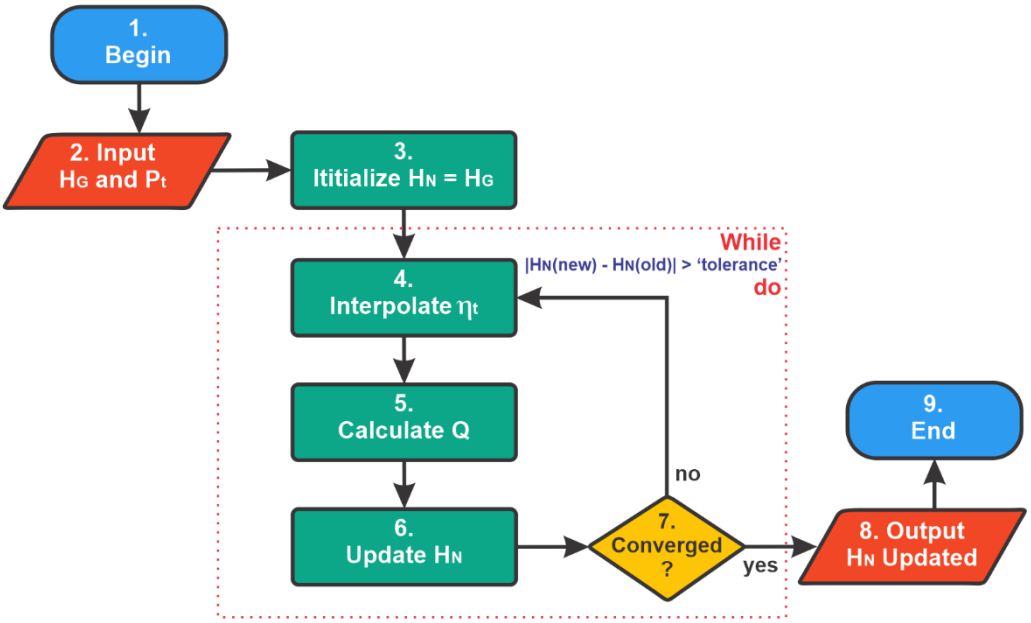

Figure 4 - Iterative procedure to determine the net head.

The hill curve efficiency surface, which is essential for this method, was generated using a Python-based implementation, which interpolated a set of scattered operational data (H_N, P_t, η_t) onto a regular grid using linear interpolation via the griddata function of the SciPy library. This means that continuous 3D surfaces and 2D contour maps are generated, which represent efficiency behavior as a function of the net head and power, as presented in Section 6.3. This approach ensures a good estimate of η_t for each point during simulation and dispatch evaluation.

3.2. SIMILARITY ANALYSIS AND OPERATING EXPANSION

The similarity equations define proportional relationships among the main turbine parameters, flow rate (Q), net head (H_N), and turbine power (P_t) as functions of the rotational speed N. These equations [64] maintain identical performance parameters for turbines while ensuring flexibility in operations. The equations below consider machines with the same diameter:

$$\frac{Q_1}{Q_2} = \frac{N_1}{N_2} \quad (4)$$

$$\frac{H_{N1}}{H_{N2}} = \left(\frac{N_1}{N_2}\right)^2 \quad (5)$$

$$\frac{P_{t1}}{P_{t2}} = \left(\frac{N_1}{N_2}\right)^3 \quad (6)$$

$$\eta_{t1} = \eta_{t2} \quad (7)$$

Additionally, the H_N and power equation must be satisfied at any operating speed. The turbine power at a given rotational speed N_i is determined by:

$$P_{ti} = \rho . g . H_{Ni} . Q_i . \eta_{ti} \quad (8)$$

To demonstrate similarity equations with speed variation for machines of the same diameter, an example region was defined by 4 reference points, which represent the maximum and minimum P_t at the minimum and maximum H_N. A variation of +10% and another variation of -10% is applied to the synchronous (current) speed, and homologous regions are produced. As shown in Figure 5, these values graphically indicate how the operating range either expands or contracts with the variation in speed. In dimensioning the influence of VSO on turbine behavior, the graphical approach offers much deeper insight in terms of flow and power adjustments.

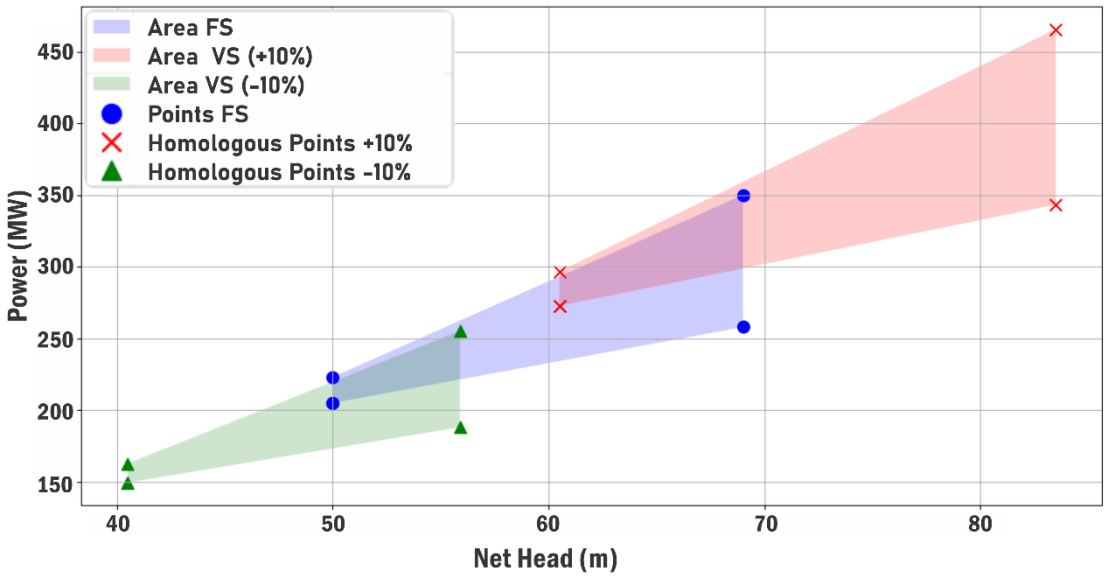

Figure 5 - Use of the similarity equations (steps ±10%).

In addition, the increased flexibility resulting from VSO necessitates stringent definitions of new operating limits to mitigate risks such as cavitation, mechanical vibrations, and structural fatigue. Establishing safe hydrodynamic and mechanical boundary conditions ensures the long-term reliability of the system while maximizing the benefits of VSO. The present stage also comprises the application of similarity equations to determine the expanded operating range at different rotational speeds. The results of this expansion for the case study in this work are presented in Section 7.1.

3.3. UNIVERSAL DIAGRAM ANALYSIS

The universal diagram is a powerful tool for analyzing turbine performance by representing the relationship between reduced quantities under different operational conditions [77]. This diagram is particularly useful in hydropower studies for comparing and evaluating turbine efficiency and performance across varying net heads and flow rates. The reduced quantities that represent the universal diagram are calculated using the following equations:

$$n_{ED} = \frac{ND}{\sqrt{gH_N}} \quad (9)$$

$$Q_{ED} = \frac{Q}{D^2\sqrt{gH_N}} \quad (10)$$

$$P_{ED} = \frac{P_t}{D^2\sqrt{gH_N{}^3}} \quad (11)$$

where n_{ED} is the speed factor, which correlates the rotational speed (N, in rpm) to geometric and hydraulic parameters, such as the turbine diameter (D, in m) and net head (H_N, in m). Similarly, Q_{ED} is the discharge factor, which relates the actual flow rate (Q, in m^3/s) to the turbine diameter and net head, with g representing gravitational acceleration (9.81 m/s^2). P_{ED} is the power factor (where P_t denotes turbine power, in W), and ρ is the water density. These dimensionless factors enable standardized comparisons across turbines under varying operational conditions, adhering to hydrodynamic similarity principles. For a better understanding of the universal diagram representation, the same operational regions shown in Figure 5 are presented through the universal diagram in Figure 6.

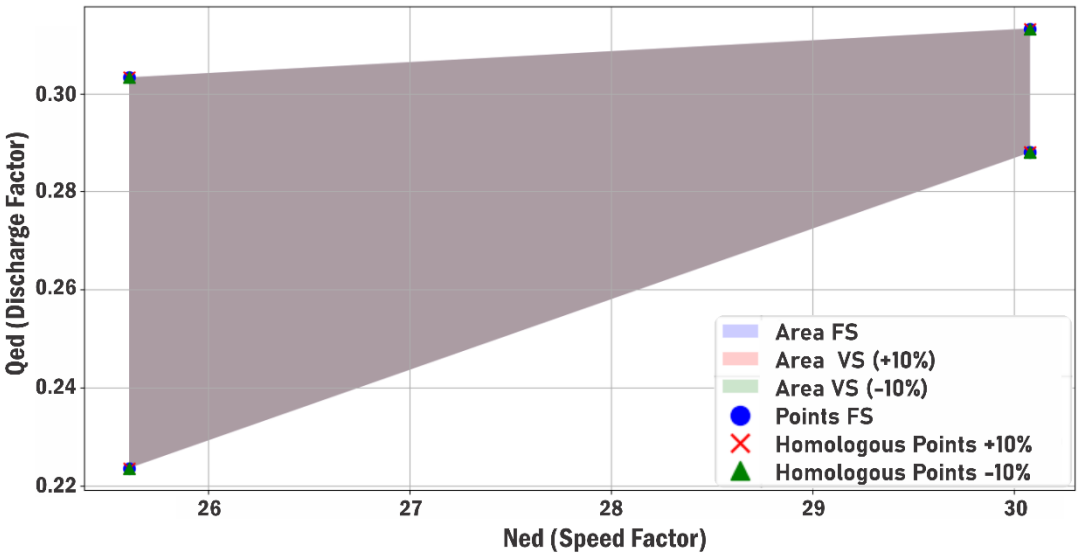

Figure 6 - Use of the reduced quantities equations.

This visualization confirms that homologous points at different rotational speeds fall within the same operational boundary when viewed in terms of reduced quantities. The universal diagram, which uses a dimensionless n_{ED} on the x-axis, can normalize different speed conditions. Homologous points coincide under the influence of rotational speed or net head change. In addition, since n_{ED} depends directly on both the rotational speed and the net head, as shown in equation (9), its application toward VSO interprets a qualitative change in parameters related to operation and, therefore, optimizes turbine performance dynamically.

3.4. SPEED VARIATION EFFECTS

The VSO has a significant impact on the performance envelope of the hydraulic turbine. Figure 7 and Figure 8 present a graphical examination of how variations in rotational speed affect the location of the operating point within the head–discharge–efficiency domain, demonstrating this effect.

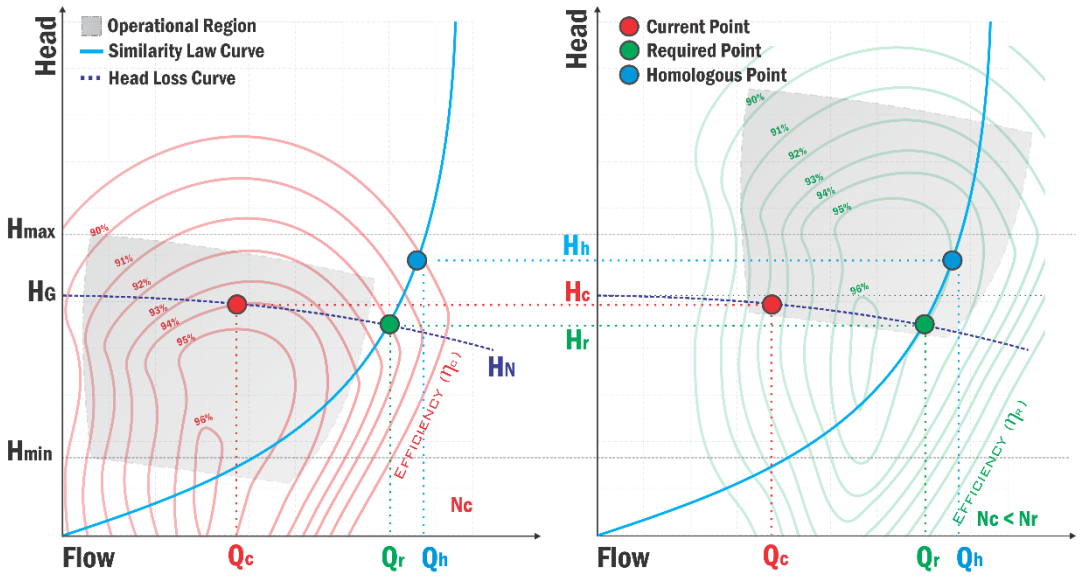

Figure 7 - Effects of increasing the rotational speed on the operating range and efficiency.

The case of increasing rotation speed is detailed in Figure 7, which shows the head loss curve derived from equation (3), the operational zone, and the similarity law curve (as discussed in Section 4.2.). The left-hand side shows the current operating point (Q_c, H_c) at the current speed (N_c), as well as the required point (Q_r, H_r) where the machine is expected to operate. Nevertheless, efficiency curves at speed η_C (in red) are displayed on the left. If the machine operates at a synchronous speed, the transition from the current point to the target point would require opening or closing the guide vanes. However, this would result in operation with low efficiency and potentially outside the permissible operating range. On the right side of the figure, increasing the rotational speed allows the required point to be brought within the permissible operating range and still improves the efficiency through the similarity curves indicated by the efficiency curves at speed η_r (in green).

The opposite situation, a decrease in rotational speed, is depicted in Figure 8. Similar to the last example, the left-hand side displays the undesirable result of attempting to maintain the current speed while reaching the necessary point. The homologous point (Q_h, H_h) corresponding to the new speed, however, falls within the operational region and follows a more efficient trajectory when the speed is decreased, as shown on the right-hand side.

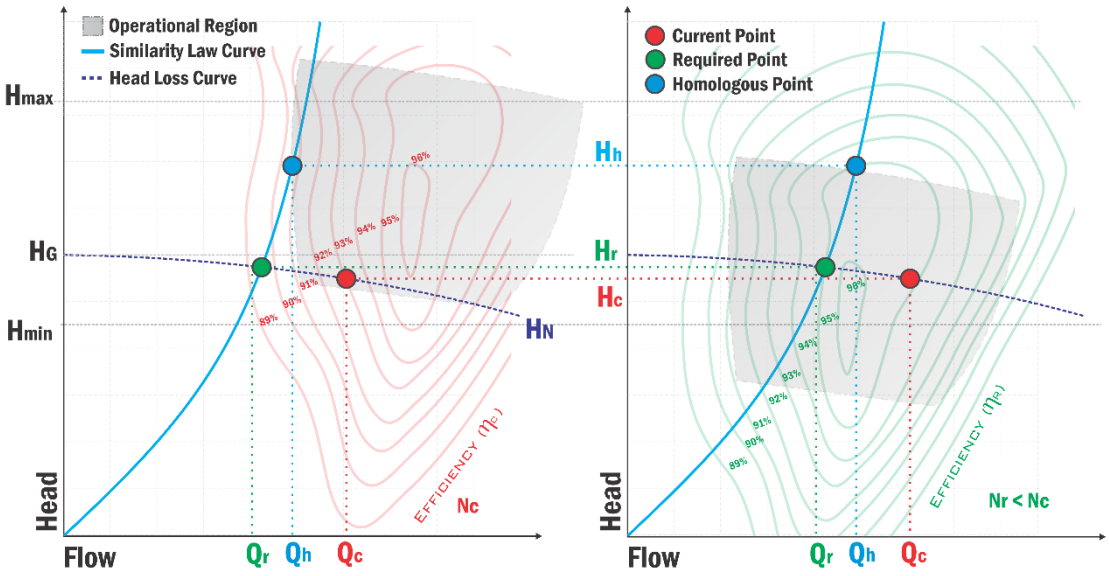

Figure 8 - Effect of decreasing rotational speed on the operating range and efficiency.

Moreover, increasing speed shifts both the hill curve and the operational region upward and to the right. Conversely, reducing the speed results in downward and leftward displacement. These effects confirm that VSO enables more flexible dispatch and increased efficiency under conditions that would otherwise be suboptimal or even unfeasible.

4. METHODOLOGY

4.1. METHODOLOGY OVERVIEW

This section presents an operational analysis to evaluate the feasibility and impacts of converting a large hydropower plant from FSO to VSO. A technical and operational evaluation of the hydropower plant operating at the FSO is the first step in the suggested technique. Its hydrodynamic characteristics, turbine–generator arrangement, and capacity are assessed. Operational bottlenecks that reduce dispatch efficiency and increase mechanical wear are identified as FSO-imposed limitations, such as limited operating ranges and rigidity in response to load fluctuations.

Following this diagnostic phase, the technique models the plant's behavior under varying rotational speeds, utilizing the principles of hydraulic similarity. These formulas, which have been verified for turbines with the same diameter, enable the conversion of performance parameters (power, head, and flow rate) under various operating conditions. An extended operating range is obtained for every machine by fusing the hill curve efficiency data with similarity concepts. This newly specified environment ensures safe operation while increasing the plant's flexibility by adhering to mechanical and hydraulic limits, as indicated by the manufacturer on the hill curve. Subsequent phases, such as dispatch optimization and performance analysis under VSO conditions, are then based on the enlarged range.

Finally, this methodology systematically integrates VSO procedures to address three key operational challenges: minimizing the number of turbine start-stop cycles, reducing exposure to cavitation-prone conditions, and enabling a potential to increase the energy generation. These aspects are explored in the following sections through targeted algorithmic implementations and operational simulations that reflect real-world constraints and technical capabilities of the studied hydropower plant.

4.2. START-STOP MINIMIZATION

One of the primary objectives of adopting VSO in hydropower plants is to minimize the frequency of turbine start and stop events. In this context, this section presents a

methodological approach to minimizing start-stop cycles through the implementation of a power dispatch strategy tailored to the expanded operational range made possible by VSO. By leveraging the additional flexibility provided by variable speed, the strategy enables a more balanced redistribution of load among available generating units, favoring those already in operation and operating within efficient and safe regions of the hill curve. The approach is formalized through the development of an algorithm that identifies the most suitable configuration of units to meet power demand with the lowest number of operational transitions, enhancing both equipment longevity and system stability.

4.3.1. Definition of Starts and Stops

To ensure accurate measurement of turbine starts and stops, the analysis was based on the internal system of Eletrobrás Eletronorte, as mentioned by [78]. This system records all operational states of the generating units, documenting every state transition, such as start-ups and shutdowns. These transitions occur due to various factors, including operational convenience, scheduled and emergency maintenance, or grid disturbances.

For this study, the data was carefully filtered to focus exclusively on start and stop events occurring due to operational convenience, aligning with the dispatch adjustments requested by the National System Operator (ONS). The following criteria were applied:

i. *Excluded Events:* Start-ups and shutdowns associated with scheduled maintenance, forced outages due to internal or external disturbances, and test runs following maintenance interventions were removed.
ii. *Considered Events:* Only Shutdowns Due to Operational Convenience (DCO) and start-ups due to increased power demand (OPR) were retained in the analysis.

The DCO events represent instances where generation was reduced by ONS requirements, necessitating the shutdown of specific generating units. Conversely, OPR events correspond to situations where the plant had to increase its power output, necessitating the start-up of additional turbines.

By applying this methodology, the analysis accurately reflects the number of turbine starts and stops directly associated with grid dispatch needs, eliminating other influencing factors such as maintenance schedules and external grid disturbances. These

refined data provide a solid foundation for comparing fixed-speed operation and variable-speed operation, enabling a more precise assessment of the impact of VSO on reducing turbine cycling.

4.3.2. Determination of the Operation Point in VSO

4.3.2.1. Determining Turbine Power and Net Head (P_r, H_r)

The first step in the implementation of the VSO strategy is the identification of the new operational point (required point) for each generating unit, defined in terms of turbine power (P_r) and net head (H_r). This point must lie within the expanded operational envelope previously established through hill curves and similarity laws, ensuring compliance with mechanical and hydraulic constraints. The selection of the operating point is objective-dependent and varies according to the specific performance goal being pursued:

i. For start-stop minimization, the determination of P_r and H_r is based on the redistribution of power among the generating units, as defined by a dispatch algorithm specifically designed to reduce the number of turbine startups and shutdowns (as shown in Section 4.3.2). This algorithm considers machine availability, operational flexibility under VSO, and the possibility of reallocating load dynamically in real time.

ii. For cavitation minimization, the operating point must be selected with the goal of avoiding flow conditions associated with cavitation-prone regions of the turbine hill chart. Although the algorithm used for dispatch minimization may provide a preliminary power allocation, additional criteria, such as operating away from regions of low pressure and high specific speed, must be incorporated. The final selection of P_r and H_r in this case will depend on the cavitation risk mapping and may be refined using simulations or empirical models that estimate the cavitation index under VSO conditions.

iii. For firm energy enhancement, the selected operating points should aim to increase the plant's energy output during critical periods, as defined by the firm energy calculation methodology. In this context, P_r and H_r may be determined to

maximize energy generation while preserving reservoir levels and avoiding operational extremes. This requires integrating historical inflow series, reservoir storage capacity, and system-wide optimization techniques.

Therefore, although the definition of P_r and H_r follows the same procedural foundation, it must be adapted for each analysis focus. The selected points will serve as inputs for the subsequent steps in the methodology, such as the determination of reduced variables, efficiency calculations, and the application of the universal diagram for dynamic simulations under variable speed operation.

4.3.2.2. Determining Speed and Efficiency (N_r, η_r)

After the power redistribution is enabled by the dispatch algorithm (Section 4.3.2), it generates the point where each machine must operate, that is, the required operating point (P_r, H_r). To determine the new rotational speed (N_r) and efficiency (η_r) for each generating unit, a secondary algorithm uses the homologous points approach, which leverages similarity equations to map the required operating point to an equivalent synchronous speed (N_s) condition while ensuring compliance with the operational limits of the plant. These homologous points (P_h, H_h) serve as operational references that adhere to the known operational boundaries of the plant. This procedure is detailed below (Figure 9).

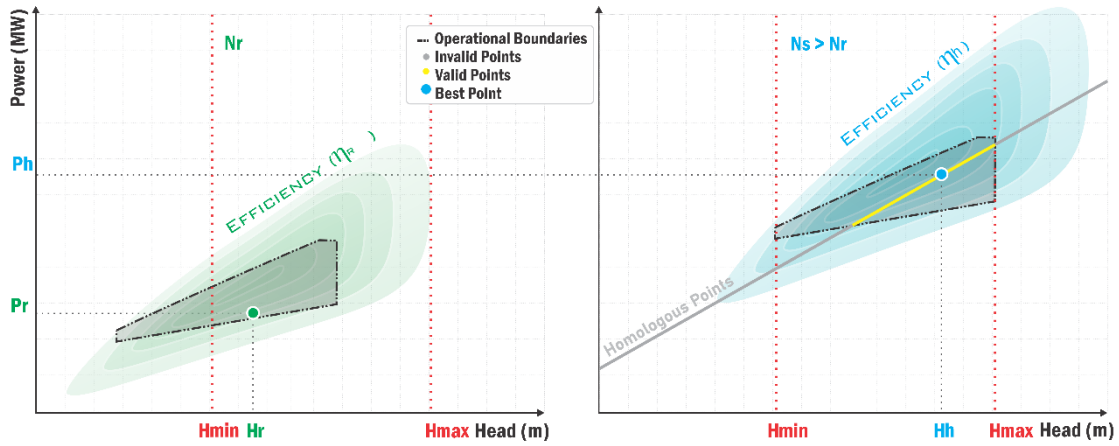

Figure 9 - Homologous points approach.

where Figure 9(a) shows the required operating point (P_r, H_r) determined by the dispatch algorithm at rotational speed N_r and Figure 9(b) highlights the straight line depicting the homologous points at synchronous speed (N_s). The gray points are those that are out of the head and power constraints and hence disregarded. The yellow points correspond to homologous points that satisfy both limits and are thus considered valid options. The blue point is the best operating condition and is taken as the optimal solution. The step-by-step process for this approach is presented as follows:

i. Definition of the Required Operating Point (Input)

The process begins with the input values obtained from the dispatch algorithm: the required power (P_r) and the available net head (H_r). This represents the expected operating point under VSO.

ii. Homologous Points Calculation

Using the similarity equations, a set of homologous points is generated by incrementally varying the rotational speed (N_r) within a predefined range. For each increase in speed, a corresponding homologous point at synchronous speed (N_s) is computed:

$$H_h = H_r.\left(\frac{N_s}{N_r}\right)^2 \qquad (12)$$

$$P_h = P_r.\left(\frac{N_s}{N_r}\right)^3 \qquad (13)$$

At this stage, a collection of homologous points (H_h, P_h, N_r) is generated, representing possible operating conditions at synchronous speed.

iii. Filtering Based on the Net Head and Power Limits

The first filtering stage ensures that only homologous points within the allowable range of the net head for FSO are retained. Because each hydropower plant has a predefined maximum and minimum operational head, any points falling outside this range are discarded. A second filter is applied on the basis of the power constraints. Each head value (H_h) has an associated minimum and maximum allowable power range in FSO. Only the points that satisfy the following conditions are retained:

$$H_{min,N_s} \leq H_h \leq H_{max,N_s} \quad (14)$$

$$P_{min,N_s}(H_h) \leq P_h \leq P_{max,N_s}(H_h) \quad (15)$$

Figure 10 shows this filtering step, in which any points outside the known operational power and head range are removed. If no points remain within the allowable region, the closest homologous point to the permitted boundary is selected as a contingency.

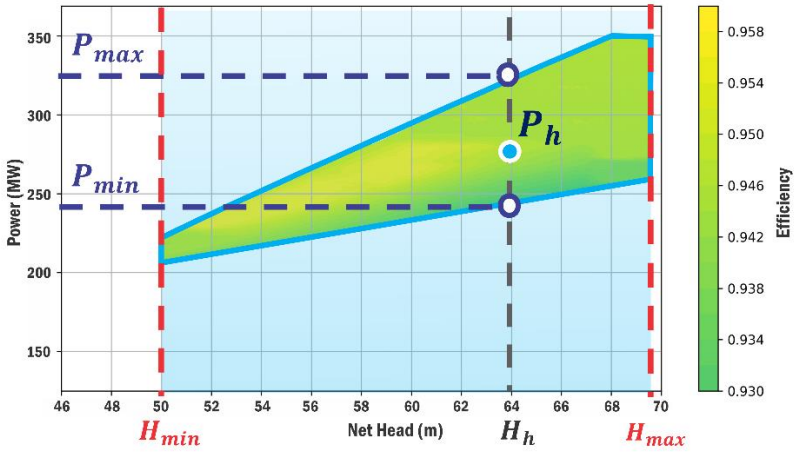

Figure 10 - Filtering based on the net head and power limits.

iv. Selection of the Best Homologous Point (FS)

After the filtering step, the remaining homologous points are within the known operating range of the plant. The efficiency (η_r) of each remaining homologous point is retrieved from the plant's hill curve to select the optimal point:

$$\eta_h = f_{hill,N_s}(P_h, H_h) = \eta_{req} \quad (16)$$

This final step outputs the optimal efficiency (η_r) and the corresponding rotational speed (N_r). These values are then used to define the operational strategy for each generating unit. This approach ensures that units operate at optimal efficiency while adhering to the constraints of VSO.

4.3.2.3. Determining the Flow Rate (Q_r)

Once the P_r, H_r, N_r and η_r have been established through the procedures outlined in the previous sections, the volumetric flow rate (Q) can be determined using the fundamental hydraulic power equation rearranged for Q. This step completes the

characterization of the operating point under variable speed conditions. The flow rate is calculated by:

$$Q_r = \frac{P_r}{\rho . g . H_r . \eta_r} \qquad (17)$$

4.3.3. Dispatch Algorithm to Minimize the Start-Stop Cycle

After the new expanded operating range is defined, a dispatch algorithm is implemented to simulate power redistribution among the generating units (GUs) for each considered scenario. The target is to redistribute power within the updated operating limits presented by VSO to optimize the number of start-stop cycles. Figure 11 presents the logical flow of the dispatch algorithm, which uses a structured and iterative approach as follows.

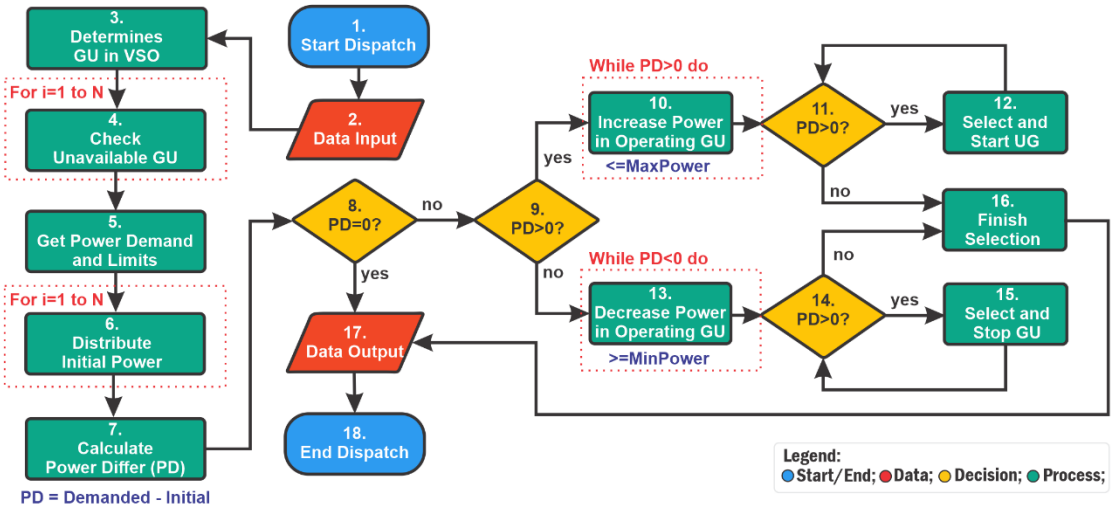

Figure 11 - Dispatch algorithm flowchart.

The algorithm starts by importing data (step 2) with the operational limits (VF and VS) that are previously defined and base hourly operational data, including the total generation demand, the operational status of each GU, and the initial H_N. In step 3, the algorithm determines which units will operate in the FS and VS modes for each scenario. In step 4, the algorithm creates a loop to go through all generating units, ranging from 1 to N, where N is the number of machines in the plant. The algorithm searches the database for the operational status of each generating unit to identify if any machine is unavailable

at that moment. Unavailable units are disregarded in the dispatch, allowing the model to adapt dynamically.

After the operational modes (VS and FS), operational status, and initial H_N are defined, the algorithm searches (step 5) the power demand and the minimum and maximum power limits for each generating unit, ensuring that each unit operates within safe and efficient limits, according to the established hydraulic conditions. In step 6, another loop was defined to pass through all the machines, and for those already in operation, the minimum power was assigned as the initial power to deliver the power that was demanded. In step 7, the power that still needs to be dispatched is calculated through the power difference (PD) between the power demanded and the sum of the minimum powers that were initially assigned. From the PD, it is possible to identify whether adding or removing power will be necessary.

If PD=0 (step 8), the power demand is equal to the power delivered; thus, the algorithm ends the dispatch (steps 17 and 18). For PD>0 (9), the power delivered thus far is less than the power demanded, in which case it is necessary to add power to the generating units. Thus, the algorithm increases the power of the units in operation (step 10), prioritizing the machines in VS mode up to their maximum limits. It is assumed that all the operating machines are already at their maximum limit and that the PD is still greater than zero (step 11). In this case, more power is needed, the algorithm selects and starts an available generating unit (step 12) on the basis of its operational history, giving preference to those in VSO mode (if available) and with fewer start-up events, doing this until the power demand is completely delivered.

On the other hand, if there is a surplus of delivered power (PD<0), the algorithm reduces the power up to the minimum limit of the machines that are operating (step 13); if it is necessary to reduce more power (step 14), it selects a unit to be turned off (step 15), also prioritizing the machines to maintain the balance of shutdowns between them.

When the difference between the power to be dispatched and the sum of the machines' power is zero, the power demand supplied by the plant is distributed among the machines in operation, and the algorithm ends the selection (step 16). The algorithm records the status and power supplied by each unit and generates output data (step 17) for subsequent analysis, including metrics on the frequency of starts and stops and machine utilization. The algorithm is implemented in Python using structured data frames and

dictionaries, which allow systematic tracking of machine states, interpolation of power limits, and intelligent selection of units to be started or stopped.

4.4. CAVITATION MINIMIZATION

The second part of the study evaluates whether VSO)can also be used to mitigate cavitating operation of Francis units. The methodology can be applied to any plant for which a representative turbine hill chart and historical operating data are available. The analysis is based on the hourly operating records of the selected year and on the same hydraulic and efficiency model employed in the energy-gain assessment, but now focusing on the σ–N_s cavitation criterion and on local adjustments in discharge and rotational speed. Regions derived from model-test data and represented in the turbine hill chart are used to define safe and forbidden operating zones; these zones are typically associated with undesired phenomena such as pressure pulsation, low efficiency, noise and vibration. In the present work, however, only cavitation is explicitly evaluated.

i. For each historical operating point, the procedure consists of three main steps:
   detection of cavitating operation using the Thoma cavitation coefficient and the σ–N_s envelope;
ii. generation of alternative operating points by means of the VSO model and the turbine hill chart, exploring admissible variations in discharge and rotational speed; and
iii. selection of the best mitigation strategy among the available options, subject to power-balance constraints and to the operational limits of the units.

4.4.1. Detection of cavitating operating points

The identification of cavitating operation is based on the classical Thoma cavitation coefficient σ and on the analytical–experimental criterion reviewed in [5] for hydraulic turbines. In this approach, acceptable operation is ensured when the absolute pressure at the runner outlet does not fall below an experimentally established limit. Using operational, geometrical and design data, the Thoma coefficient σ is computed for each

historical operating record and compared with a critical value (σ_c). Cavitation is assumed to occur whenever σ falls below this limit.

The definition of levels and geometric elevations follows the convention shown in Figure 12 (adapted from [6]), which depicts the reference elevations for a hydraulic turbine and the main quantities used in the suction-side energy balance.

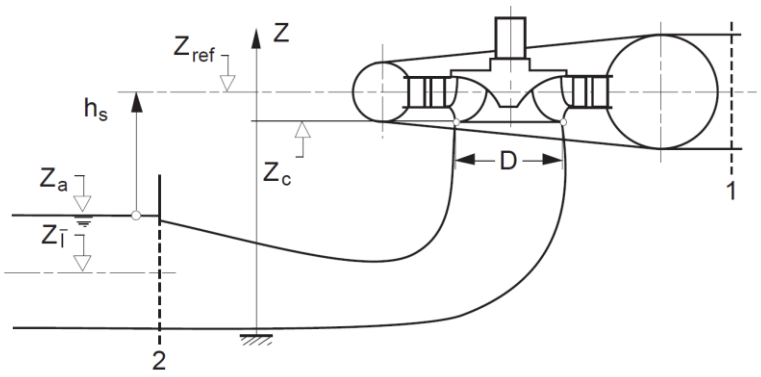

Figure 12 - Definition of the set of levels for a hydraulic turbine.

The suction-side energy available at the runner outlet is expressed as:

$$\text{NPSE} = \frac{p_2}{\rho g} + Z_2 + \frac{C_2^2}{2g} - \frac{p_v}{\rho g} - Z_{\text{ref}}, \qquad (18)$$

where p_2 is the absolute pressure at the runner outlet, $Z_2$is the elevation of the measurement section, $C_2$is the local velocity, $p_v$is the vapour pressure and $Z_{\text{ref}}$is the reference elevation of the tailrace. The specific energy at the runner inlet is given by $E = gH_{\text{N}}$. The Thoma coefficient is then:

$$\sigma = \frac{\text{NPSE}}{E} \qquad (19)$$

and the corresponding specific speed is calculated as:

$$N_s = N\frac{\sqrt{Q}}{H_N^{3/4}} \qquad (20)$$

where N is the rotational speed and Q the discharge.

To classify each operating point, the pair (σ, N_s) is compared with an empirical cavitation envelope obtained from Arndt's diagram, fitted as lower and upper bounds $\sigma_{\text{low}}(N_s)$ and $\sigma_{\text{up}}(N_s)$ by power-law relations: $\sigma_{\text{low}}(N_s) = 10^{b_\ell} N_s^{a_\ell}$, $\sigma_{\text{up}}(N_s) = 10^{b_u} N_s^{a_u}$

Points with $\sigma < \sigma_{\text{low}}(N_s)$ are classified as **cavitating**, points with $\sigma > \sigma_{\text{up}}(N_s)$ as **safe**, and the intermediate band as a transition region with light or intermittent cavitation.

4.4.2. Variable-speed homology model

The mitigation procedure relies on the same universal hill chart and similarity relations used in this study (see Section 3.2.), now employed to generate alternative operating points in the neighborhood of each cavitating record. For a given H_N and target active power P_t, the hill chart η(H,P) provides the corresponding efficiency and discharge at synchronous speed.

When the rotational speed is changed from the synchronous value N_s to a candidate speed N, the corresponding homologous point (H_h, P_h)on the chart is obtained from the classical affinity laws (12) and (13). From (H_h, P_h) the interpolated efficiency η_h is retrieved, and the physical discharge at the actual head is reconstructed by enforcing power balance:

$$P_t = \rho g Q_{new} H_N \eta_h \qquad (21)$$

This homology step ensures that each candidate (Q_{new}, N) is dynamically consistent with the manufacturer's chart and with the net head of the hour under analysis.

4.4.3. Definition of feasible candidates

For every cavitating historical point, the algorithm generates a set of candidate operating points through controlled variations in discharge $Q$and/or rotational speed N. A candidate is considered feasible if it simultaneously satisfies:

- *Cavitation constraint:* $\sigma_{new} \geq \sigma_{low}(N_{s,new})$, the new point lies outside the cavitating region in the σ–Ns plane.
- *Power-balance constraint:* the active power remains within a tolerance band around the original value, $| P_{new} - P_0 | \leq \Delta P_{max}$, so that the remaining units in the plant can compensate the deviation without violating the daily generation schedule.
- *Operational limits:* all candidates must respect the admissible H-Q envelope, guide-vane travel limits and the allowable VSO range defined in Section 6.1.1.

If no feasible candidate is found, the original historical point is kept and counted as residual cavitating operation.

4.4.4. Cavitation-mitigation strategies

To explore different combinations of control actions, five mitigation strategies are defined. They differ in the sequence and degree of discharge and speed adjustments, but all of them use the same feasibility criteria described above.

4.4.4.1. Q-only strategy (Q)

The rotational speed is kept fixed at synchronous value. The discharge is varied in a one-dimensional search around the historical value Q_0, following the actual dispatch trajectories to preserve realistic operating patterns. For each trial discharge, the corresponding power is obtained from the hill chart, and only candidates within the power tolerance are retained. Among all successful candidates, the one with minimum absolute discharge deviation $| \Delta Q | = | Q_{\text{new}} - Q_0 |$ is selected.

4.4.4.2. N-only strategy (N)

The discharge is initially kept equal to the historical value and the speed is varied within the admissible VSO range. For each candidate speed, the homology model is used to reconstruct $Q_{\text{new}}$and verify cavitation and power constraints. The selected point is the one with the smallest speed deviation $| \Delta N | = | N - N_{\text{s}} |$.

4.4.4.3. Sequential N→Q strategy (NQ)

This strategy first applies the N-only procedure to move the operating point towards the safe region through a speed change, obtaining an intermediate point with discharge Q_{h}. A local refinement in discharge is then performed around Q_{h}(Q-only step) to further increase the safety margin or reduce the power error. The final candidate is chosen by minimising a scalar cost function that combines both adjustments;

$$J = w_Q \, | \Delta Q | + w_N \, | \Delta N | \qquad (22)$$

with weights w_Q and w_N set to reflect the relative difficulty of modifying discharge or speed.

4.4.4.4. Sequential Q→N strategy (QN)

In this case, the algorithm first executes the Q-only search to guarantee consistency with power and discharge limits, obtaining an intermediate point with modified discharge. Starting from this point, a secondary N-only search is carried out, using the homology model to adjust speed and reconstruct the new discharge. The same cost function J is used to select the best candidate.

4.4.4.5. Best-of-all strategy (OPT)

For each cavitating hour, all four previous strategies are executed (whenever they produce feasible candidates). The resulting candidates are compared according to the following hierarchy:

1. Preference is given to solutions that eliminate cavitation (σ above the safe boundary);
2. Among these, the candidate with the lowest cost J is selected;
3. In case of ties, the solution with the largest safety margin in σ and Ns is chosen.

The OPT strategy thus defines an optimal operating envelope in the σ–Ns plane, combining the most effective combination of discharge and speed adjustments for each operating condition.

4.4.5 Performance indicators

Finally, the impact of each strategy is quantified by comparing the number of cavitating hours before and after the mitigation procedure, as well as the residual share of operating points falling in the transition band of the σ–Ns diagram. For the selected tolerance $\Delta P_{\max}$, the percentage reduction in cavitating hours is computed for the Q, N, NQ, QN and OPT strategies, allowing a direct comparison of their effectiveness and of

the incremental benefit brought by VSO when combined with modest adjustments in discharge.

4.5. INCREASING THE ENERGY GENERATION

4.5.1. Introduction

This section presents a generic methodology to quantify the additional energy that can be obtained when one or more generating units of an existing hydropower plant are converted from fixed-speed to variable-speed operation. The procedure is formulated in a plant-independent way and can be applied to any site for which turbine hill charts and a sufficiently long historical operating record are available. The real hourly operation of the plant is used as a reference trajectory, and for each time step the method evaluates how much extra power could be produced with exactly the same water usage, by exploiting the interaction between net head, discharge and turbine efficiency on the hill chart.

The central idea is to keep the discharge fixed, either at unit level or at plant level, and use VSO to move the operating point to a more efficient region of the turbine performance surface. For each historical operating point, similarity relations are applied to identify a homologous VS condition with higher efficiency, this improved efficiency is then used to recompute the turbine and generator powers, so that any energy gain is obtained without increasing the total volume of water turbined over the period. When appropriate, the same framework can be combined with an additional optimization layer in which the total plant discharge prescribed by the system operator (e.g. ONS) is kept equal to the historical value, but its distribution among the available units is reallocated under variable speed in order to maximize the instantaneous electrical power. In both cases, the turbine hill chart remains the common reference for fixed-speed and variable-speed operation, what changes is the selection of the operating point on this chart and, when optimization is activated, the way the fixed total discharge is shared among units.

4.5.2. VSO for Energy Gain

The estimation of additional energy under VSO is based on a point-wise simulation of each generating unit along the historical time series. For every hour t and for every unit j that is in operation, the method reconstructs a consistent operating triplet (H_0, Q_0, η_0) and the corresponding electrical power $P_{g,0}$ from the measured plant data. The gross head $H_B(t)$, the net head $H_N(t)$ (or the variables required to compute it), the unit discharge $Q_j(t)$, and the active power at generator terminals are used as primary inputs. When efficiency is not directly measured, the turbine efficiency η_0 associated with the historical operating point (H_0, Q_0) is obtained from the hill chart interpolator $\eta(H, Q)$, and can be cross-checked against manufacturer data or calibrated efficiency curves.

Turbine performance is represented by hill charts that relate efficiency to net head and either discharge or power. Manufacturer data, originally provided as discrete points and contour lines in (H, Q) and (H, P) planes, are digitized and converted into numerical tables. In a pre-processing stage, these scattered points (H_i, Y_i, η_i), where Ydenotes either discharge Q or mechanical power P, are mapped onto a regular grid using a combination of linear interpolation, nearest-neighbour extrapolation and inverse-distance weighting to fill possible gaps in the domain. This yields two continuous surfaces:

$$\eta_Q = \mathrm{f}_{hill,\mathrm{N_s}}(\mathrm{Q}, \mathrm{H}) \qquad (23)$$

$$\eta_P = \mathrm{f}_{hill,\mathrm{N_s}}(P, \mathrm{H}) \qquad (24)$$

Implemented as two-dimensional interpolating functions. The resulting efficiencies are clipped to a physically meaningful interval $[\eta_{\min}, \eta_{\max}]$to avoid artefacts near the boundaries of the chart. The surface $\eta_Q(H, Q)$is used to evaluate the efficiency associated with any admissible pair (H, Q), whereas $\eta_P(H, P)$ is later employed to convert head-dependent power limits into equivalent discharge limits.

For units allowed to operate in variable speed, the efficiency used to recompute power is not restricted to the original historical point (H_0, Q_0). Instead, the method exploits the similarity relations introduced in Section 3.2, which link discharge, head and power to rotational speed for turbines with the same runner diameter. Starting from the original point, a similarity line is constructed on the hill chart: for each admissible head value $H_h$within the valid range of the chart, the corresponding discharge $Q_h$is obtained from the similarity relation.

$$Q_{\mathrm{h}} = Q_o \cdot \sqrt{\frac{H_h}{H_o}} \qquad (25)$$

Which is consistent with the affinity laws presented in (4)-(8) under constant runner diameter. Candidates (H_h, Q_h) that lead to non-positive discharge or fall outside the support of the hill chart are discarded. Along this similarity line, turbine efficiency is evaluated using the interpolator (23) producing a set of candidate values $\eta(H_h, Q_h)$.

The best homologous point is defined as the point on the similarity line that maximizes efficiency:

$$\eta_{best} = \max_{\eta}(H_{\mathrm{h}}, Q_{\mathrm{h}}) \qquad (26)$$

If η_{best} exceeds the original efficiency η_0 by more than a small numerical tolerance, the corresponding homologous point is accepted as an improved operating condition for that unit. Otherwise, the historical condition is retained. The associated VS rotational speed N_{VSO} is derived from the affinity relation between discharge and speed.

$$N_{VSO} = N_{\mathrm{s}} \frac{Q_o}{Q_h^*} \qquad (27)$$

Were Q_h^* is the discharge of the selected homologous point and N_{s} is the synchronous speed of the original machine. In the present framework, the net head and discharge used in the power equation remain equal to the historical values H_0 and Q_0. The similarity search is therefore employed as a *lookup mechanism* on the manufacturer hill chart: it identifies the efficiency that would be achievable under an equivalent, more favorable operating condition, and this improved efficiency η_{best} is then used to recompute turbine and generator powers for the actual head and discharge observed in the time series. For units that remain in FSO, the similarity search is bypassed and the efficiency is simply evaluated as $\eta_Q(H_0, Q_0)$, with rotational speed fixed at N_{s}.

The mechanical power on the turbine shaft is calculated by equation (8) where η_{ti} is either the original efficiency η_0 or the improved value η_{best}, and ρg is the specific weight of water. The corresponding electrical power is obtained by multiplying by the downstream electro-mechanical efficiency. For fixed-speed units, only generator efficiency is considered.

$$P_{g,new} = P_{t,new} \cdot \eta_{gen} \qquad (28)$$

The algorithm is applied independently to each unit and each hour of the historical series, producing a new time series of powers $P_{g,\text{new}}(t)$ under VSO, while preserving the original water usage.

4.5.3. VSO with Original Dispatch Strategy

In the first energy-gain scenario, VSO is applied without modifying the historical distribution of flow among units. The objective is to quantify how much additional energy can be obtained solely by adjusting the rotational speed of the converted units, exploiting the efficiency gains available on the hill chart, while preserving the original unit discharges and the original set of units that are in service at each hour.

For each generating unit j and each time step t, the historical discharge $Q_{j,0}(t)$ and net head $H_{N,j}(t)$ are treated as fixed inputs. The configuration of the plant with respect to VSO is represented by a binary flag c_j, where $c_j = 1$ indicates that unit j has been converted to VSO and $c_j = 0$ indicates that it remains in FS mode. This framework allows the same methodology to be applied to *partial conversion* (only a subset of units with $c_j = 1$) and *full conversion* (all units with $c_j = 1$).

For units that remain in FSO ($c_j = 0$), the turbine efficiency is evaluated directly on the hill chart as $\eta_{j,\text{FSO}}(t) = \eta_Q(H_{N,j}(t), Q_{j,0}(t))$, the rotational speed is kept at synchronous speed, and the turbine and generator powers are recomputed using the adopted electromechanical chain efficiency. For units that operate under variable speed ($c_j = 1$), the similarity-based search described in Section 4.5.2 is invoked along the line of homologous points associated with the historical operating condition $(H_{N,j}(t), Q_{j,0}(t), \eta_{j,0}(t))$.

This search identifies the candidate point $\left(H^*_{h,j}(t), Q^*_{h,j}(t), \eta_{j,\text{best}}(t)\right)$ on the hill chart that maximizes efficiency while respecting the chart domain and similarity constraints. If $\eta_{j,\text{best}}(t)$ exceeds the original efficiency $\eta_{j,0}(t)$ by more than a small tolerance, the turbine and generator powers are updated using $\eta_{j,\text{best}}(t)$ and the corresponding variable-speed rotational speed ($n_{j,\text{VSO}}(t)$) obtained from the similarity relations; otherwise, the historical efficiency and synchronous speed are retained.

In this scenario, neither the plant-level total discharge nor its allocation among units is altered. For each unit and each time step, $Q_{j,\text{new}}(t) = Q_{j,0}(t)$, and units that were historically out of service at time $t$remain disconnected ($Q_{j,\text{new}}(t) = 0$). The total discharge therefore satisfies:

$$Q_{\text{tot,new}}(t) = \sum_j Q_{j,\text{new}}(t) = \sum_j Q_{j,0}(t) = Q_{\text{tot},0}(t) \qquad (29)$$

Ensuring strict conservation of water at both unit and plant level. The only degrees of freedom are the efficiency and rotational speed of the units configured for VSO.

The total electrical power at each hour is obtained by summing the updated unit powers:

$$P_{g,\text{tot,new}}(t) = \sum_j P_{g,j,\text{new}}(t), \qquad (30)$$

And is compared to the historical total power $P_{g,\text{tot},0}(t)$. To avoid spurious numerical degradations, a safeguard is implemented: whenever the VSO-based calculation yields:

$$P_{g,\text{tot,new}}(t) < P_{g,\text{tot},0}(t) - \varepsilon_P \qquad (31)$$

With ε_Pa small tolerance, the original fixed-speed powers are retained for that hour. In this way, the scenario provides a conservative estimate of the energy benefit achievable by variable-speed operation alone.

The simulation is repeated for different conversion configurations $\{c_j\}$, ranging from partial conversion (only a subset of machines equipped with variable speed drives) to full conversion (all units converted). The resulting energy gains for each configuration will later serve as inputs to the economic and financial assessment of VSO implementation.

4.5.4. VSO with Optimized Flow Allocation

The second scenario exploits not only the additional flexibility provided by VSO, but also the freedom to redistribute the total plant discharge among the available units, while still preserving the historical water usage at plant level. The objective is to determine, for each hour, the combination of unit discharges that maximizes the total

electrical power under the extended operating ranges enabled by VSO, subject to the mechanical and hydraulic limits of each unit and to the chosen conversion configuration (partial or full).

For a given time step t, the gross head $H_B(t)$ and the historical unit discharges $Q_{j,0}(t)$ are used to compute the historical total discharge:

$$Q_{\text{tot},0}(t) = \sum_j Q_{j,0}(t), \qquad (32)$$

Which is treated as an invariant in the optimization problem:

$$Q_{\text{tot,new}}(t) = \sum_j Q_{j,\text{new}}(t) = Q_{\text{tot},0}(t) \qquad (33)$$

Units that were historically unavailable at time t remain unavailable and are enforced to have $Q_{j,\text{new}}(t) = 0$. For each unit, a simple quadratic loss model, previously calibrated in the hydraulic modelling stage, is employed to approximate the net head as a function of unit discharge in (3), with k obtained from hydraulic calibration and H_N bounded to the valid head range of the hill chart. The operating limits of each unit are expressed in terms of minimum and maximum admissible power as a function of net head, based on manufacturer information in the (H, P) plane. These power limits $P_{\min}(H_N)$ and $P_{\max}(H_N)$ are converted into equivalent discharge limits $[Q_{\min,j}(H_{N,j}), Q_{\max,j}(H_{N,j})]$ by means of the interpolator $\eta_P(H, P)$, ensuring consistency between the hill chart and the operational envelopes:

$$Q_{\min,j}(H_{N,j}) \leq Q_{j,\text{new}}(t) \leq Q_{\max,j}(H_{N,j}) \qquad (34)$$

Under these assumptions, the hourly optimization problem can be stated conceptually as:

- **Given:** gross head $H_B(t)$, total discharge $Q_{\text{tot},0}(t)$, unit availability, and the VSO/FSO status c_j of each unit;
- **Find:** a set of unit discharges $\{Q_{j,\text{new}}(t)\}$such that:
  - discharge conservation is respected:
  - each unit operates within its admissible region:

    $$Q_{\min,j}(H_{N,j}(t)) \leq Q_{j,\text{new}}(t) \leq Q_{\max,j}(H_{N,j}(t)), \qquad (35)$$

  - and the total electrical power is maximized:

$$P_{g,\text{tot,new}}(t) = \sum_j P_{g,j,\text{new}}(t) \text{ is maximal.} \quad (36)$$

And the corresponding net heads $H_{N,1}(t)$ and $H_{N,2}(t)$ are computed using the loss model. Candidate pairs that violate the discharge limits of any unit are discarded. For the remaining feasible candidates, each unit is evaluated with the hill chart:

- If $c_j = 1$(unit converted to VSO), the similarity-based procedure is applied as in Section 4.5.2 to obtain an improved efficiency $\eta_{j,\text{VSO}}(t)$ and rotational speed $n_{j,\text{VSO}}(t)$;
- If $c_j = 0$ (unit kept in FSO), the efficiency is evaluated directly at synchronous speed as $\eta_{j,\text{FSO}}(t) = \eta_Q(H_{N,j}(t),\ Q_{j,\text{new}}(t))$, with fixed rotational speed n_s.

The corresponding turbine and generator powers $P_{g,j,\text{new}}(t)$ are then computed for each candidate, and the combination $\{Q_{j,\text{new}}(t)\}$ that maximizes $P_{g,\text{tot,new}}(t)$ is selected as the optimal solution for that hour. As in the previous scenario, a safeguard is applied at plant level: if the optimized configuration leads to:

$$P_{g,\text{tot,new}}(t) < P_{g,\text{tot,0}}(t) - \varepsilon_P, \quad (37)$$

The historical fixed-speed powers are retained for that time step, ensuring that the estimated benefit of VSO plus optimized flow allocation is conservative.

By changing the conversion vector $\{c_j\}$, the same optimization engine can be used to analyze partial conversion, where only a subset of units is equipped for VSO, and full conversion, where all units operate under VSO. The comparison of energy gains between these configurations, obtained through the aggregation procedure in Section 4.5.5, provides a direct quantitative basis for subsequent financial analyses of different VSO implementation strategies.

4.5.5. Energy Aggregation and Performance Indicators

Once the hourly simulation under VSO has been completed for all units and all time steps, the resulting power time series are aggregated into energy-based indicators. For each scenario and for each hour t, the methodology provides (i) the historical total electrical power $P_{g,\text{tot,0}}(t)$ under FSO and (ii) the corresponding total electrical power $P_{g,\text{tot,new}}(t)$ obtained with VSO, with or without optimized flow allocation. Assuming a

constant time step Δt (1 h in this study), the total energies over the analysis horizon $\mathcal{T}$ are computed by numerical integration of the power curves:

$$E_{\text{orig}} = \sum_{t \in \mathcal{T}} P_{g,\text{tot},0}(t)\,\Delta t, E_{\text{new}} = \sum_{t \in \mathcal{T}} P_{g,\text{tot,new}}(t)\,\Delta t, \qquad (38)$$

With energies usually expressed in MWh or GWh. The global energy gain attributable to variable-speed operation is then given by:

$$\Delta E = E_{\text{new}} - E_{\text{orig}}, \qquad \Delta E_{\%} = 100\,\frac{\Delta E}{E_{\text{orig}}} \qquad (39)$$

These metrics provide a compact measure of the cumulative benefit of VSO over the entire simulation period, while ensuring that the comparison is carried out under identical water usage, as both scenarios preserve the historical discharge time series at unit or plant level.

In addition to the plant-wide indicators, the methodology computes energy contributions and gains at unit level. For each generating unit j, the historical and VSO-based energies are calculated as:

$$E_{j,\text{orig}} = \sum_{t \in \mathcal{T}} P_{g,j,0}(t)\,\Delta t, E_{j,\text{new}} = \sum_{t \in \mathcal{T}} P_{g,j,\text{new}}(t)\,\Delta t, \qquad (40)$$

With the corresponding energy gain $\Delta E_j = E_{j,\text{new}} - E_{j,\text{orig}}$. This decomposition makes it possible to identify which units benefit the most from VSO and how the gains are distributed among machines with different operating roles (base-loading versus peaking units). To characterize the temporal distribution of the gains, additional performance indicators are derived from the hourly power differences:

$$\Delta P_g(t) = P_{g,\text{tot,new}}(t) - P_{g,\text{tot},0}(t). \qquad (41)$$

The number of hours with positive gain, N_{gain}, is obtained by counting the time steps for which $\Delta P_g(t)$ exceeds a small numerical tolerance. The methodology also records the maximum instantaneous power gain, the distribution of $\Delta P_g(t)$ over the year (or over specific hydrological seasons), and the frequency with which the similarity-based efficiency improvement is effectively used in each unit. When Scenario 2 (VSO + optimized flow allocation) is activated, the same indicators are computed, allowing a direct comparison between the gains achieved by VSO alone and those obtained when VSO is combined with an optimized redistribution of discharge. Together, these energy

and performance indicators provide a comprehensive quantitative basis to assess the potential of VSO to enhance the annual energy production of existing hydropower plants.

5. CASES STUDY

5.1. TUCURUÍ HYDROPOWER PLANT

5.1.1. Overview Of Plant

The Tucuruí Hydropower Plant (THP) is one of the largest hydropower plants in the world and serves as a cornerstone in the country's energy matrix. The plant site is located in Tucuruí, Brazil, at approximately 3.79°S, 49.64°W, on the Tocantins River. The total installed capacity is 8,535 MW, comprising 25 generating units. Powerhouse I (CFI) consists of 12 turbines, each with a capacity of 350 MW. In contrast, Powerhouse II (CFII) has 11 turbines, each with a capacity of 390 MW, and two additional generator auxiliaries (GA) of 22.5 MW each. Given this large installed capacity, the THP plays a crucial role within the Brazilian National Interconnected System (SIN) as a vital contributor to the country's electricity supply. Figure 13 provides an aerial view of the THP. The structural magnitude and configuration of the THP justify the application of the proposed methodology for partial or total retrofitting to VSO.

Figure 13 – Tucuruí Hydropower Plant on the Tocantins River.

5.1.2. THP and the Renewable Generation in Brazil

According to national and international evaluations, large-scale hydropower facilities such as THPs are essential for balancing intermittent sources such as solar and wind in Brazil's energy grid [10,11,79]. This plant has great potential but some major operational challenges, especially with the increasing share of renewable energy sources in the grid, as shown in Figure 14. This figure shows the total generation from all hydropower plants, the combined generation from wind and solar sources, and the specific contribution of the THP. The graph highlights the growing share of variable renewable energy in the national grid and the relative importance of Tucuruí in this context.

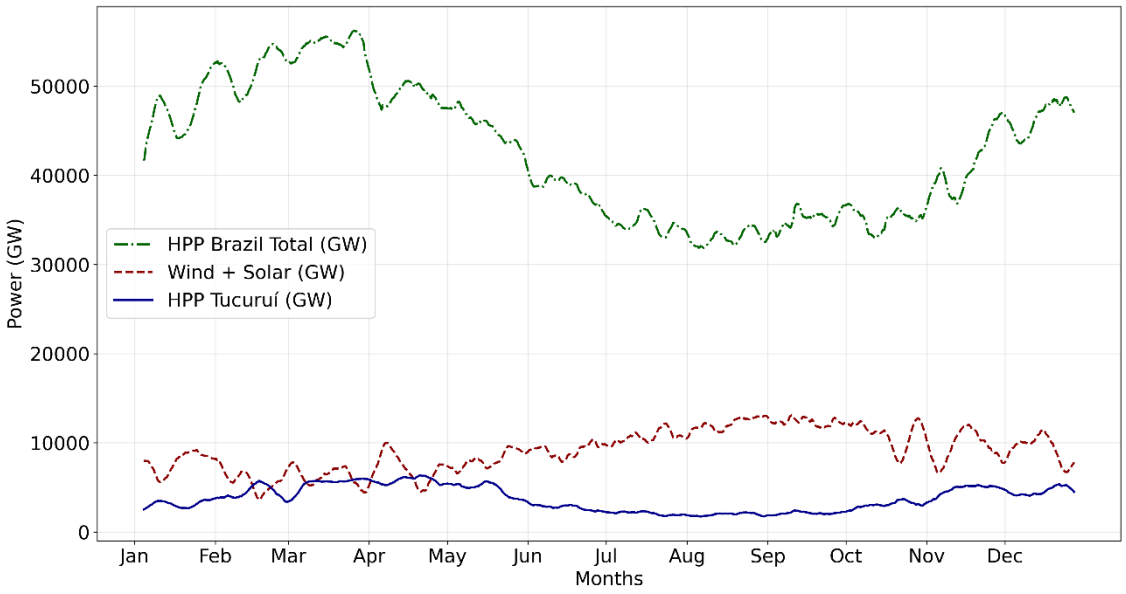

Figure 14 - Comparison of Wind and Solar Power Generation with THP.

The plant is based on FS turbines, which creates a limitation for the plant to manage the grid that is constantly changing. Consequently, the generating units have been operating at more frequent starts and stops, resulting in increased mechanical stress and subsequently reduced equipment life, as well as increased maintenance costs.

5.1.3. Hill Curves THP

Hill charts which represent the efficiency of the generating units across different head and flow conditions are shown in Figure 15 and Figure 16. In addition, these charts

show the limits within which the machines can operate, aiming to avoid major problems like cavitation and other constraints.

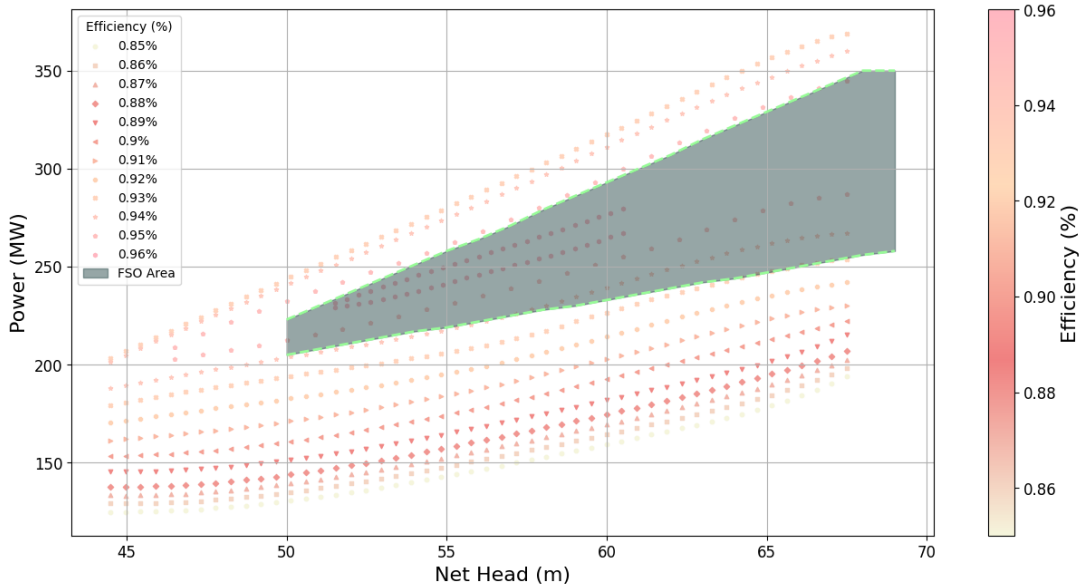

Figure 15 - Hill Chart with Operation Range: CFI.

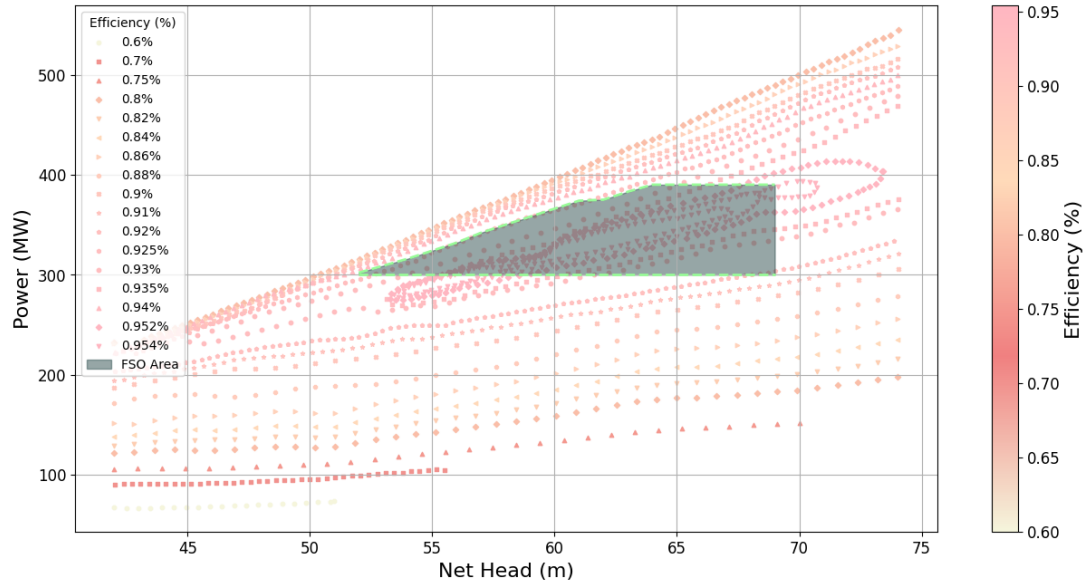

Figure 16 - Hill Chart With Operation Range : CFII.

These images summarize the current operational limits for the units of THP Tucuruí, CFI and CFII respectively, and provide a clear view of the operational boundaries for the generating units of hydropower plant. Understanding these limits is crucial for evaluating how variable speed operation can be used to expand the operational range and improve plant performance.

Figure 17 shows the interpolated hill curves, as described in Section 4.1. Figure 17(a) corresponds to the CFI turbines, and Figure 17(b) refers to the CFII turbines. These maps highlight the best-performing regions where efficiency reaches its peak values and the operational margins.

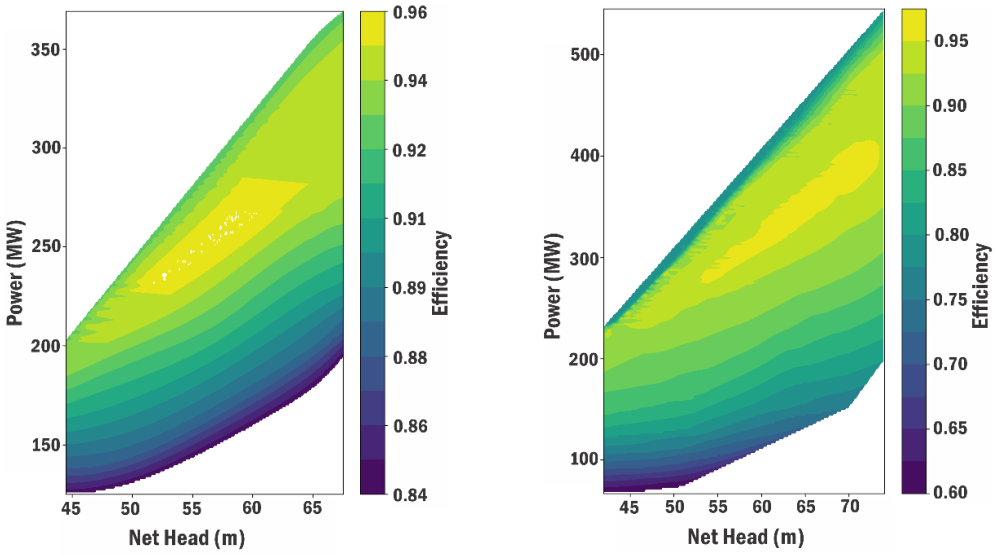

(a) *(b)*

Figure 17 - Hill Curve THP: (a) CFI units. (b) CFII units.

5.1.4. Universal Diagram

The equations (9), (10) and (11) were used to create the universal diagram. Where the turbine rotor diameters, obtained from Eletrobras Eletronorte, were used in the calculations and are as follows:

$$D_{CFI} = 8004\ mm\ (\ D\ for\ CFI)$$

$$D_{CFII} = 8277\ mm\ (\ D\ for\ CFII)$$

Using these equations, two universal diagrams were constructed: $n_{ED}\ x\ Q_{ED}$ and $n_{ED}\ x\ P_{ED}$, for the generating units of the THP. These diagrams provide a detailed visualization of the performance characteristics of the turbines under fixed-speed operation.

Figure 18 and Figure 19 present the universal diagrams for the CFI and CFII units, respectively. These diagrams highlight the operational limitations and performance trends under fixed-speed conditions, forming the basis for evaluating the potential benefits of variable speed operation.

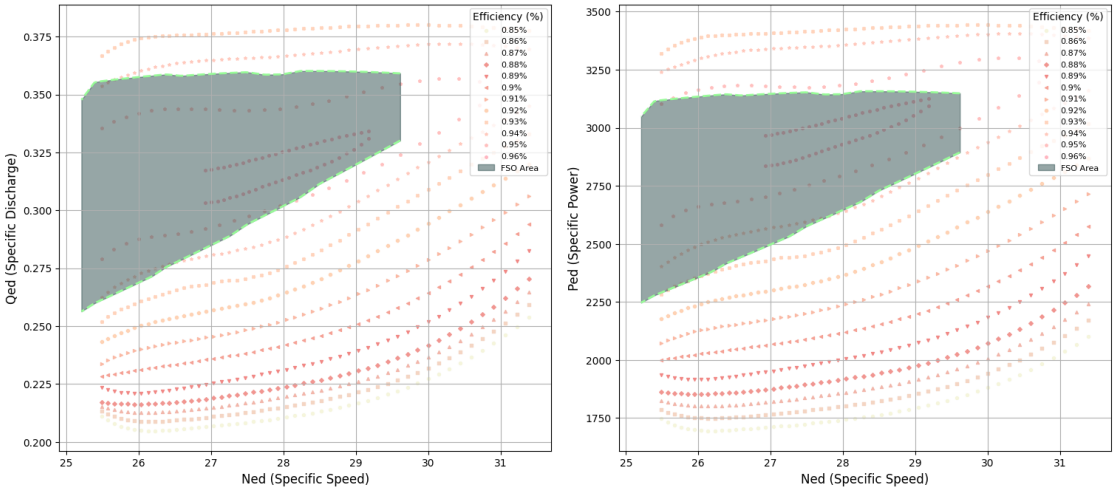

Figure 18 - Universal Diagram with Operation Range: CFI.

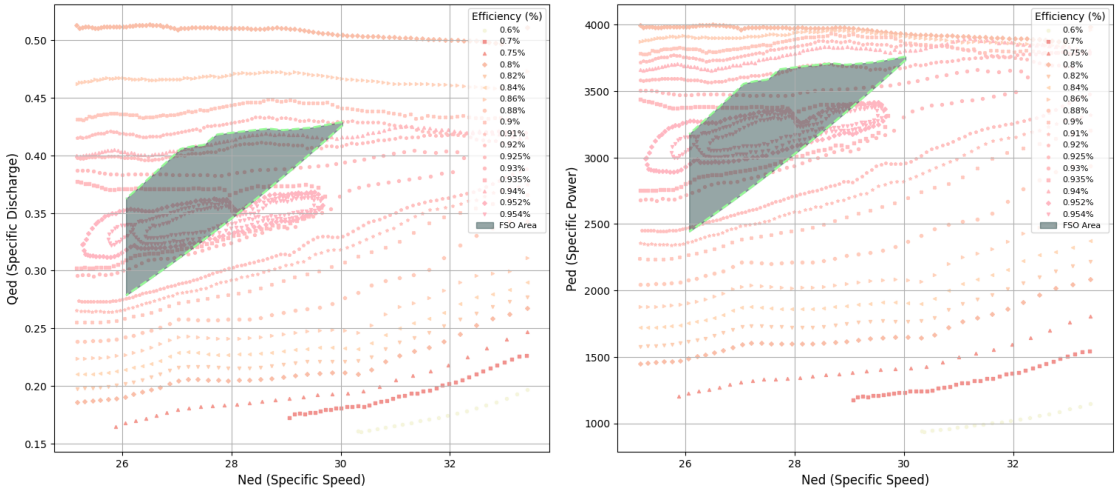

Figure 19 - Universal Diagram with Operation Range: CFII.

5.1.5. Typical Operation

Furthermore, the data from the 2021 flow provide insight into the valuable behavior of hydrology and the operational challenges of the THP. Figure 20 summarizes this hydrology and operating conditions using the influent (blue), turbinated (green) flows, and the dashed red line shows the gross head. A clear seasonal pattern is observed, with peak inflows from March to May, when the plant operates at higher turbine discharge to meet demand while managing reservoir levels. From July to November, inflows are much lower, and generation relies more on storage, which is reflected in reduced turbine discharge.

The gross head varies approximately from 53 m to 69.5 m over the year, tracking the balance between inflows, releases, and storage. Spill occurs only during brief wet-season episodes; otherwise, the spilled flow is zero (not shown). This annual flow behavior further indicates the need for operational flexibility to adjust to the vagaries of hydrological conditions.

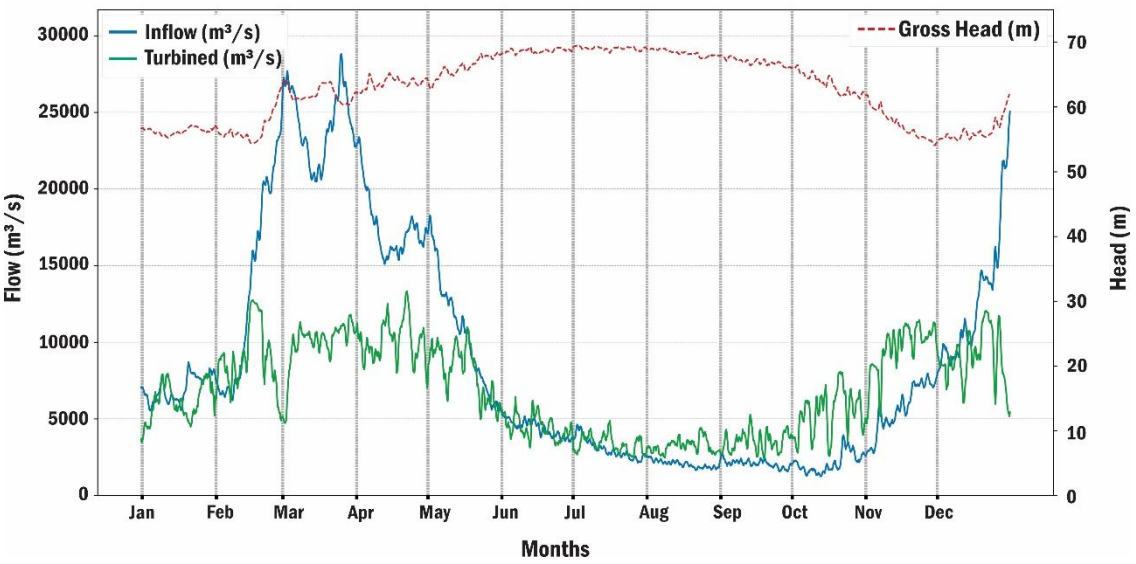

Figure 20 - Flow and the gross head throughout 2021 (THP).

The case study utilized a highly comprehensive, real-time operational dataset monitored during 2021 at the THP. The dataset represents one of the actual 365 days of the whole operation, depicting actual plant behavior, including turbine status, current generation, and other significant operational factors. The same dataset will be referred to later to determine the effects of VSO, in which case it simulates how the plant would have worked under VSO conditions. The simulation results will be directly contrasted with the real 2021 dataset, which operates under FSO conditions to explain the differences in performance, efficiency, and operational flexibility between the two modes.

For this case, the H_N was not directly available in the dataset and had to be determined through an iterative computational process. This calculation was performed for every operational point in the dataset using the methodology presented in Section 4.1, which is illustrated in Figure 4. The iterative approach enabled accurate reconstruction of the net head by accounting for hydraulic losses, represented by the coefficient *k*, which

varies depending on the type of turbine. The k-values regarding the calculations themselves originated from the source [80] and are defined as follows:

$$k_{CFI} = 3.5878130298969 \text{ x } 10^{-6} \text{ (} k \text{ for } CFI\text{)}$$

$$k_{CFII} = 2.0841481394822 \text{ x } 10^{-6} \text{ (} k \text{ for } CFII\text{)}$$

This method was essential to accurately reconstruct the operational conditions of the plant, ensuring that the net head values used in subsequent analyses reflect the actual hydraulic behavior of the turbines. Because of this, we were able to accurately analyze the operational limits and ensure the validity of the simulations for both FSO and the expanded operational range under VSO. Figure 21 illustrates all operational points recorded in this data set for the FSO, using the previously calculated H_N.

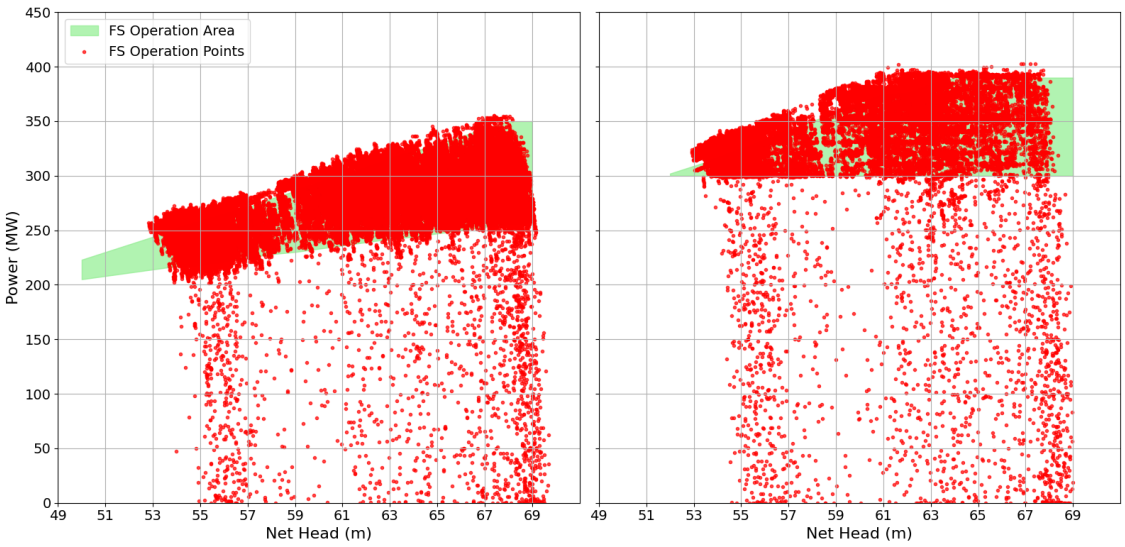

Figure 21 – All operationg points which was recorded in 2021 (THP): H x P.

It is worth noting that the dataset includes transition points that occur during work when a turbine is starting or stopping. Such transition points would exhibit sudden power variations as the machinery would shift from one operating state to another. Hence, to ensure the accuracy and reliability of the operational data used in this study, a filtering process was implemented to identify and remove transition points. These points correspond to unstable operating conditions, which typically occur during the startup and shutdown phases of generating units. Since these transient states do not represent steady operational performance, their presence in the dataset could distort analyses related to efficiency, power redistribution, and the benefits of VSO.

The logic used for detecting and eliminating these transition points is illustrated in Figure 22. This flowchart outlines the step-by-step process, from data loading to the identification and removal of unstable points based on real and maximum allowable flow rates. By applying this systematic approach, only stable operational points remain in the dataset, ensuring a more accurate assessment of power plant performance.

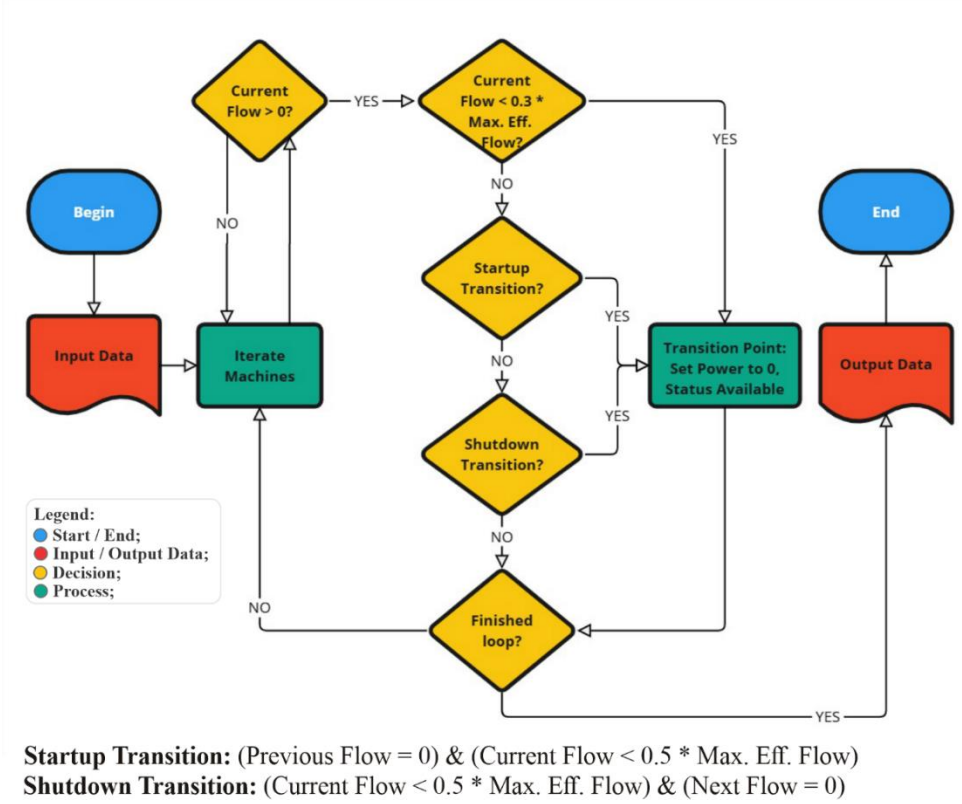

Figure 22 - Flowchart of the Transition Points Removal Process.

This flowchart illustrates the logical process used to identify and eliminate transition points (startup and shutdown phases) from the dataset. The methodology involves checking flow generation levels, interpolating turbine efficiency, and calculating real and maximum allowable flow (previous, current and next). By applying predefined thresholds, unstable operational points are detected and removed, ensuring that only steady-state operation data is retained for further analysis.

After implementing this filtering process, the dataset was updated, and a new visualization of the operational points was generated. Figure 23 presents the refined dataset, highlighting the stable operational points after the removal of transition states.

The results of this calculation serve as the foundation for all subsequent operational analyses and simulations.

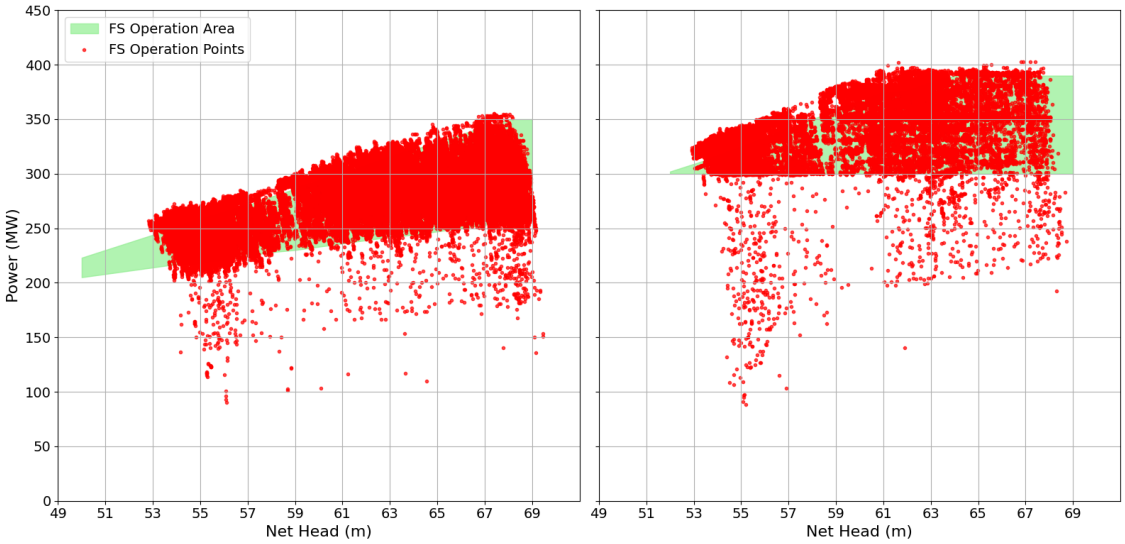

Figure 23 - Operating points without transition points.

To further analyze the impact of transition point removal on the dataset, Figure 24 presents two pie charts comparing the distribution of operational points before and after applying the logic. The charts classify the points into three categories: Within the Allowed Zone, Below the Allowed Zone, and Above the Allowed Zone.

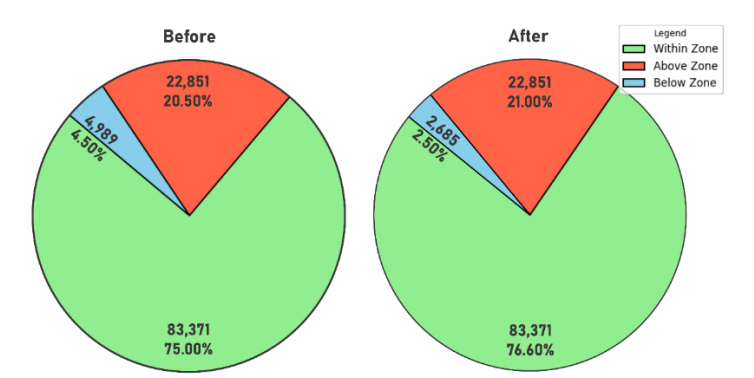

(a) *(b)*

Figure 24 - Number of operational points before (a) and after (b) removing transition points.

Since the applied methodology specifically identifies and eliminates transition points (startup and shutdown phases), only the number of points below the allowed operational zone was affected, while the points within and above the operational limits remained unchanged. A detailed comparison shows that in the original dataset (Figure

24.a), there were 4,989 points (4.5% of the total) classified as below the lower operational limit. After applying the transition point removal logic (Figure 24.b), this number was reduced to 2,685 points (2.5% of the total). This means that 2,304 points (46% of those below the allowed zone) were identified as transition points and subsequently removed, ensuring that only steady-state operational points remain for further analysis. This refinement significantly improves the dataset's reliability, as the removal of transition points prevents misleading interpretations regarding the plant's performance and ensures that further analyses focus solely on stable operating conditions.

5.2. MEDIUM-HEAD 200 MW HYDROPOWER PLANT

5.2.1. Overview Of Plant

The second case study considered in this work is a medium-head hydropower plant with an installed capacity of approximately 200 MW. The scheme is composed of a relatively recent development with two identical Francis generating units and a single reservoir, commissioned in the last two decades, and designed to supply electricity to a large urban load under typical Brazilian consumption patterns.

The main dam is a mixed structure combining roller-compacted concrete sections with an earthfill section with clay core, with a maximum height of about 92 m. Under normal operating conditions, the impounded reservoir presents a water surface area on the order of 200 km^2 and a total storage volume of approximately 5×10^9 m^3, with an average depth close to 20–25 m. The flooded area extends along several tens of kilometres of the river valley and partially affects multiple municipalities in the surrounding region.

The hydraulic layout includes a gated surface spillway equipped with two radial gates, providing a maximum discharge capacity of about 2,700 m^3/s, and a surface water intake with two independent gate slots feeding the penstocks. The powerhouse is of the semi-underground/abutment type and houses two identical vertical-axis Francis units. Each unit is rated at roughly 100 MW, with a runner diameter of about 4.2 m and a nominal rotational speed of 171.4 rpm, directly coupled to a 13.8 kV, 60 Hz synchronous generator. The resulting total installed capacity is in the 200 MW range, representative of a typical medium-head, two-unit configuration.

Grid connection is achieved through a double-circuit transmission line at sub-transmission voltage level, linking the plant's step-up substation to the regional grid over a distance of a few tens of kilometres. The implementation of the project required a set of associated infrastructure works, including road paving and relocation, new bridge construction over the reservoir and the reorganization of local access roads and river crossings.

From the hydropower-system perspective, this 200 MW case-study plant is a relatively recent two-unit scheme operating under medium head, for which detailed manufacturer hill charts and operational records are available. These characteristics make it a suitable test bed for evaluating the potential energy gains from converting existing fixed-speed Francis units to VSO, complementing the large-scale case study presented previously. All plant description and technical data in this subsection are based on the original project documentation and operator records made available to the authors.

5.2.2. Hill curves of the 200 MW case-study plant

For the 200 MW case-study plant, the turbine hill curves were derived from the manufacturer's original performance data for the two Francis units and subsequently converted into numerical tables. The discrete points of net head, discharge, power and efficiency were cleaned, converted to consistent SI units and assembled into a single dataset. Following the general procedure described in Section 4.5.2, these scattered measurements were interpolated on a regular grid in the (H,Q) and (H,P) planes using a two-dimensional Clough–Tocher scheme, with inverse-distance weighting used only to fill small gaps near the convex hull of the data. The resulting efficiency values were clipped to a physically meaningful range and checked against the original samples, which are superimposed as white markers in the plots for validation.

Figure 25(a) shows the efficiency map $\eta(H,Q)$ as a function of net head and discharge. The chart covers heads from approximately 46 m to 92 m and discharges between 40 m^3/s and 180 m^3/s, thus encompassing the full admissible operating range of the case-study units. The isolines, drawn every 2 %, highlight a broad high-efficiency plateau above 90 % for intermediate heads (about 60-80 m) and discharges around 110-130 m^3/s, gradually decreasing towards low-flow and high-flow regions. This

representation is used throughout the study to evaluate turbine efficiency for any operating point (H,Q) encountered in the historical record or generated by the VSO algorithms.

The second map, η(H,P), is presented in Figure 25(b) and describes efficiency as a function of net head and mechanical power. In this case, the power axis spans from roughly 10 MW to 135 MW, covering deep part-load, nominal and moderate overload conditions with respect to the 106.29 MW rated output of each unit. The isolines again reveal a well-defined high-efficiency region above 92 %, whose position shifts with head, while lower efficiencies appear at very low power and near the upper operating limits. This (H,P) formulation is used mainly to convert manufacturer power envelopes into equivalent discharge limits, ensuring consistency between the admissible operating region and the efficiency surface adopted in the simulations.

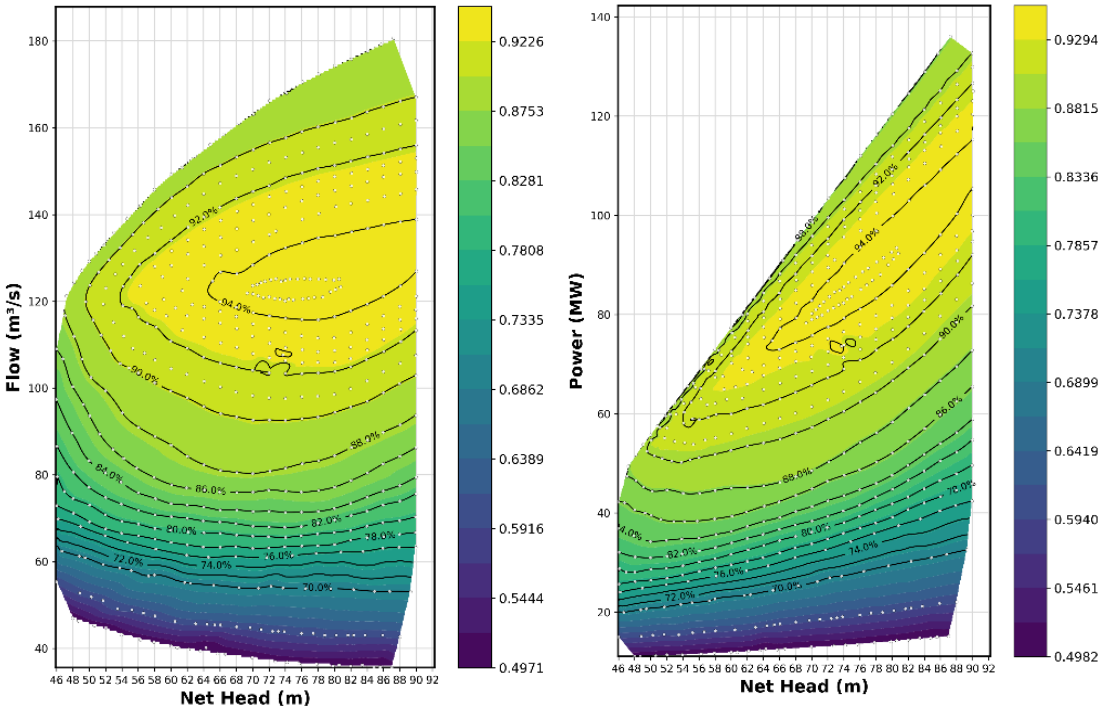

(a) *(b)*

Figure 25 - Hill curve for the 200 MW case-study plant: (a) $\eta(H,Q)$ (b) $\eta(H,P)$.

Taken together, the η(H,Q) and η(H,P) maps constitute the turbine performance model of the 200 MW case-study plant used in this work. All subsequent analyses for this plant, VS similarity searches, energy-gain scenarios and, when applicable, optimized flow

allocation, are based on these hill curves, which provide a plant-specific and hydraulically consistent description of turbine efficiency over the entire relevant operating domain.

5.2.3. Typical Operation

The typical operation of the 200 MW case-study plant was characterized using the historical hourly records for the year 2021. **Error! Reference source not found.** presents the annual evolution of reservoir inflow, total turbined discharge and gross head. The inflow exhibits a marked seasonal pattern, with higher values during the wet season (approximately from January to April and again in December) and a pronounced reduction during the dry months in mid-year. In contrast, the turbined discharge remains comparatively smoother, close to the plant's preferred operating band for most of the year, with short periods of increased generation when inflows rise sharply. The gross head varies in a relatively narrow interval around 60–65 m, reflecting the regulating effect of the reservoir and the operational strategy aimed at keeping the net head close to the nominal design value.

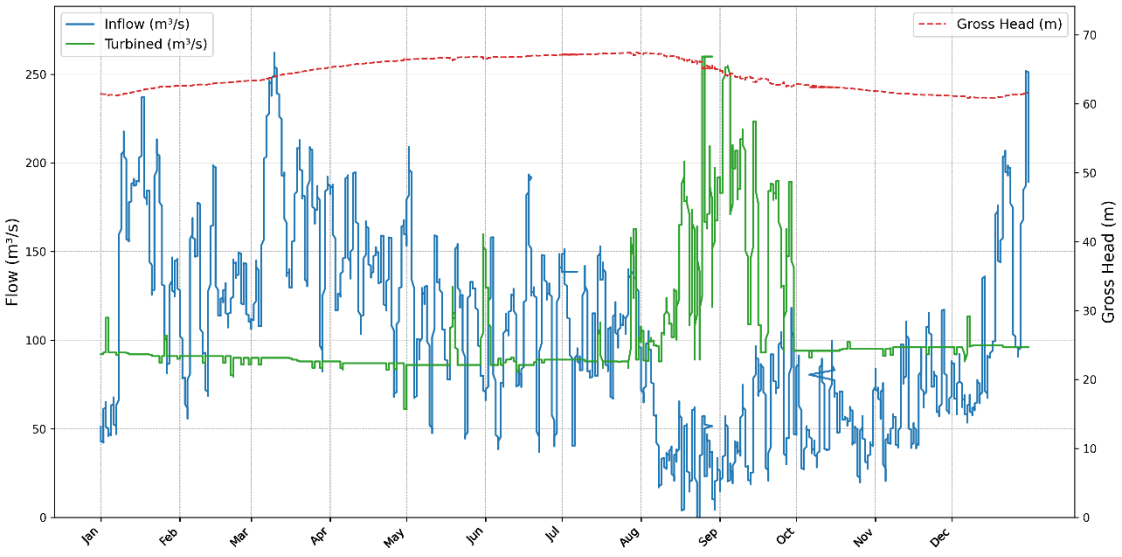

Figure 26 - Flow and gross head throughout 2021 for the 200 MW case-study plant.

To better understand how the plant is dispatched over the turbine hill chart, **Error! Reference source not found.** shows all operating points of units UG1 and UG2 during 2021 plotted in the H–Q plane and colored according to the FS efficiency. The

background contours correspond to the efficiency map η(H,Q) derived in Section 5.2.2, while the light-blue polygon represents the admissible FSO range in terms of net head and discharge. The operating points of both units are largely concentrated inside this region and clustered around the high-efficiency ridge of the hill chart, roughly between 60–66 m of net head and 85–135 m³/s of discharge, where efficiencies above 0.90 are achieved. Only a few points approach the lower-efficiency boundaries, indicating that, under current FSO, the plant is already dispatched close to its best-efficiency band for most of the time.

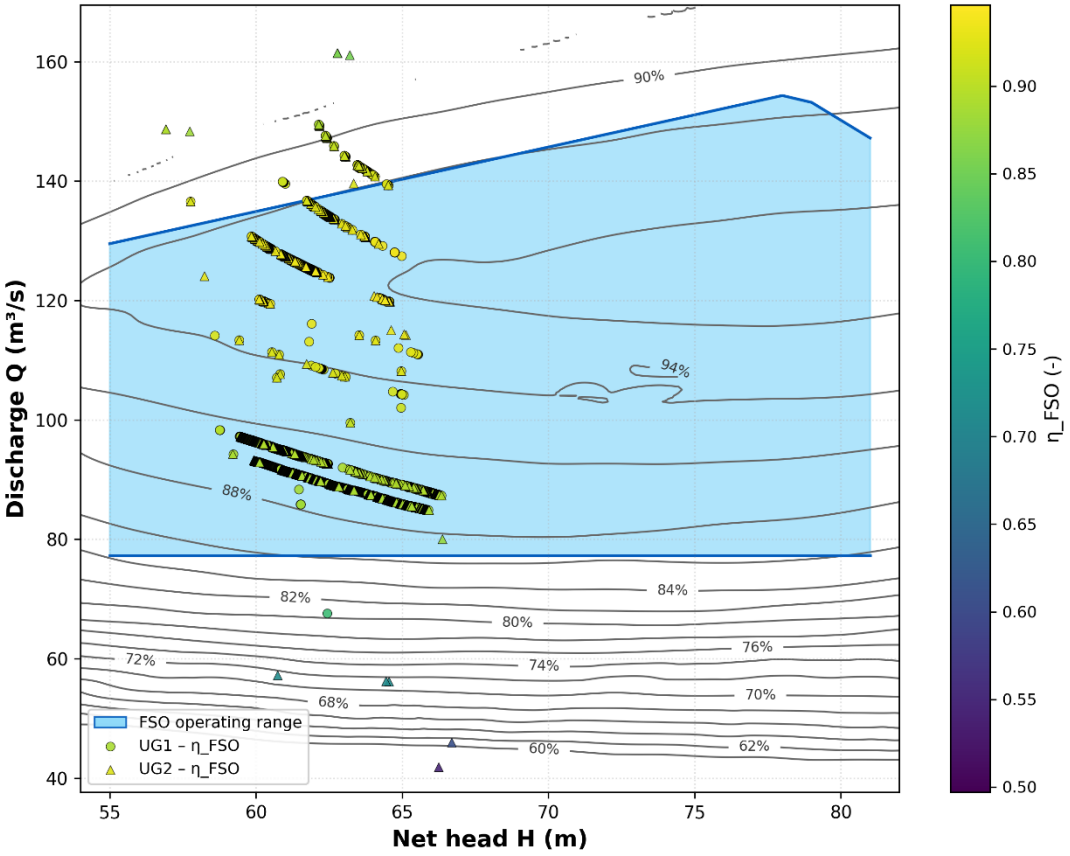

Figure 27 - All operating points recorded in 2021 for the 200 MW case-study plant – H x Q.

These results provide a reference description of the current operating pattern of the 200 MW case-study plant. The annual inflow–head behavior and the distribution of operating points over the hill chart will be used as the baseline for the subsequent simulations, in which alternative operating strategies with VS units are evaluated and compared against the existing FS configuration.

6. RESULTS AND DISCUSSIONS

6.1. NEW OPERATIONAL RANGE

6.1.1. New Operational Range THP

Upon applying the similarity equations shown in Section 4.2, it was assumed that the turbine diameter is constant even as the rotational speed changes. The simulations were conducted by applying a ±20% variation around the nominal speed. This is the operational flexibility that can be achieved with variable-speed turbines. Figure 28 and Figure 29 shows the expanded operational ranges for CFI and CFII turbines under VS and FS conditions, respectively.

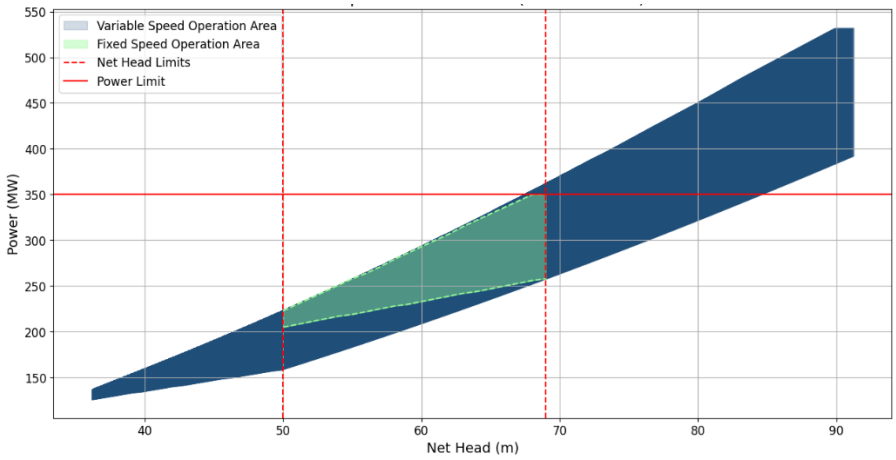

Figure 28 - Operation Area CFI with Limits – VS and FS (THP).

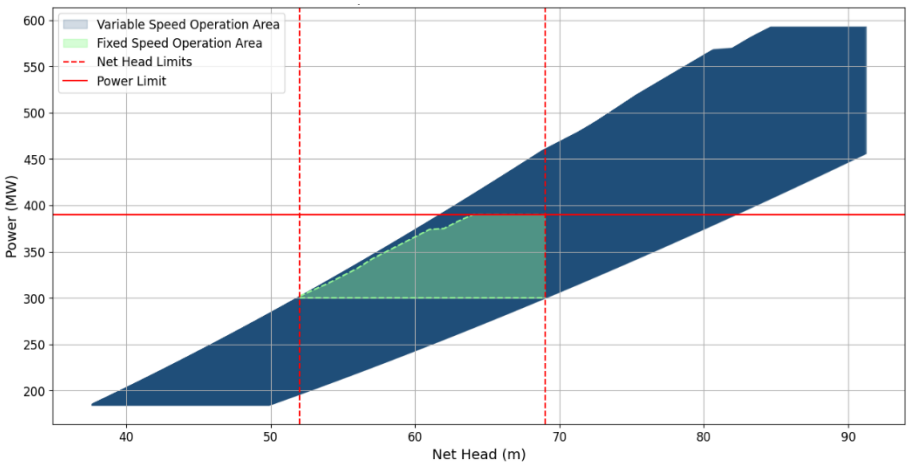

Figure 29 - Operation Area CFII with Limits – VS and FS (THP).

Figure 28 shows the operational areas for CFI turbines, with shaded regions indicating the areas of operation under both VS and FS conditions. The red dashed lines represent the net head limits that must be within the actual operational range of the plant. The solid red line represents the turbine power limit, which cannot exceed 350 MW, as this is the turbine's nominal capacity. Figure 29 shows the operational areas to be expanded for CFII turbines under similar conditions, with a nominal power limit of 390 MW.

Only the expanded operational areas are shown in Figure 30 and Figure 31 after applying these limits. The regions, defined by the net head range and nominal power constraints, will be used as a basis for FSO comparison with VSO during simulation.

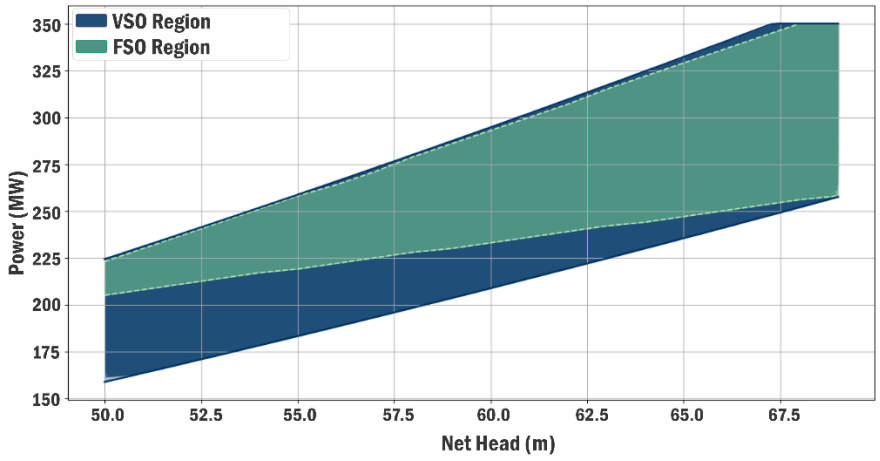

Figure 30 - Expanded Operation Area VS and FS (THP): CFI.

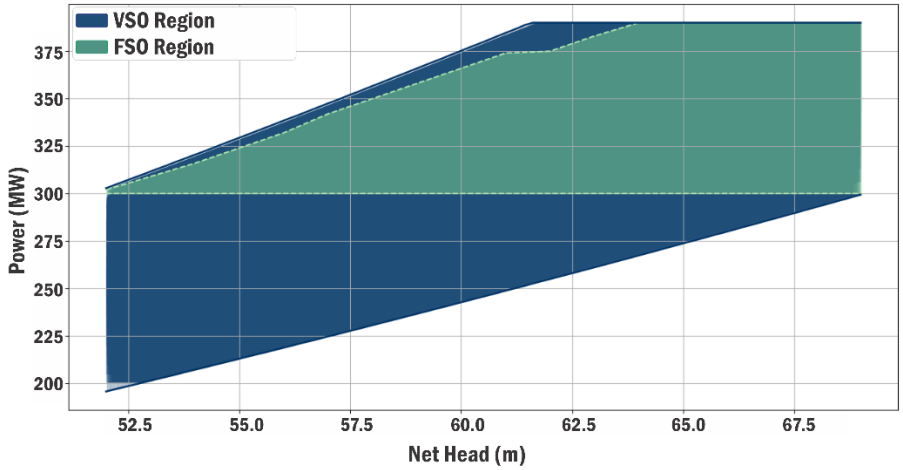

Figure 31 - Expanded Operation Area VS and FS (THP): CFII.

The green region represents the current operating range under FSO conditions, whereas the blue region represents the expanded operational domain enabled by VSO. These regions, defined by the H_N range and P_t, are used as a basis for FSO comparison with VSO during simulation.

This study highlights the substantial operational flexibility benefits that can be achieved with VSO, particularly in terms of adapting to changes in grid requirements and optimizing energy dispatch under diverse hydraulic conditions. These widened operational scopes stand as potential enhancements of efficiency and grid support that could be achieved by retrofitting Tucuruí's turbines to VSO.

6.1.2. New Operational Range SFHP

For the Serra do Facão hydropower plant the new operational range under VSO was obtained by applying exactly the same procedure described for Tucuruí. First, the original fixed-speed limits in the H–P plane , the minimum and maximum unit power as a function of net head, were taken directly from the manufacturer's characteristic curves and from the plant operating guide. This information defines the green polygon in Figure 32, which represents the current admissible range of unit power for each net head, and is fully consistent with the corresponding H–Q envelopes and with the η(H,Q) hill chart presented in Section 5.

In a second step, the similarity relationships previously described, together with the η(H,Q) and η(H,P) hill charts derived for Serra do Facão, were used to recompute the admissible operating region when variable speed is allowed. For each value of net head in the interval approximately between 55 and 80 m, several operating points were generated within the speed band defined for the VSO retrofit. Points violating cavitation limits or exceeding generator, transformer or mechanical constraints were discarded, and only points with efficiency above the minimum design threshold were retained. The extremal values of power for each head form the blue envelope in Figure 32, which defines the VSO region.

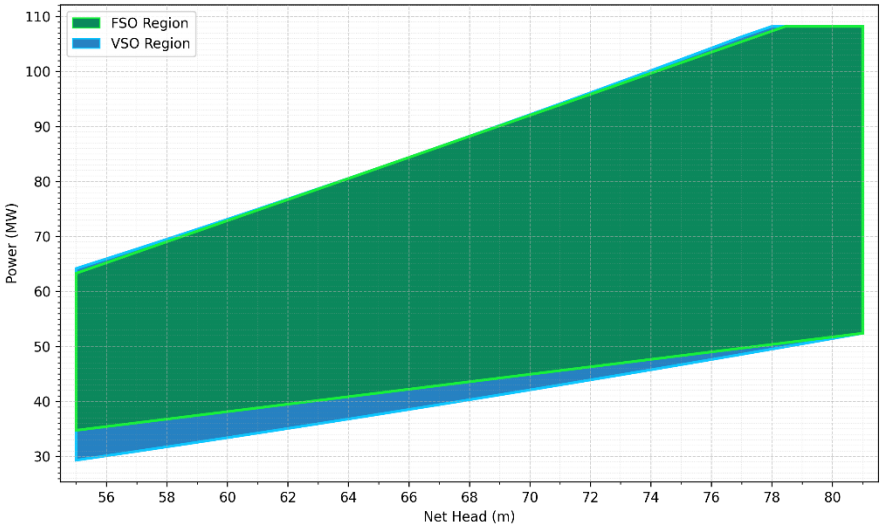

Figure 32 - Expanded Operation Area VS and FS (SFHP).

The comparison between the two polygons shows that, for Serra do Facão, the VSO region almost fully covers the existing FSO range and provides an additional area at higher power levels, particularly for heads above roughly 70 m. In this upper-head region, the maximum unit power can be slightly increased while keeping the operation closer to the best-efficiency island of the hill chart. At low heads the envelopes nearly coincide, indicating that cavitation and discharge limits dominate and leave little room for expansion.

It is also worth noting that, as in Tucuruí, the new VSO range for Serra do Facão was defined so that all historical operating points from 2021 lie inside the admissible region. Therefore, the green polygon in Figure 32 represents the status-quo operation, whereas the blue polygon corresponds to the technically feasible operating space after the retrofit. This enlarged region will be used in the next subsections as the constraint set for the dispatch simulations, allowing a consistent comparison of turbine starts and stops, cavitation exposure and energy production between FSO and VSO for the Serra do Facão case study.

.

6.2. IMPACT ON TURBINE STARTS AND STOPS

The analysis evaluates the reduction in turbine starts and stops achieved through the implementation of VSO compared with the baseline FSO. Five different scenarios

were considered, wherein the number of GUs operating under VSO progressively increased. The dispatch algorithm from Section 5.2 was applied to simulate the following scenarios (Table 2):

Table 2 - Scenarios considered

Item	***Scenario***	***Description***
1	FS	Current scenario with all 23 units operating in FS (reference).
2	3GU-CFII	Partial conversion with 3 CFII units operating in VS.
3	6GU	Partial conversion with 6 units operating in VS: 3 in CFI and 3 in CFII.
4	12GU	Partial conversion with 12 units operating in VS: 6 in CFI and 6 in CFII.
5	23GU	Full conversion with all 23 units operating in VS.

The results for each of these scenarios will be presented in detail in the following subsections, and finally, a comparative analysis will be conducted in the last subsection, where the performance of all scenarios will be evaluated side by side, highlighting the benefits and trade-offs of transitioning from FSO to VSO at different levels of implementation.

6.2.1. Current Scenario (FS)

In the current operational scenario, all 23 generating units (GUs) of the THP operate under whole steam operation (FSO). This configuration imposes certain constraints on the system's flexibility, requiring frequent start-ups and shutdowns to balance grid demands. The operational limitations of FSO often lead to an increased number of turbine starts and stops, resulting in greater mechanical wear, reduced efficiency, and increased maintenance costs.

To analyze this behavior, the first step was to assess the distribution of start and stop events across all generating units over one year. Figure 33 presents the number of turbine starts and stops for each generating unit in 2021. It is observed that some units experience significantly higher operational cycling than others, suggesting an uneven distribution of operational demand among the available turbines. This imbalance can contribute to increased mechanical stress on certain units, leading to premature wear and higher maintenance requirements.

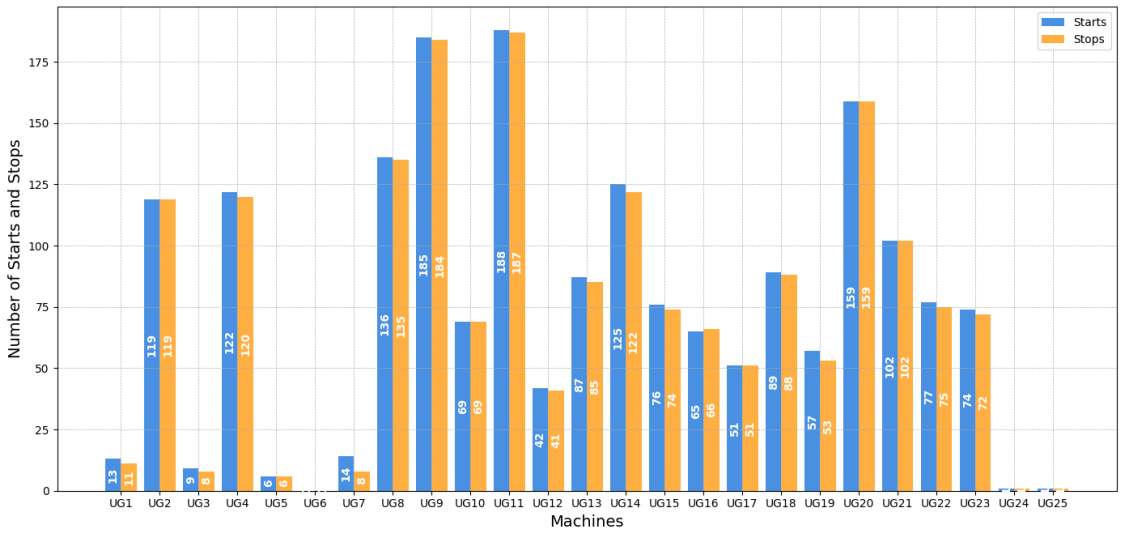

Figure 33 - Number of starts and stops per machine (FS).

Furthermore, Figure 34 illustrates the monthly distribution of turbine starts and stops throughout the year. The data indicate that the frequency of these events varies across different months, likely influenced by seasonal demand variations and hydroelectric dispatch strategies. Some months exhibit a higher concentration of start-stop events, highlighting periods of more intense operational adjustments to match energy demand fluctuations.

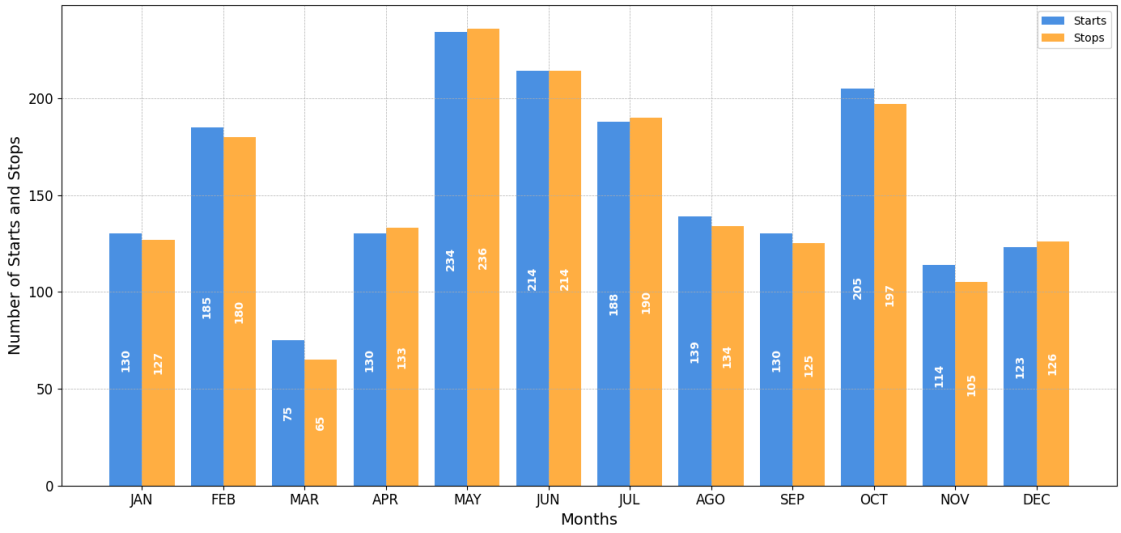

Figure 34 - Number of Starts and Stops per Month (FS).

To quantify the overall impact of FSO on turbine cycling, Figure 35 summarizes the total number of starts and stops recorded in 2021. The plant registered 1,867 starts

and 1,837 stops during the year, underscoring the high frequency of turbine cycling in the current operational framework. This frequent cycling not only increases mechanical stress on the equipment but also results in inefficiencies related to ramp-up periods and energy losses during transitional states.

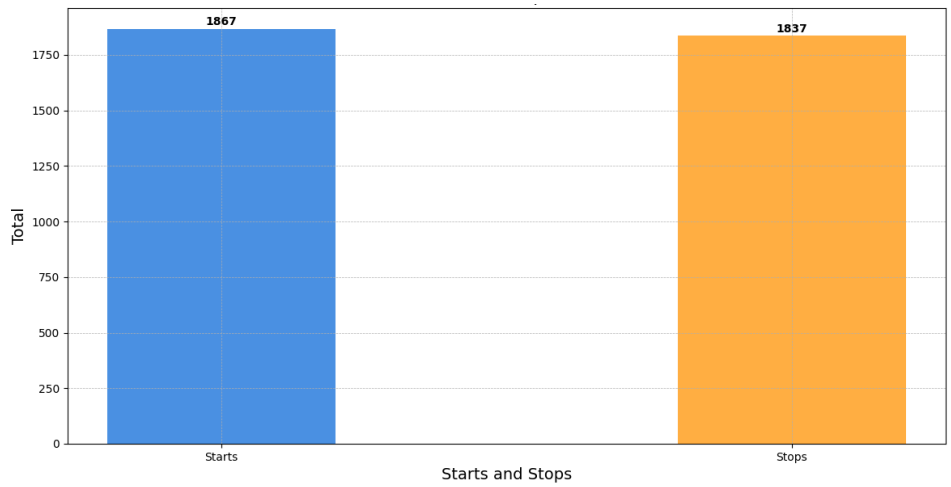

Figure 35 - Total number of starts and stops recorded (FS).

These findings serve as a baseline for comparison with the VSO scenarios presented in the subsequent sections. By evaluating the reduction in starts and stops under different levels of VSO implementation, this study aims to quantify the potential benefits of transitioning from FSO to VSO in terms of operational stability, mechanical longevity, and efficiency improvements.

6.2.2. VSO Scenarios Conversion

This section presents the simulated scenarios involving the application of VSO to a subset or all generating units of the hydropower plant. The goal is to evaluate the progressive impact of integrating VSO on the reduction of turbine start-stop cycles and on the operational flexibility of the plant. The following VSO scenarios were defined and analyzed:

- *Partial Conversion (3UG):* Three generating units from CFII (UG 13, UG 15, UG 17) operate under VS.
- *Partial Conversion (6UG):* Three generating units from CFI (UG 1, UG 3, UG 5) and three from CFII (UG 13, UG 15, UG 17) operate under VS.

- *Partial Conversion (12UG):* Six generating units from CFI (UG 1, UG 3, UG 5, UG 7, UG 9, UG 11) and six from CFII (UG 13, UG 15, UG 17, UG 19, UG 21, UG 23) operate under VS.
- *Full Conversion (23UG):* All generating units from both CFI and CFII operate under VSO.

The dispatch algorithm was applied to simulate each scenario by incorporating the new operational limits for VSO units while maintaining FSO units within their current constraints. The results are analyzed below.

6.2.2.1. Partial Conversion (3UG)

In this scenario, only three units (UG 13, UG 15, UG 17) operate in VS. Figure 36 presents a bar chart comparing the number of starts (top subplot) and stops (bottom subplot) before and after the partial conversion. The results indicate a visible reduction in the number of starts and stops across all machines, with a more uniform distribution among the units.

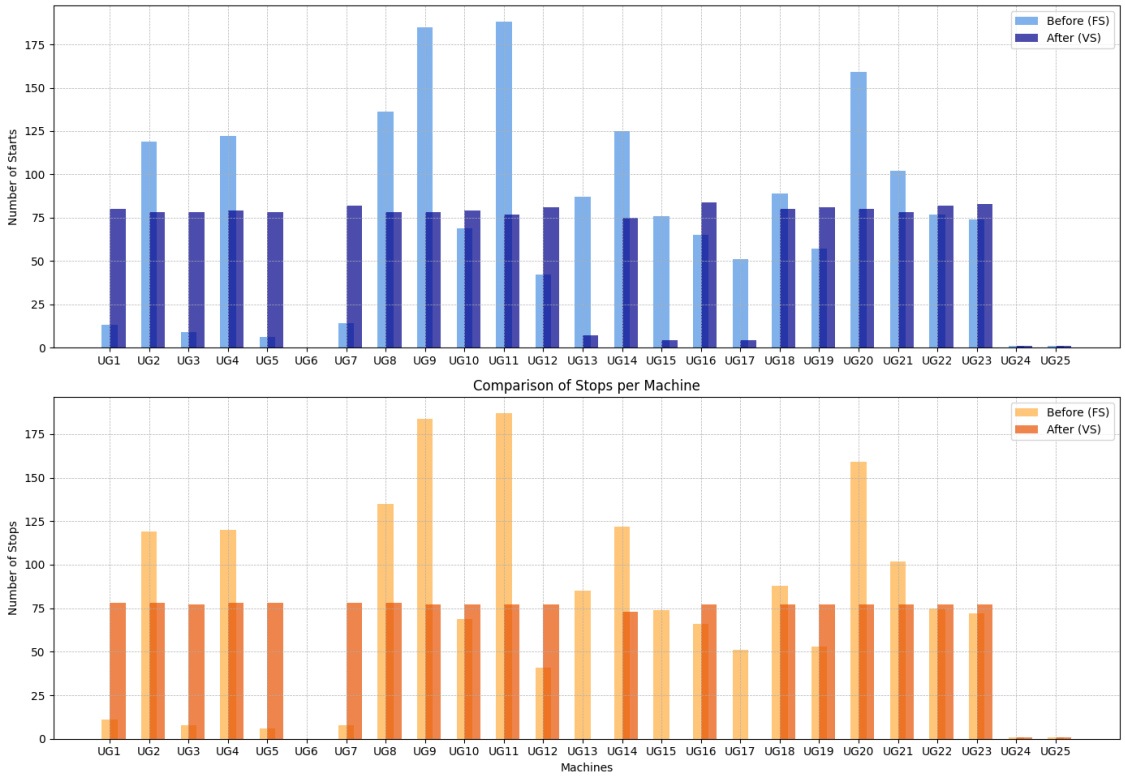

Figure 36 - Number of starts and stops per machine FS (Before) and VS (After): 3UG.

The dispatch algorithm prioritizes keeping VSO units continuously operating, reducing their start-stop cycles significantly. This behavior is evident in the selected VSO units, which exhibit minimal shutdown occurrences.

Figure 37 provides a monthly breakdown of starts and stops before and after the conversion, demonstrating how the reduction in operational transitions is distributed over the year.

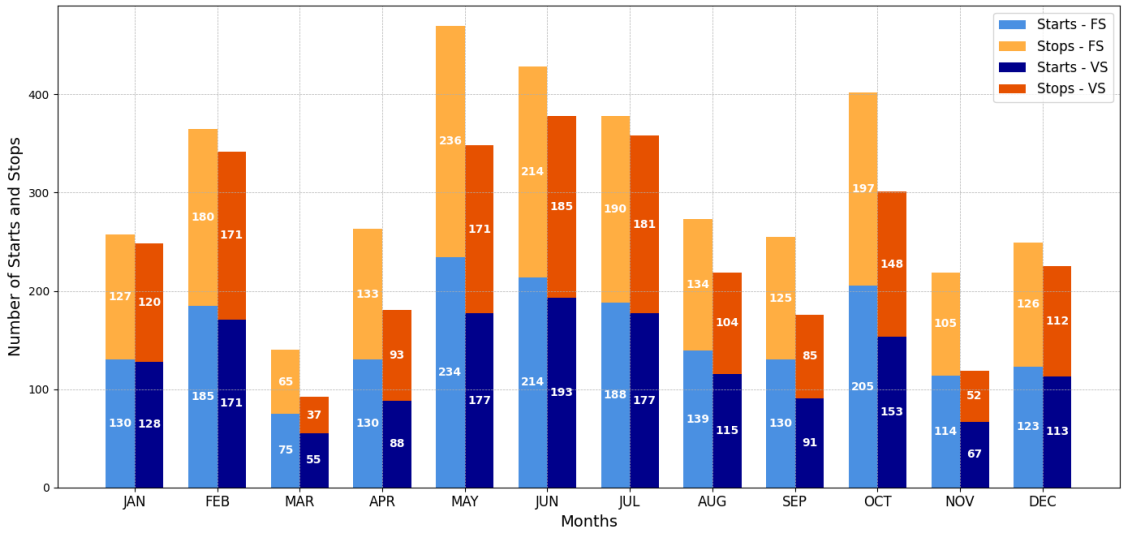

Figure 37 - Number of starts and stops per month FS (Before) and VS (After): 3UG.

Figure 38 highlights the overall reduction in starts and stops for the entire power plant. The total number of starts decreased from 1867 to 1528, a reduction of 339 starts (18.50%), while stops dropped from 1837 to 1467, a reduction of 370 stops (20.15%).

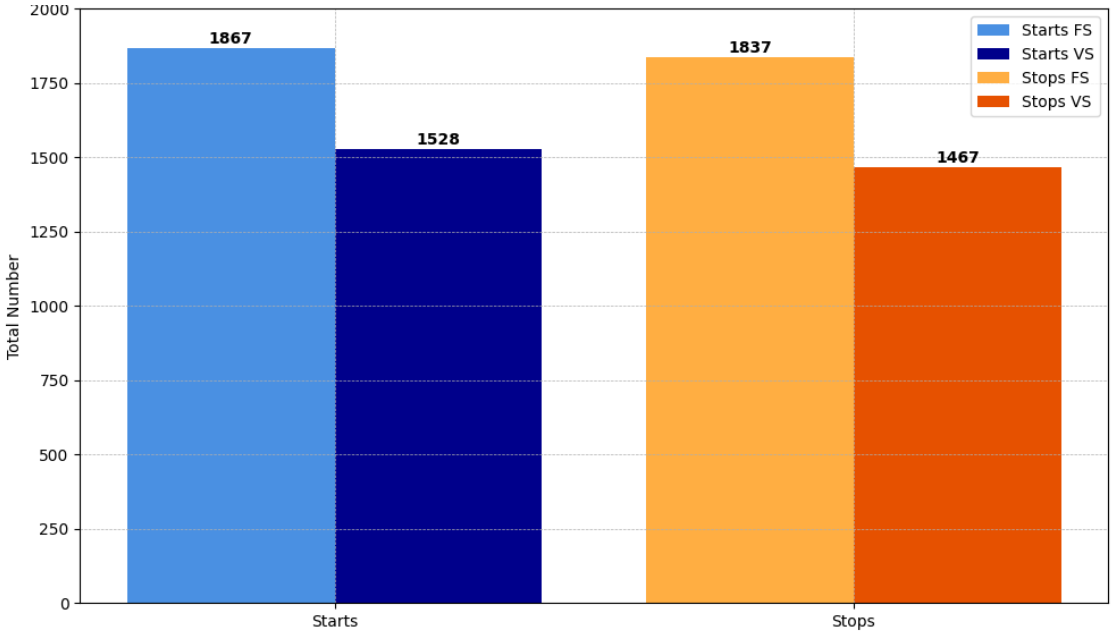

Figure 38 - Total number of starts and stops recorded FS and VS: 3UG.

6.2.2.2. Partial Conversion (6UG)

For this scenario, an additional three units (UG 1, UG 3, UG 5) from CFI were converted to VSO, totaling six units operating under variable speed. Figure 39 shows the impact on starts and stops per machine. Similar to the previous scenario, the VSO units experience significantly fewer transitions, with a more balanced operation among all units. The monthly trend is illustrated in Figure 40, where the reduction in starts and stops is more pronounced compared to the 3GU scenario.

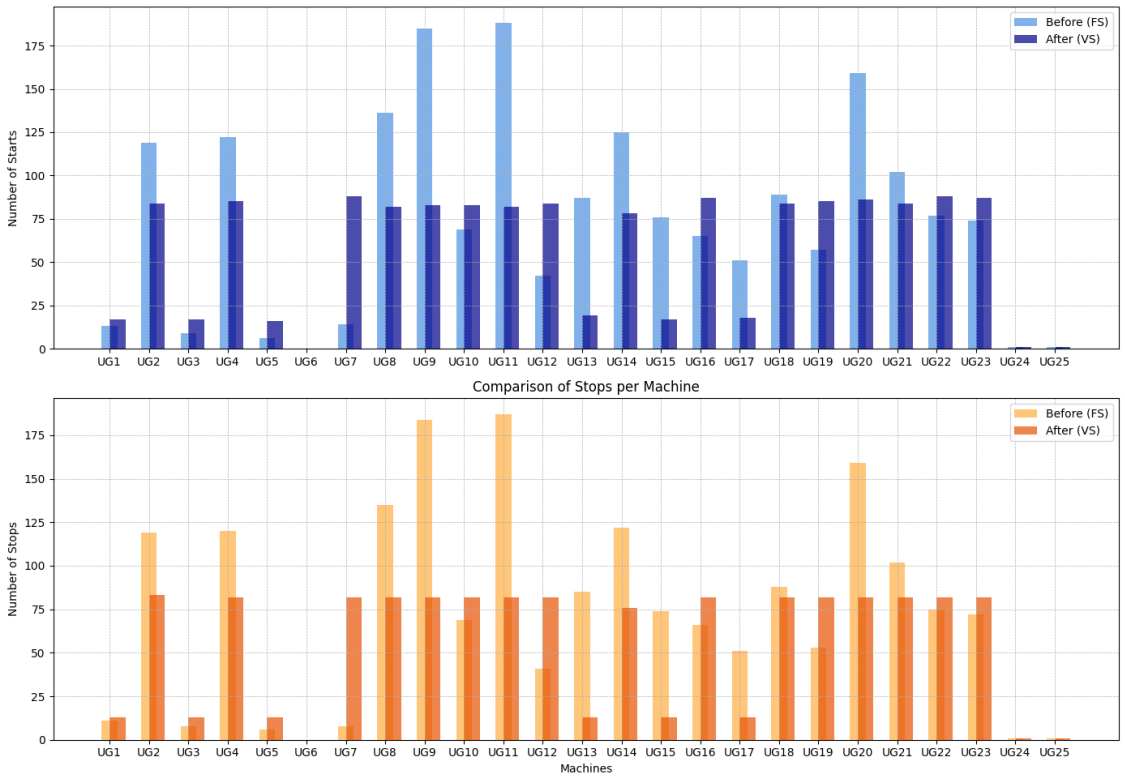

Figure 39 - Number of starts and stops per machine FS (Before) and VS (After): 6UG.

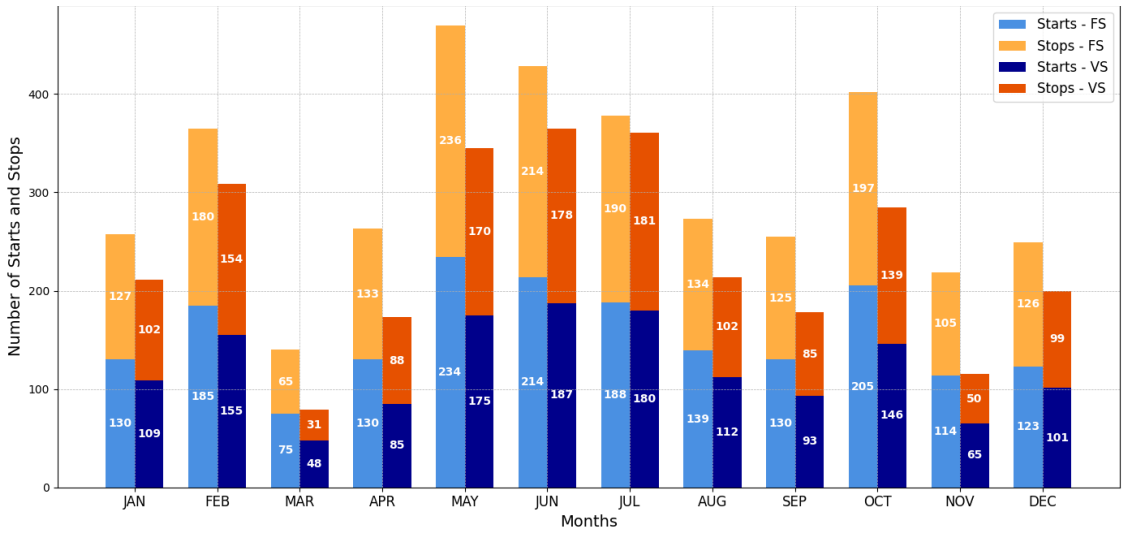

Figure 40 - Number of starts and stops per month FS (Before) and VS (After): 6UG.

The overall reduction is captured in Figure 41, where the total starts dropped from 1867 to 1456, representing a 22% reduction (411 starts avoided). Similarly, stops decreased from 1837 to 1387, a 24.50% reduction (450 stops avoided). Compared to the

3GU scenario, this configuration led to an additional 21% (72 starts) and 21.6% (80 stops) being avoided.

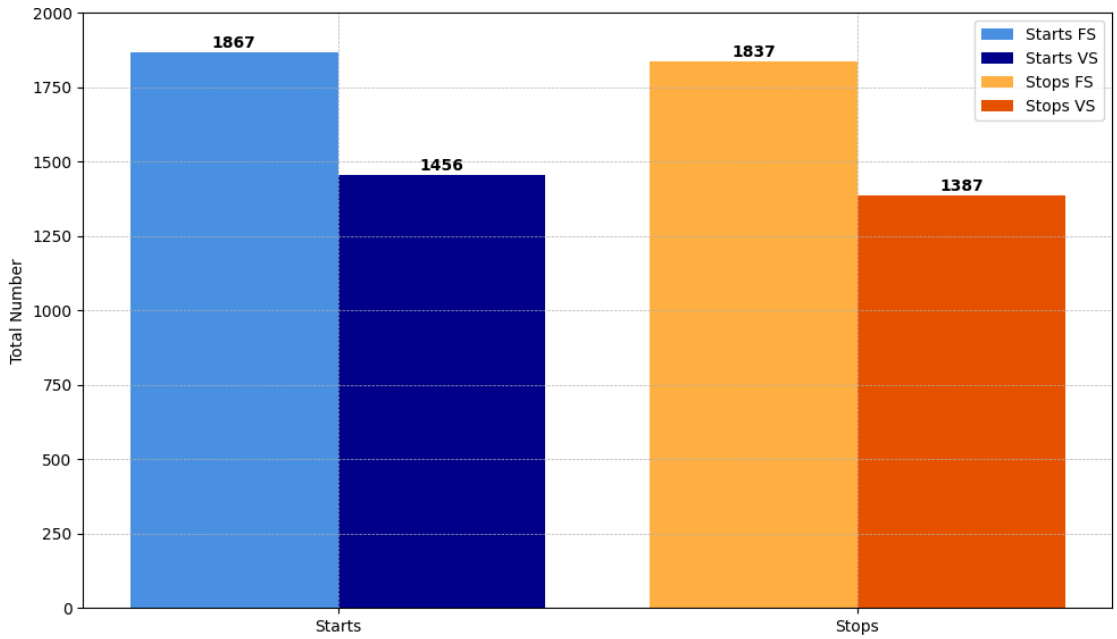

Figure 41 - Total number of starts and stops recorded FS and VS: 6UG.

6.2.2.3. Partial Conversion (12UG)

The final partial conversion scenario involves 12 generating units operating under VSO, representing a more balanced distribution between FSO and VSO machines. As shown in Figure 42, the reduction in starts and stops across the entire plant becomes more substantial. Unlike the previous scenarios, where VSO units were prioritized to remain in continuous operation, in this case, the workload is more evenly distributed across both FSO and VSO units. Figure 43 presents the monthly comparison, demonstrating the effectiveness of VSO in stabilizing plant operation over time.

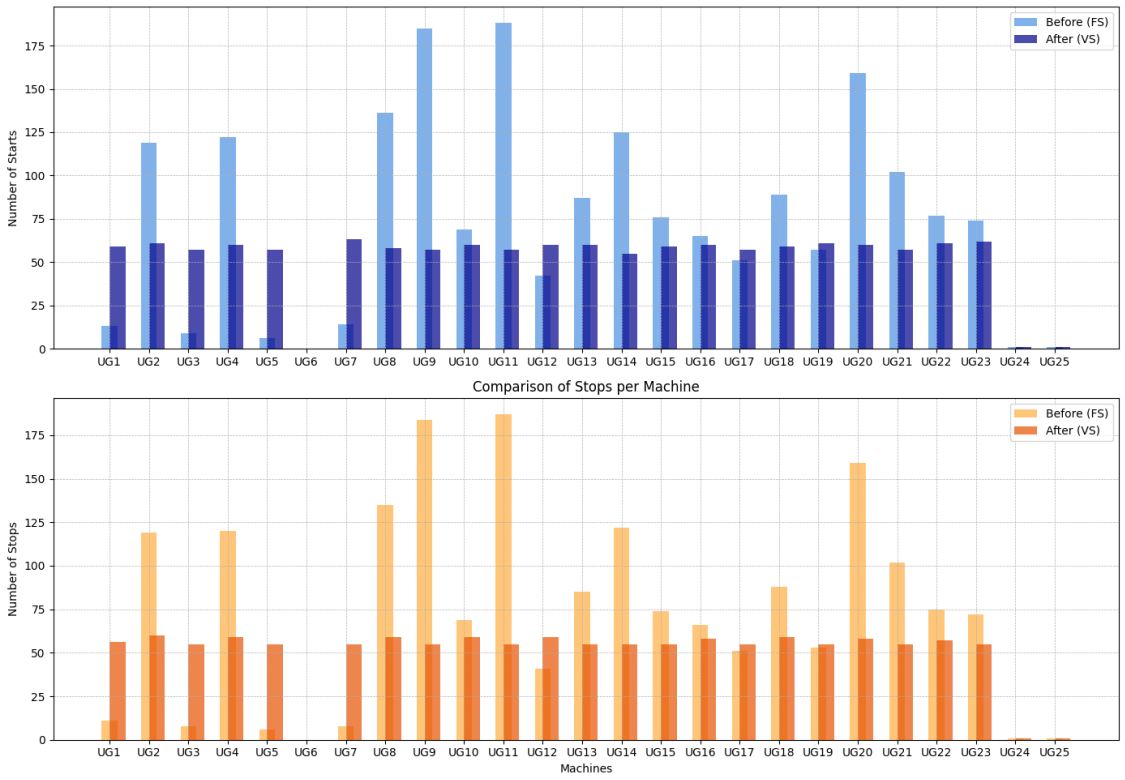

Figure 42 - Number of starts and stops per machine FS (Before) and VS (After): 12UG.

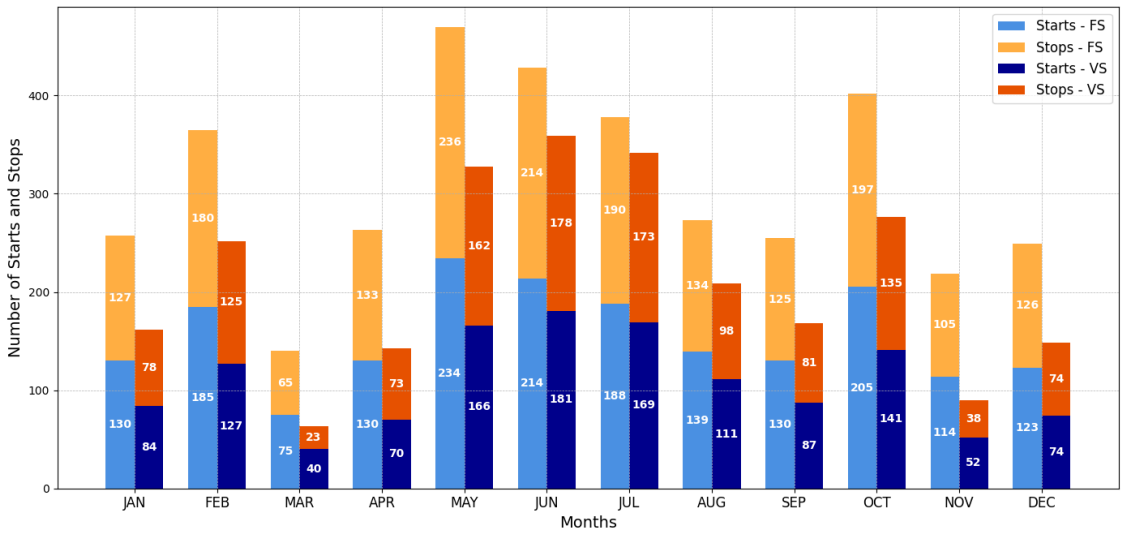

Figure 43 - Number of starts and stops per month FS (Before) and VS (After): 12UG.

The cumulative impact is depicted in Figure 44, where the total starts decreased from 1867 to 1302, achieving a 30.20% reduction (565 starts avoided). Stops followed a similar trend, dropping from 1837 to 1246, a 32.17% reduction (591 stops avoided).

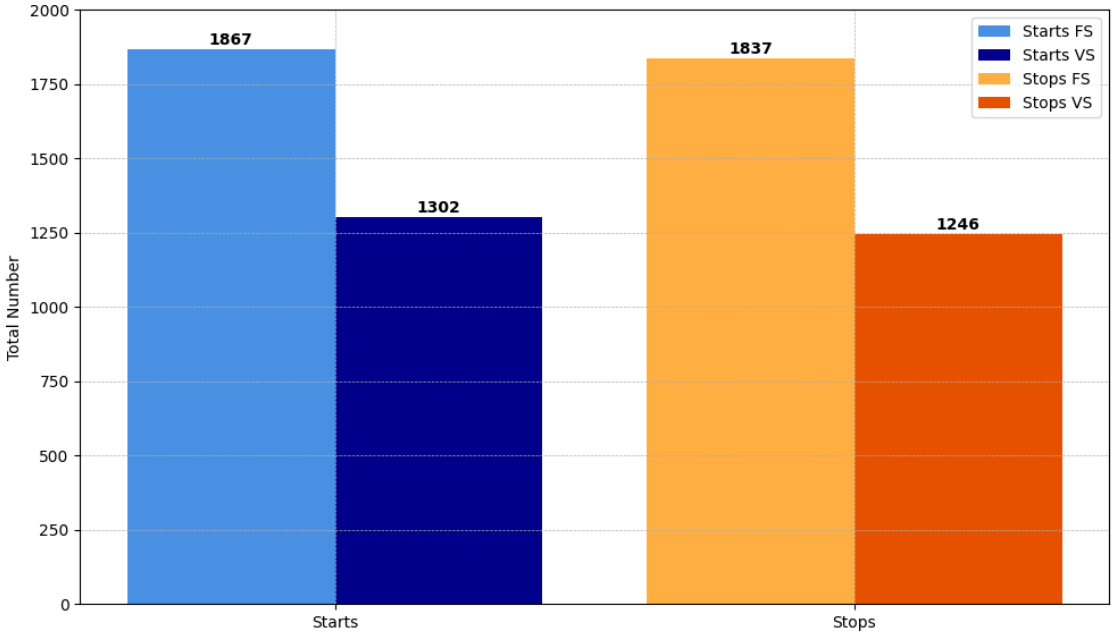

Figure 44 - Total number of starts and stops recorded FS and VS: 12UG.

Comparing this with the 3GU scenario, the 12GU configuration avoided an additional 226 starts (66.50%) and 221 stops (60%). Against the 6GU case, the reductions were 154 more starts (37.50%) and 141 more stops (31.30%), confirming the incremental benefits of expanding VSO across more units.

The progressive implementation of VSO significantly reduces the number of starts and stops, leading to fewer mechanical stresses, extended equipment lifespan, and enhanced operational efficiency. The analysis demonstrates that even partial conversion to VSO delivers measurable improvements, with greater benefits as more units transition to variable speed operation. The following section explores the full conversion scenario to assess the maximum achievable impact of VSO implementation.

6.2.2.4. Total Conversion (23UG)

In this scenario, all 23 generating units of the THP operate under VSO. This represents a complete transition from FSO to VSO, allowing all machines to take full advantage of the expanded operational range and improved efficiency.

To present the results for this scenario, the same graphical analysis used in previous cases is applied for comparison. Figure 45 shows a bar chart with two subplots: the upper subplot highlights the number of starts per generating unit before and after total

conversion, while the lower subplot displays the number of stops. As expected, a significant reduction in the number of starts and stops is observed across all machines, reinforcing the impact of VSO in minimizing operational transitions.

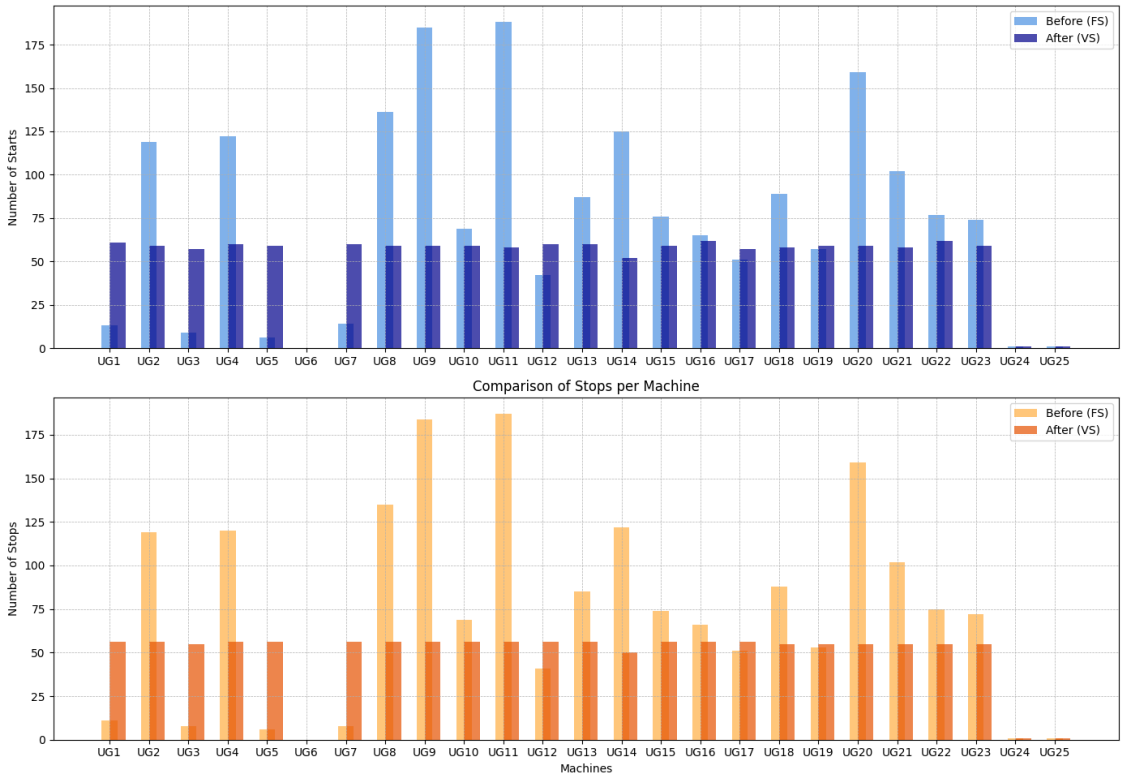

Figure 45 - Number of starts and stops per machine FS (Before) and VS (After): 23UG.

Figure 46 illustrates a monthly comparison of starts and stops, showing how the reduction in operational transitions is distributed throughout the year. The decrease is consistent across different months, indicating that VSO helps stabilize unit dispatch by reducing unnecessary machine activations and shutdowns.

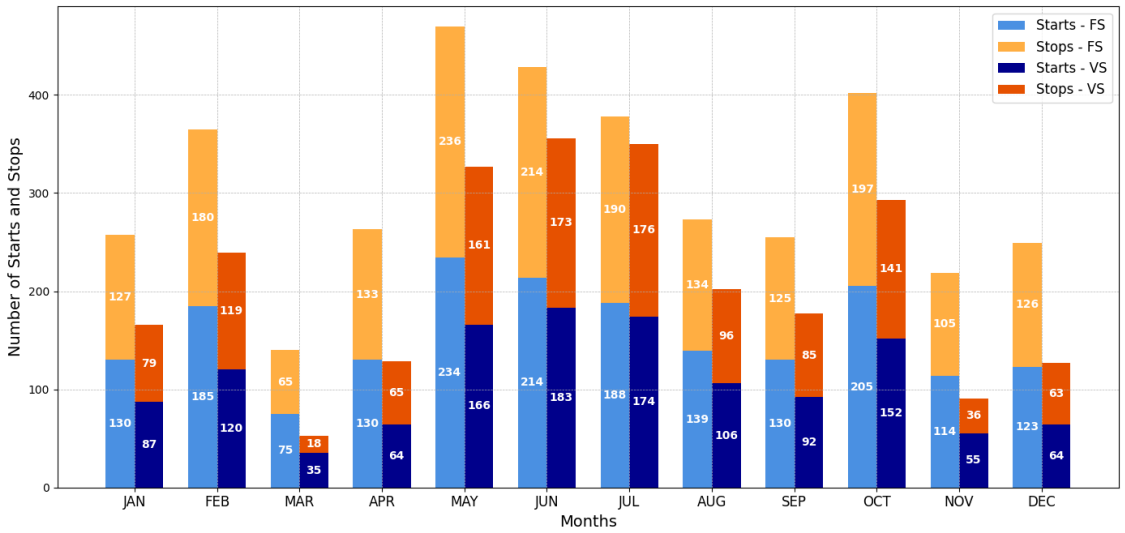

Figure 46 - Number of starts and stops per month FS (Before) and VS (After): 23UG.

Lastly, Figure 47 presents a summary of total starts and stops before and after the full conversion. The total number of starts decreased from 1867 to 1298, representing a 30.5% reduction (569 fewer starts). Similarly, the number of stops decreased from 1837 to 1221, leading to a 33.6% reduction (616 fewer stops). These results confirm the effectiveness of VSO in reducing machine transitions, which in turn can lead to lower maintenance costs and increased equipment lifespan.

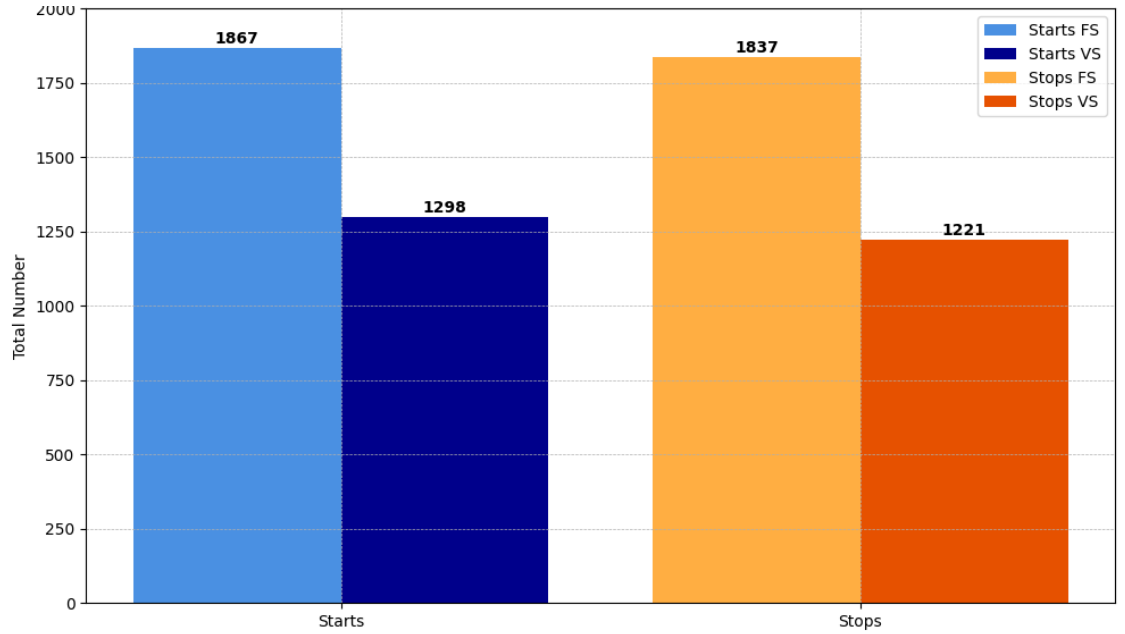

Figure 47 - Total number of starts and stops recorded FS and VS: 23UG.

6.2.3. Conversion Analysis

This section provides a comprehensive comparison of the impact of VSO on turbine starts and stops across different conversion scenarios. The results demonstrate that increasing the number of VSO machines effectively reduces the frequency of starts and stops, leading to a more stable and efficient operational profile.

Figure 48 displays a time series line chart of the monthly total number of starts and stops for each of the five scenarios examined. A notable trend in the results is the steady decrease in the number of turbine starts and stops, accompanied by an increasing share of GU being converted to VSO, indicating the extensive operational improvements and potential cost savings that this technology can bring. This figure demonstrates that applying VSO can enhance operational stability and efficiency, particularly at a hydroelectric generating station of such a large capacity as Tucuruí, where operational flexibility is the most crucial factor. Moreover, with this figure, it becomes possible to identify the months with the most and least operational activity.

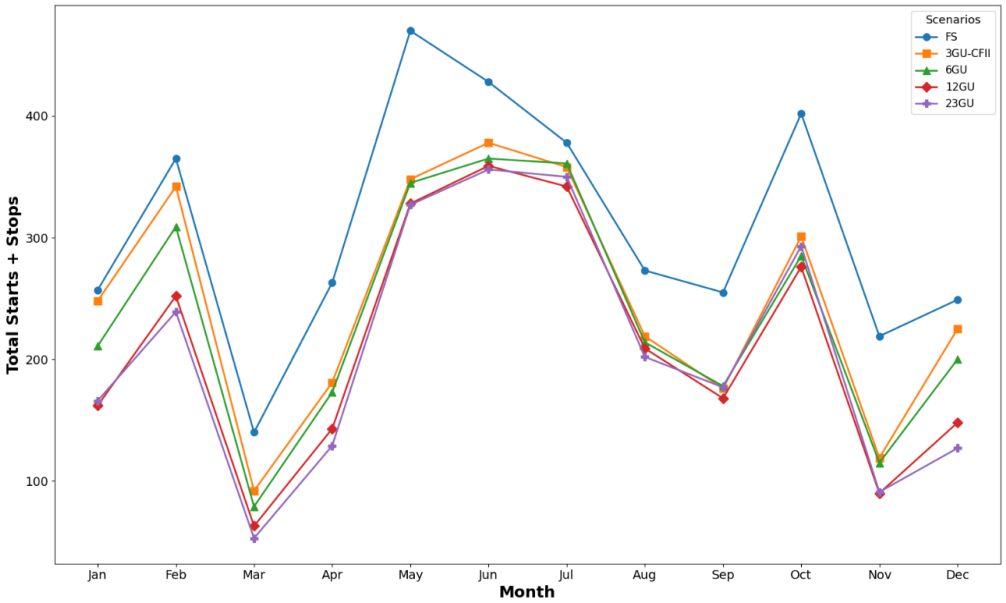

Figure 48 - Monthly Total Starts and Stops - Comparison between scenarios.

From the graph, May, June and October jump as the months with the highest total starts and stops available, in the FSO scenario, therefore reflecting increased demand during these periods. On the other hand, months like March and November show much lower numbers and therefore represent reduced activity.

The implementation of VSO results in visible decreases in starts and stops for all months, smoothing the operational profile. These reductions are much more marked in those months that previously stood out due to a very high level of operational activity under FSO such as, for example, June and October thus serving as visible evidence of VSO's capacity to stabilize operations and reduce mechanical stress on equipment.

Figure 49 illustrates a stacked bar chart presenting the total number of starts and stops for the five scenarios, along with corresponding reductions. In the baseline FSO scenario, 3704 starts and stops were recorded.

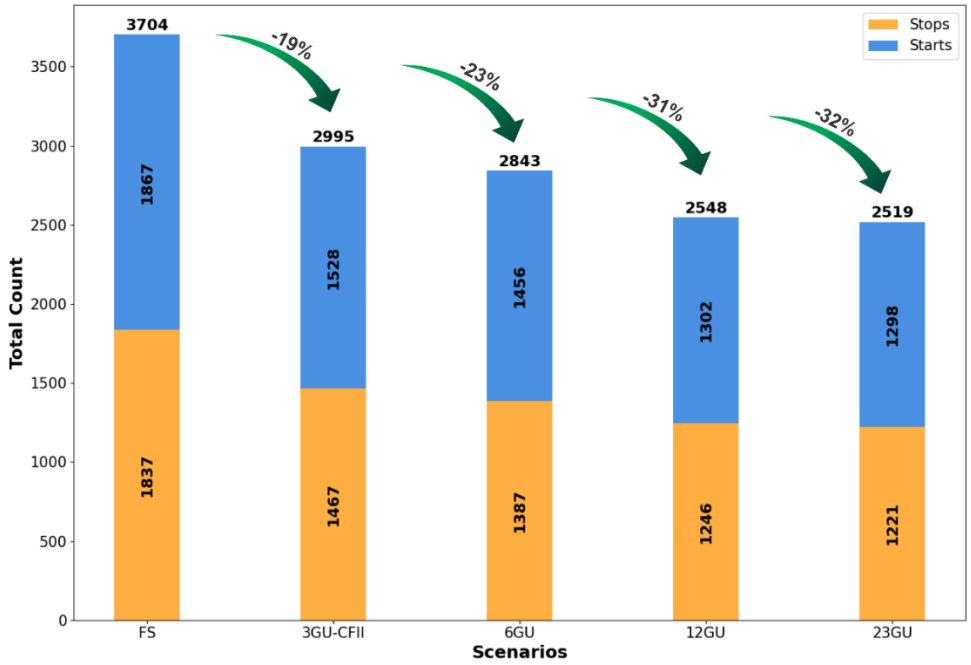

Figure 49 - Comparison of Start and Stop between Scenarios.

The methodology used in this analysis makes use of the operational points filtered in the previous section while removing transient points to make simulations more accurate. Tests on the increased operational range available when variable speed is attained were carried out under various conditions, both partial and full machine conversion to variable speed. The reductions that were achieved by introducing VSO are as follows:

- *3GU-CFII scenario:* 2927 starts and stops (reduction by 709 events, ~19%).
- *6GU scenario:* 2783 starts and stops (reduction by 861 events, ~23%).
- *12GU scenario:* 2541 starts and stops (reduction of 1156 events, ~31%).
- *23GU scenario:* 2426 starts and stops (achieving the highest reduction of 1185 events, ~32%).

The Total Conversion (23GU) scenario only provided marginal additional benefits compared to the 12GU scenario. The total conversion resulted in just four additional starts and 25 additional stops avoided compared to the 12GU scenario. This suggests that the majority of the benefits in reducing starts and stops are already achieved with 12 units operating in VSO. This last observation is particularly relevant when considering the financial feasibility of a complete conversion. Since converting from 12GU to 23GU yields minimal additional reductions in starts and stops, the cost of implementing VSO for all machines may not be justified solely by this benefit. Thus, other advantages associated with VSO, such as efficiency gains, improved frequency regulation, and enhanced operational flexibility, must be carefully evaluated in future studies to determine the economic viability of full-scale implementation.

To summarize the results, Table 3 provides a comparative overview of the number of starts and stops across all analyzed scenarios.

Table 3 - Comparison of Starts and Stops Reduction Across Scenarios.

Scenario	*Starts (FSO)*	*Starts (VSO)*	*Starts Reduction*	*Stops (FSO)*	*Stops (VSO)*	*Stops Reduction*	*Total (FSO)*	*Total (VSO)*	*Total Reduction*
FS	1867	-	-	1837	-	-	3704	-	-
3GU		1528	18.50%		1446	20.15%		2995	19.15%
6GU		1456	22.00%		1387	24.50%		2843	23.20%
12GU		1302	30.20%		1246	32.17%		2548	31.20%
23GU		1298	30.50%		1221	33.60%		2519	32.00%

From this table, it becomes evident that the most significant impact in reducing starts and stops occurs at 12GU conversion, with only marginal improvements when transitioning from 12GU to complete conversion (23GU). These findings highlight an important consideration: a partial conversion (12GU) may provide nearly the same benefits as a full conversion (23GU) at a lower cost, making it a more viable approach for practical implementation.

Thus, while the reduction in starts and stops is an important metric, future research should focus on other operational benefits of VSO, such as energy efficiency improvements, grid support capabilities, and maintenance cost reductions, to provide a holistic assessment of its economic and technical feasibility.

6.2.4. Power Redistribution Analysis

The implementation of VSO requires a strategic redistribution of power among the generating units to optimize efficiency and fully utilize the expanded operational range. This redistribution process ensures that the power demand is met while minimizing unnecessary start-top cycles, leading to more stable and efficient plant operation.

The logic behind the power dispatch algorithm was previously introduced in Section 5.2. Moreover, it is thoroughly detailed in Figure 11, which illustrates the step-by-step procedure used to dynamically adjust power allocation. The algorithm redistributes power by prioritizing variable speed units (VSUs) to maintain continuous operation, while fixed speed units (FSUs) are activated or deactivated as needed. This enables the system to strike a balance between efficiency and mechanical wear, ensuring a more uniform load distribution across the available generating units.

To illustrate the impact of this approach, this section presents graphical analyses of power redistribution across different scenarios. These analyses include comparisons of the number of operating units, power output adjustments, and average power per unit, demonstrating the algorithm's effectiveness in optimizing dispatch.

Additionally, operational points are analyzed before and after the redistribution process, followed by an evaluation of the universal diagram, which verifies the coherence and effectiveness of the operational adjustments.

6.2.4.1. Dispatch Algorithm

To evaluate the behavior and efficiency of the algorithm, we focus on May, the month with the highest incidence of starts (OPR) and stops (DCO) recorded in the dataset. Since the primary objective is to assess how the algorithm redistributes power while respecting the new VS operational limits, the month of May provides a representative case for comparing fixed-speed operation with the complete conversion to variable-speed operation scenario. Figure 50 presents a bar chart illustrating the number of starts and stops before and after the complete conversion of the plant to VS for May, where a reduction of 75 starts (34%) and 73 stops (33%) was observed when comparing both scenarios.

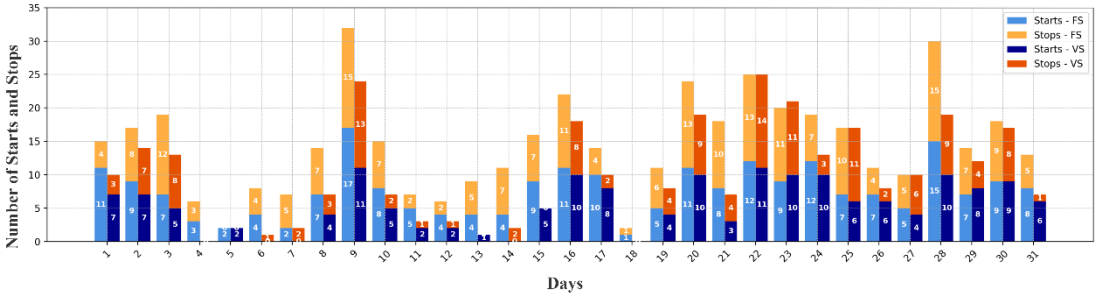

Figure 50 - Number of Starts and Stops (FS/VS): May 21.

This graphical representation highlights the daily variation in generator activations and deactivations, providing insights into how the VS operational strategy reduces the frequency of these transitions.

Figure 51 presents two key aspects of the power redistribution process in the context of FS and VS operations. The top subplot illustrates the number of operating units throughout the day for both cases, highlighting how the algorithm dynamically adjusts the number of active generating units. The results demonstrate that in the VS scenario, the algorithm aims to maintain a more stable number of operating units, minimizing unnecessary starts and stops. This behavior is evident in the VS curve, which exhibits fewer fluctuations compared to the FS case, where frequent transitions occur. By strategically controlling the number of operating units, the algorithm optimizes the dispatch process and reduces the operational stress on the turbines.

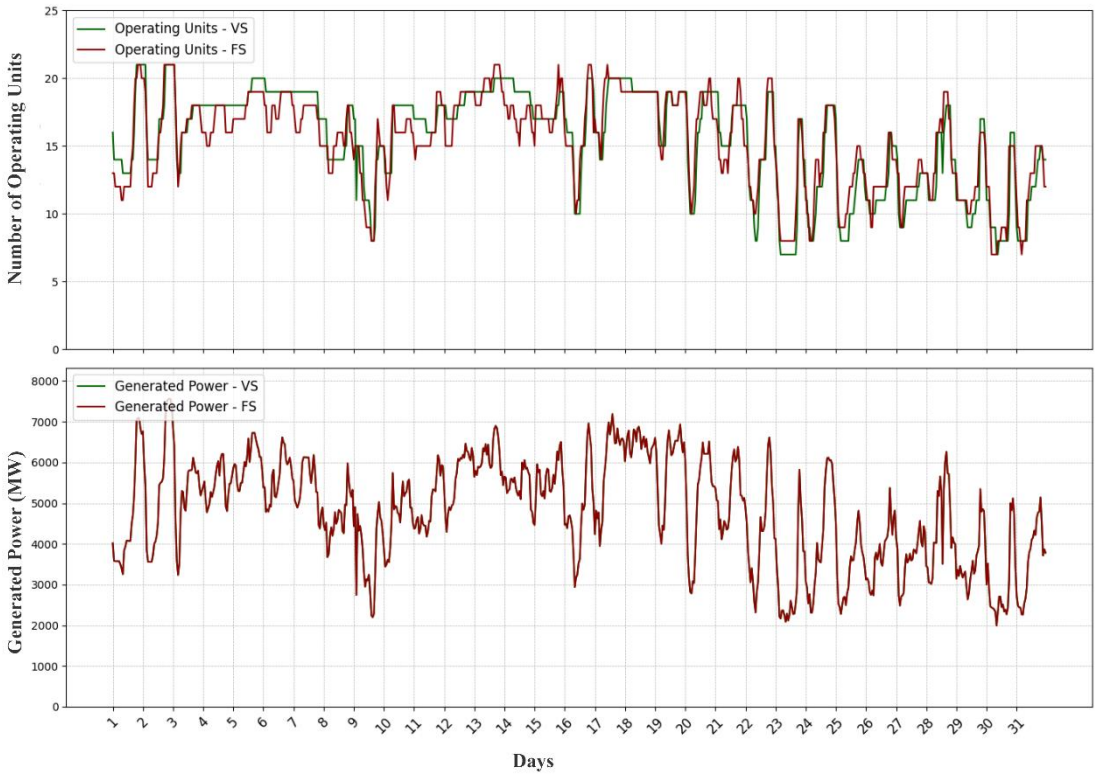

Figure 51 - Comparison of operating units and generating power: May.

The bottom subplot displays the total generated power for both FS and VS modes, confirming that the algorithm preserves the overall power output as expected. The nearly identical curves indicate that, despite variations in the number of active generating units, the total power generation remains unchanged. This consistency is crucial, as the methodology aims to simulate the baseline year while adjusting the dispatch strategy. The results reaffirm that the power redistribution algorithm effectively reallocates generation among available units while leveraging the expanded operational limits of VS to enhance stability and efficiency.

To further clarify the operational adjustments made by the algorithm, Figure 52 provides a detailed analysis for May 21st. This visualization enables a closer examination of the algorithm's real-time decision-making process for a single day. As seen in the figure, while the generated power remains constant, the green line (VS) exhibits a more stable trend compared to the red line (FS), indicating that the algorithm effectively reduces unnecessary startups and shutdowns. This demonstrates how the optimized

dispatch strategy under VS conditions enhances plant efficiency while ensuring that operational requirements are met.

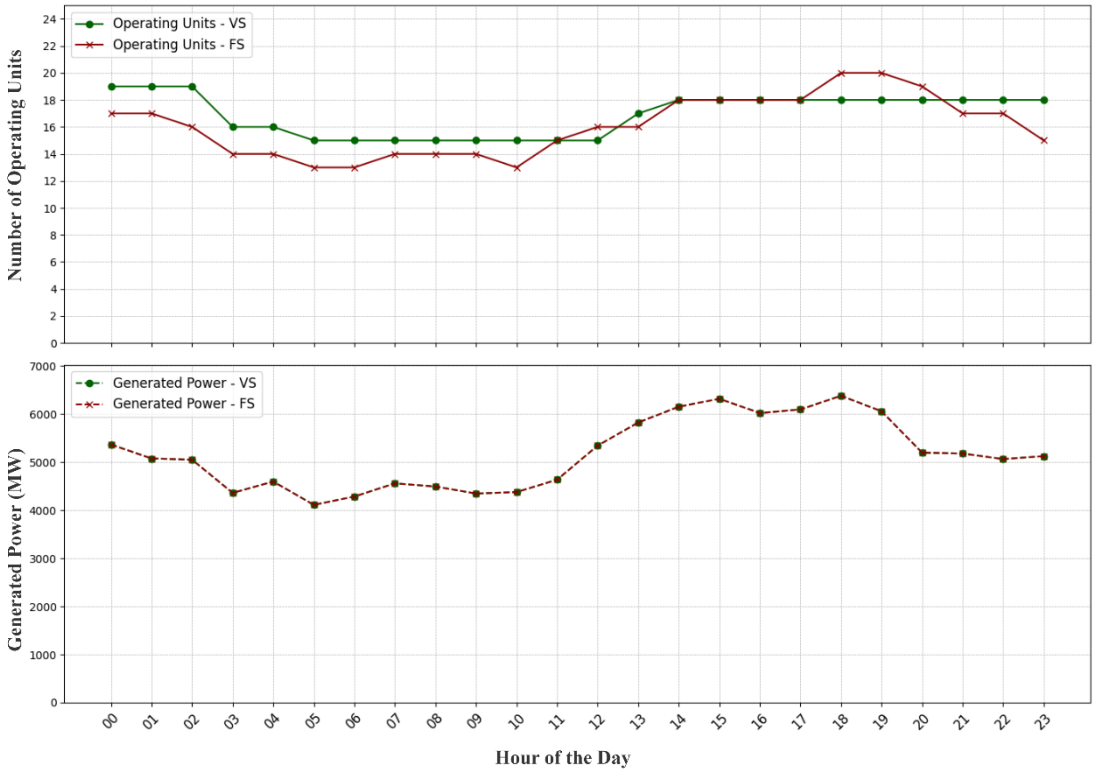

Figure 52 - Comparison of operating units and generating power: 21/05/21.

In addition, Figure 53 offers a more detailed perspective on how the balancing algorithm redistributes power to minimize starts and stops. The data shown are the same day, specifically May 21, 2021. The upper chart is the number of units operating for each hour of the day, and the lower chart is the average power per operating unit for this period.

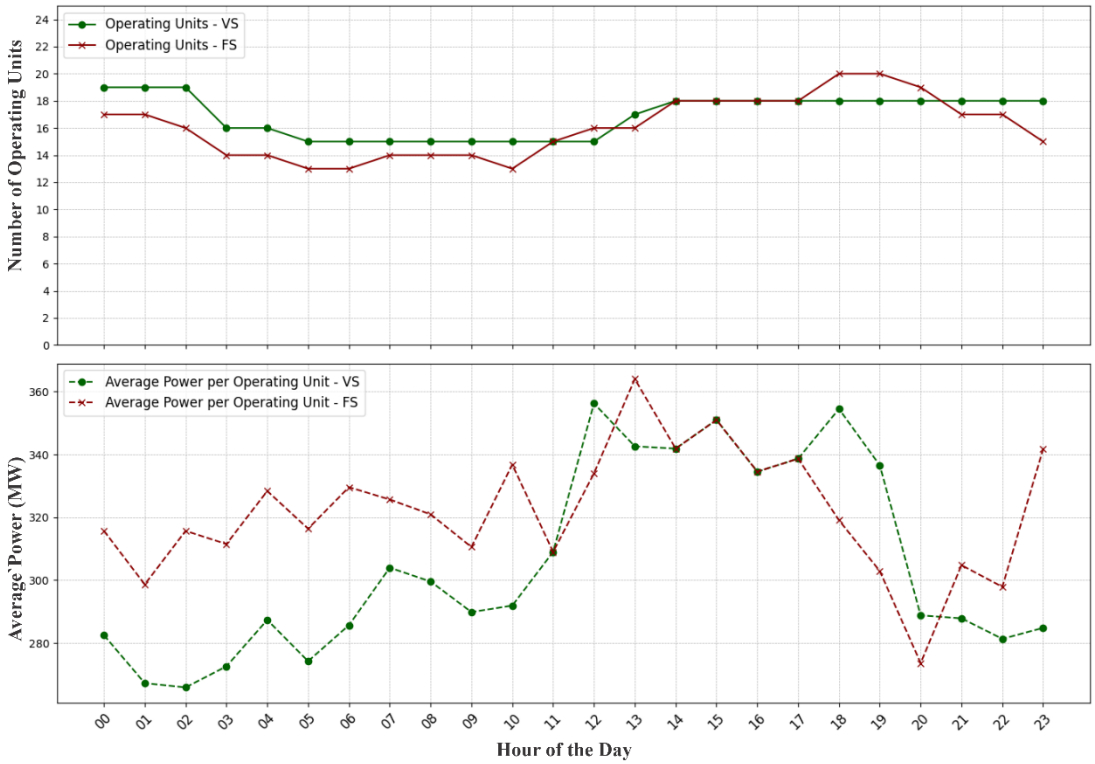

Figure 53 - Compaison of Operanting Units and Average Power: 21/05/21.

From these graphs, it is clear that the algorithm redistributes power effectively, eliminating unnecessary stops and starts. In cases where more power is needed, the average power per unit is a method for approaching the algorithm to drive the units to their upper operational limit. Moreover, vice versa, during a lower load period, the average power is decreased since it optimizes usage by moving to where each unit's lower operational bounds are utilized. Notably, units operating in VS mode exhibit significantly less variation throughout the day compared to those operating in FS mode, which is a much smoother and more stable mode of operation. On the other hand, the average power per unit in VS mode exhibits greater variability, which leverages the expanded operational range enabled by variable speed operation.

On this specific day, the advantages of VS mode are evident. If 10 starts and eight stops were recorded in FS mode and were reduced sharply to 3 starts and three stops upon entering VS mode, then a total reduction of 66% was achieved. The dynamic response of this adjustment demonstrates how VS mode maximizes flexibility, effectively controls

demand, and saves wear-in on the generators to attain their primary goal, which is to reduce starts and stops without compromising stability or efficiency at the hydro plant.

6.2.4.2. Operational Points

The following paragraphs discuss the operational points in different scenarios after the conversion to VSO. To provide better visualization and understanding, the graphs compare the operational points in the FS scenario with each of the VS scenarios, highlighting their respective operational areas. These comparisons demonstrate how the conversion to VS affects the operation of generating units and optimizes the plant's performance.

In Figure 54, the operational points for the FS scenario are compared with the scenario where three generating units from CFII are converted to VS. The graph clearly shows that only the CFII region contains points within the VS operational area. This result is expected, as only three generating units in CFII were converted to operate in VS. The operational points for these units remain within the maximum and minimum boundaries defined for VS mode, which minimizes variations in the number of units operating and, consequently, reduces the number of starts and stops.

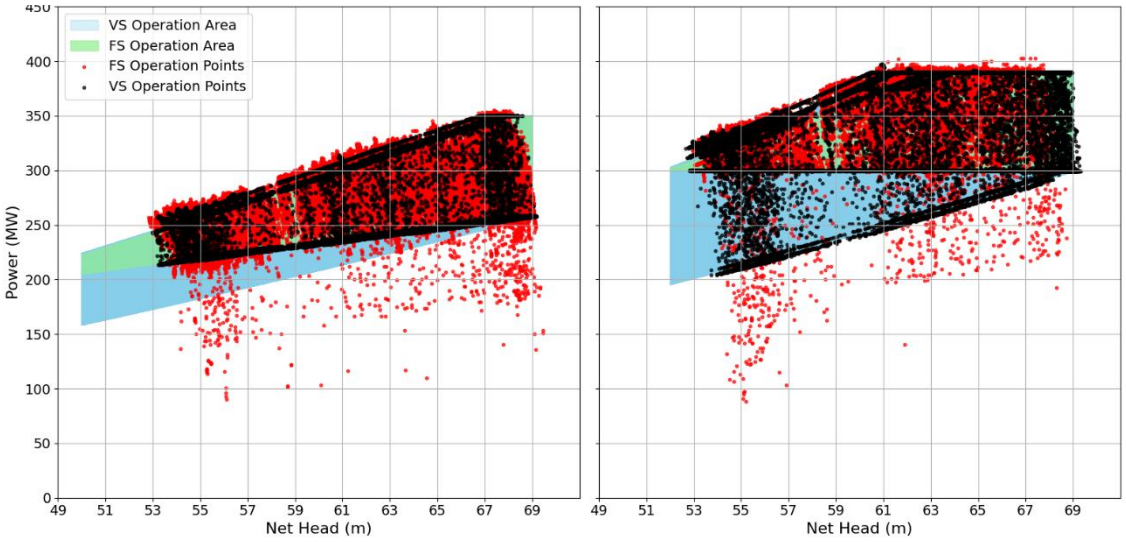

Figure 54 - Operational points: FS and 3GU-CFII.

In contrast, the operational points for CFI are entirely within the FS operational area in this scenario. Since no generating units from CFI were converted to VS, the algorithm

redistributes the load only within the FS operational limits of CFI. The absence of operational points in the VS area for CFI confirms that the VS functionality is effectively limited to the units that have been converted in CFII.

This figure demonstrates how the conversion to VS impacts the operation of the hydropower plant. The algorithm successfully redistributes the load to take full advantage of the expanded operational range offered by VS in CFII, while maintaining FS operation in CFI. This selective application of VS ensures operational efficiency and stability while gradually enhancing the flexibility of the plant as more units are converted in subsequent scenarios. The ability to adapt operational strategies to the constraints of each unit underscores the potential benefits of incremental conversion to VS.

Figure 55 and Figure 56 further analyze operational points comparing fixed speed operations with two partial variable speed operation scenarios: 6 generating units (6GU) and 12 generating units (12GU), respectively. These scenarios represent incremental conversion strategies, where half of the generating units which operate in variable speed are distributed across the two powerhouses: three in CFI and three in CFII for 6GU, and six in each powerhouse for 12GU. The graphs illustrate operational points distributed within the FS and VS regions, demonstrating how the algorithm efficiently manages the operational ranges.

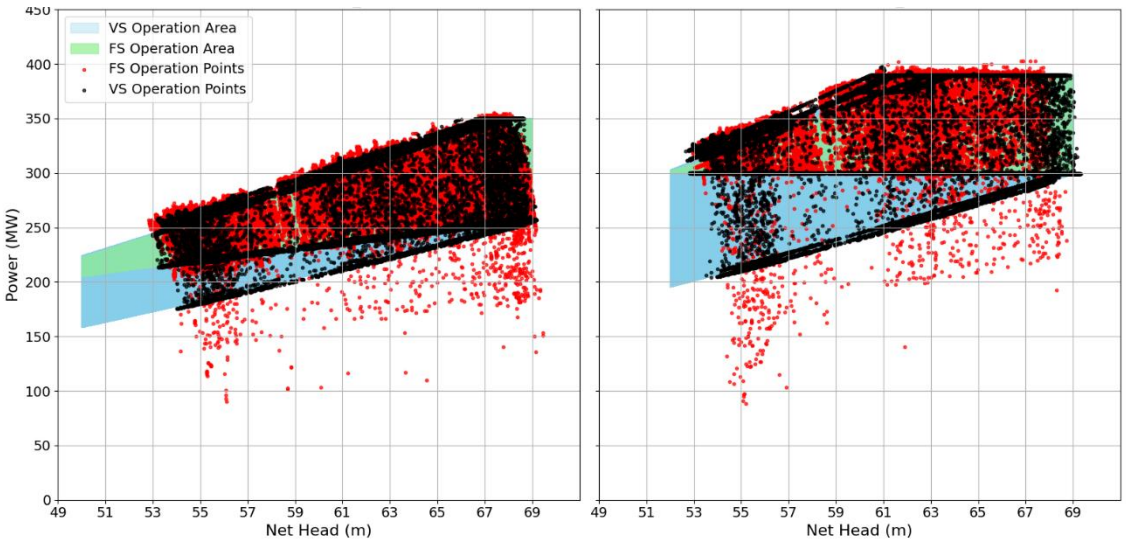

Figure 55 - Operational points: FS and 6GU.

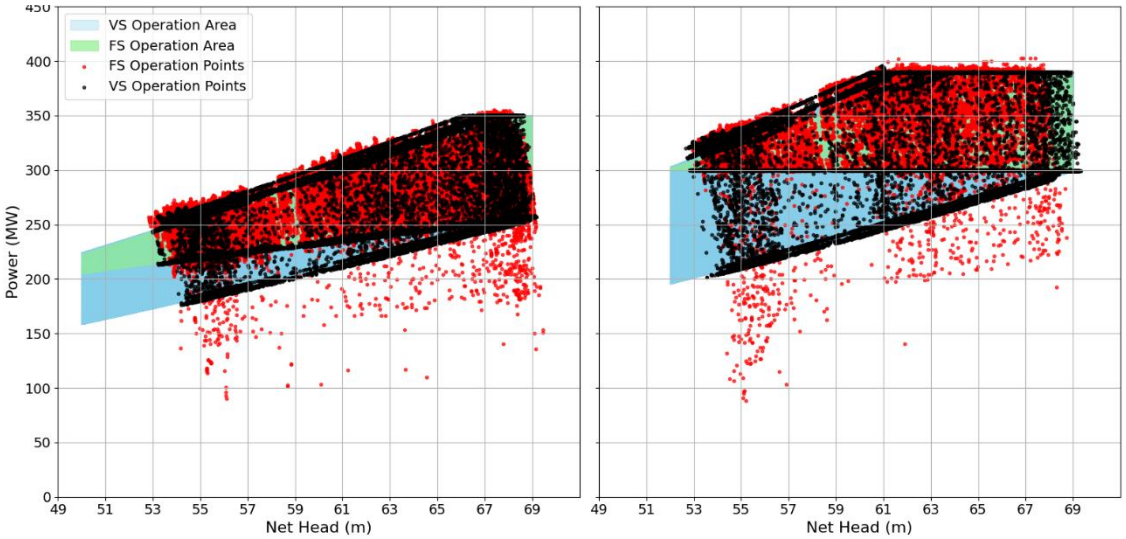

Figure 56 - Operational points: FS and 12GU.

In both scenarios, the algorithm aims to maximize operational stability by pushing the operational points closer to the boundaries of the permissible FS and VS regions. This strategy ensures that generating units avoid unnecessary starts and stops while maintaining energy production requirements. As seen in the 6GU scenario, operational points begin to populate the VS regions of both powerhouses as the algorithm adapts to the partial conversion setup (refer to Figure 55). Equilibrium becomes more complex in the 12GU scenario because the increased VS allows more freedom in managing operational stability; significant distributions can be seen at the boundaries of both FS and VS regions (see Figure 56).

Finally, Figure 57 illustrates the operational points of the hydropower plant after its complete conversion to variable-speed operation. From the graph, it is evident that there is a much greater concentration of operational points at or near the surface boundaries of the VSO region. This is entirely consistent with expectations because, in VSO, all generating units are fully capable of exploiting a much-widened operational range to balance power demands most effectively. The application of VSO strategically sets the operation of units within the prescribed limits of the extended range, ensuring that no superfluous starts and stops occur while maintaining maximum stability for operations.

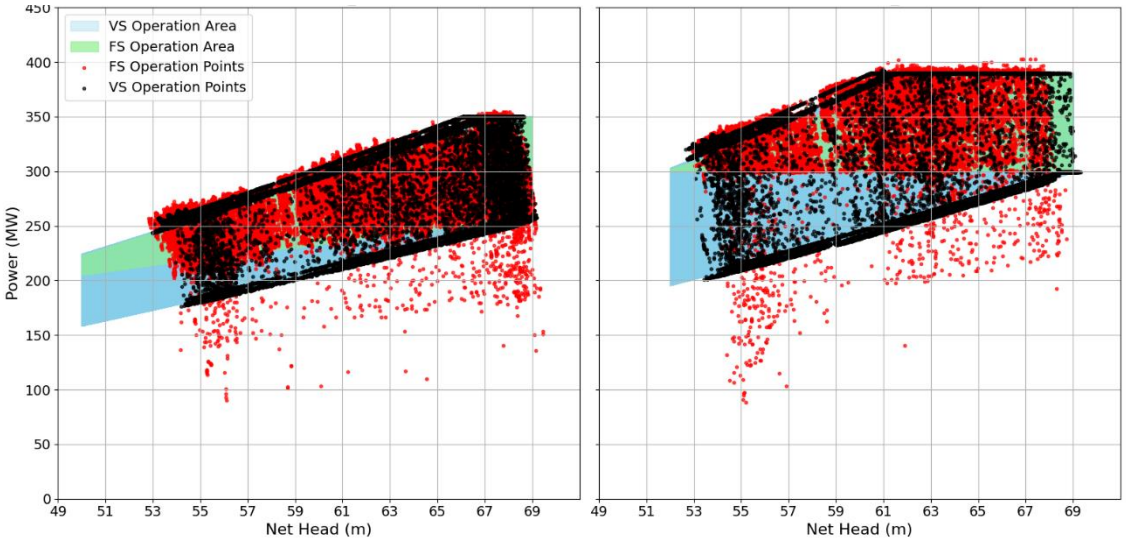

Figure 57 - Operational points: FS and 23GU.

6.2.4.3. Universal Diagram

As already mentioned, the universal diagram is a great analysis tool, and it can also be applied to analyze the behavior of the operating points in FS and VS by using the reduced equations shown in Section 5.3. The universal diagram holds special value for this assessment because the allowable operating area is the same for different speeds. This provides a good opportunity to clearly visualize how speed variation affects generating units. The n_{ED} axis which indicates specific speed is profoundly influenced by both rotational speed and net head at the operating point. Thus, enabling straightforward comparisons across diverse operating conditions.

Figure 58 gives the universal n_{ED} x P_{ED} diagram for a full month (September 2021), showing clearly the operational behavior of the units over this period. Operating points for CFI are given in Figure 58(a), while Figure 58(b) provides those for CFII. Figure 59 gives the universal diagram for a single day (December 16, 2021), allowing a much sharper view of operating points in a reduced time interval. This comparative approach brings out very clearly the impact of variable speed operation on both the distribution of operating points and the use made of the expanded operating range.

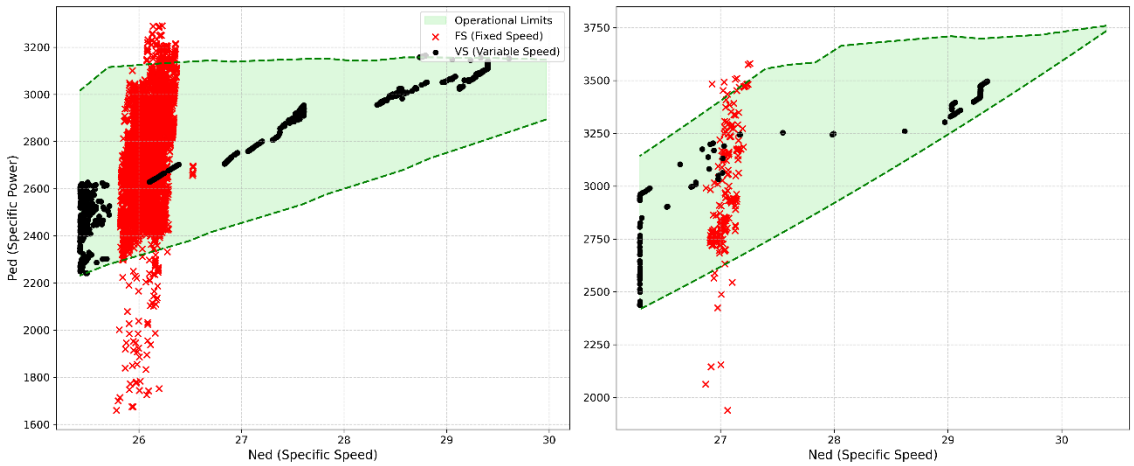

Figure 58 - Universal Diagram in FS and VS: Setember.

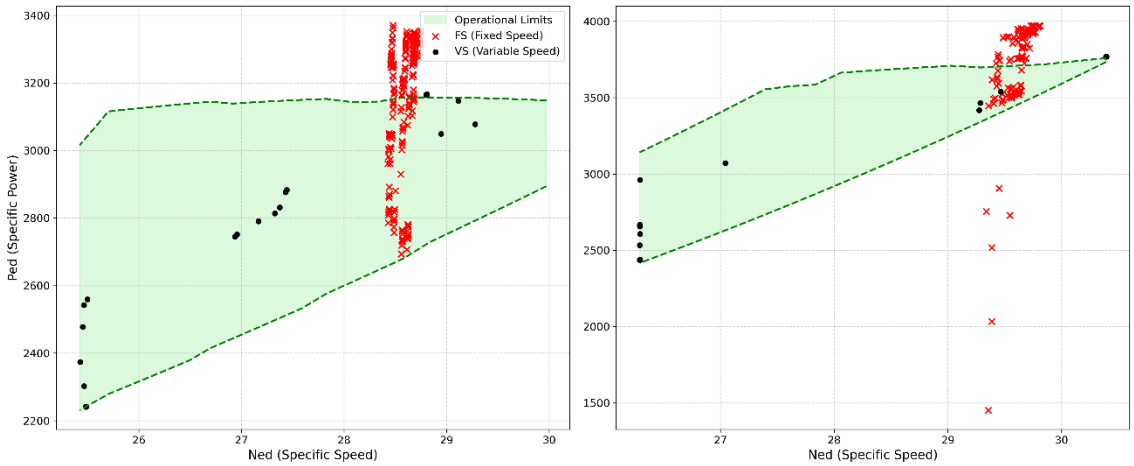

Figure 59 - Universal Diagram in FS and VS: 2021-12-16.

In FSO, where the speed of rotation remains constant, the operating points tend to be more concentrated on the x-axis. In variable-speed operation, however, the dispersion of points on the x-axis is greater because the speed of rotation can be adjusted according to different operational needs. This illustrates the greater flexibility that variable-speed control can provide and the broader distribution of operating points within the viable region of the universal diagram.

Moreover, this operational strategy also offers the added advantage of reducing the occurrence of points outside the permissible operating limits, which can lead to harmful conditions such as cavitation or excessive mechanical stress. Although addressing cavitation is not the primary focus of this study, the results highlight the potential of VSO to enhance operational safety by reducing the frequency of such extreme operating points.

To summarize, the implementation of VSO proves highly advantageous for hydropower operations, as demonstrated by this study. Significant benefits include a reduction in starts and stops, increased flexibility of unit operation within the expanded range, and a practical power redistribution strategy that enhances overall plant efficiency. Detailed conclusions will be presented in the next section; however, the installation of VSO not only improves the operation's performance but also lays the basis for addressing much broader challenges in hydropower generation.

6.3. CAVITATION MINIMIZATION ANALYSIS

This part of the study investigates whether VSO can also be used to mitigate cavitating operation of the Francis units. The methodology described in Section 4.4 is now applied to the historical hourly records of 2021 for unit UG2 in the first powerhouse of the Tucuruí hydropower plant. Starting from the measured discharge, net head, tailwater level and active power, each operating point is first classified in terms of cavitation risk in the σ–N_s plane. Then, for the hours that fall inside the cavitation risk region, alternative operating points are generated by locally adjusting discharge and rotational speed within the admissible operating envelope, while preserving the original generation schedule as closely as possible.

Five mitigation strategies are considered, combining different sequences of discharge and speed adjustments: the Q-only strategy, which keeps speed fixed and perturbs the guide-vane opening; the N-only strategy, which varies the rotational speed within the VSO capability; the sequential strategies N→Q and Q→N, which combine both types of adjustment; and the Best-of-all strategy, which selects, for each cavitating hour, the most effective candidate among all strategies according to the criteria defined in Section 4.4. For a given power-deviation tolerance ΔP_{max}, the effectiveness of each strategy is measured by the reduction in the number of cavitating hours. The following subsections first characterize the baseline cavitation behavior of UG2 and then quantify the performance of the mitigation strategies.

6.3.1. Identification of cavitating operating points

The first step consists in applying the detection procedure of Section 4.4.1 to all historical operating points of UG2 in 2021. For each hour, the Thoma cavitation coefficient σ and the specific speed N_s are computed from the measured discharge, net head and tailwater level, using the suction-side energy balance and the reference levels illustrated in Figure 12. The pair (σ, N_s) is then compared with the empirical cavitation envelope derived from Arndt's diagram, represented by the lower and upper bounds $\sigma_{low}(N_s)$ and $\sigma_{up}(N_s)$. Points that fall below the lower curve are associated with unacceptable cavitation, points above the upper curve are considered safe, and the band in between is interpreted as a region of light or intermittent cavitation, here referred to as "risk band".

Figure 60 shows the resulting σ–N_s scatter plot for all 5,335 hourly operating points of UG2. The lower and upper Arndt limits are plotted as continuous lines, while the operating points are coloured according to their classification. Green markers correspond to points that lie above $\sigma_{up}(N_s)$ and are therefore considered safe. Red markers represent the hours that fall inside the risk band between $\sigma_{low}(N_s)$ and $\sigma_{up}(N_s)$, where cavitation is expected to be mild but recurrent. For this data set no points fall below the lower limit, indicating that the unit does not systematically operate in regimes of severe cavitation, but it does spend a non-negligible fraction of the year in conditions where cavitation may occur intermittently.

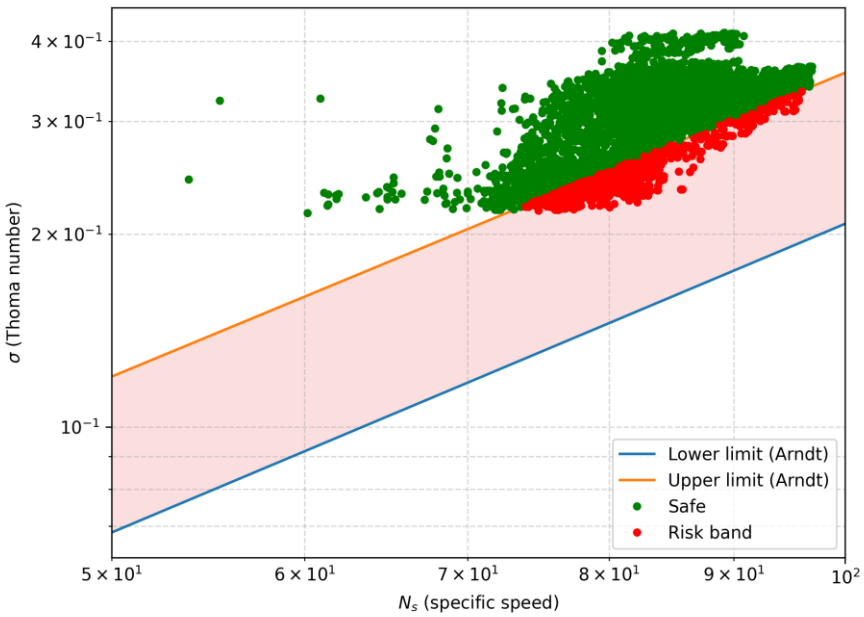

Figure 60 - Cavitation classification of UG2 operating points in the σ–N_s plane (2021).

Table 4 summarises the classification statistics. Out of 5,335 hourly records, 881 points (16.51 %) are located in the cavitation risk band, while 4,454 points (83.49 %) are in the safe region of the σ–N_s plane. These figures provide the reference against which the performance of the mitigation strategies will be evaluated in the next subsections: any successful strategy should aim at moving a significant portion of these 881 risk-band hours into the safe region, without violating the power-balance and operating constraints of the plant.

Table 4 - Classification of operating points in the safe and cavitation-risk region for UG2 (2021).

Status	***Count***	***Percent***
Risk-band	*881*	*16,51*
Safe	*4454*	*83,49*
Total	*5335*	*100*

A natural complement to the σ–N_s diagram is to visualize the same operating hours in the reduced-variables plane associated with the universal hill chart. Figure X projects all 2021 operating points of UG2 onto the *speed factor* $N_{ed}$and *discharge factor* Q_{ed}. Each point is coloured according to the cavitation classification obtained from the σ–N_s envelope: green markers represent operating conditions classified as safe, whereas red markers correspond to hours lying in the cavitation-risk band.

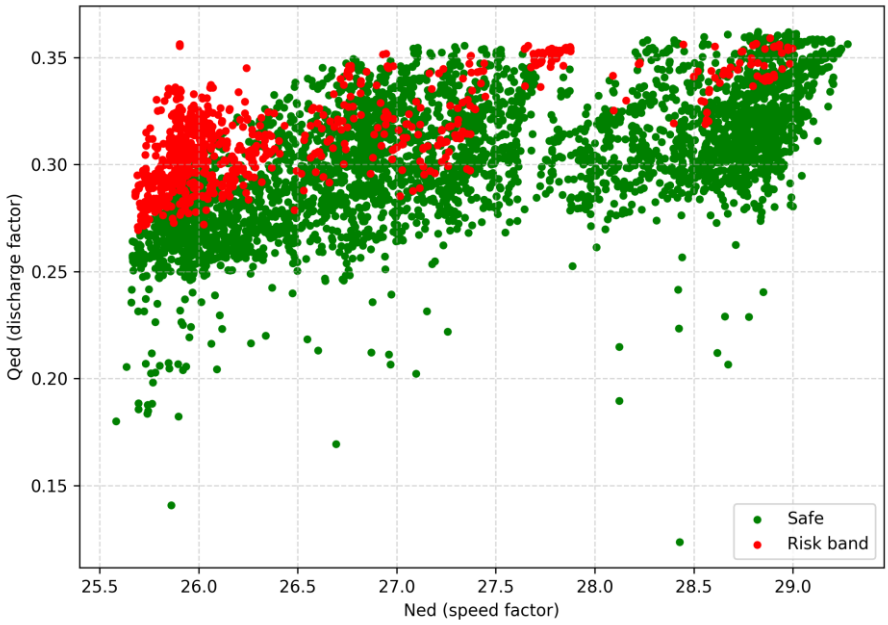

Figure 61 - Distribution of safe and cavitation-risk operating points of UG2 in the universal diagram.

This representation shows that cavitation is not randomly distributed over the operating range, but tends to cluster in specific regions of the universal diagram. The red points are concentrated in relatively narrow bands of $Q_{\mathrm{ed}}$and N_{ed}, corresponding to medium–high discharge factors and speed factors close to the normal operating region. In contrast, the low-discharge region of the diagram is practically free from cavitation-risk points. This behaviour indicates that the occurrence of cavitation is linked to particular combinations of head, discharge and speed, rather than to all partial-load conditions, and it also highlights where the mitigation strategies must act: by slightly shifting the operating point in $Q_{\mathrm{ed}}$and/or N_{ed}so as to move it away from the red bands while remaining inside the admissible hill-chart envelope.

6.3.2 Performance of mitigation strategies for different power tolerances

The mitigation algorithm was applied to all cavitating hours identified for UG2, considering the four basic strategies (Q, N, NQ and QN) and the combined *Best-of-all* option. To analyze the trade-off between cavitation reduction and adherence to the original generation schedule, three values of the active-power tolerance ΔP_max were tested: 0%, 2% and 4% of the historical hourly power.

For each tolerance level, the performance of the strategies is evaluated in two complementary ways:

- by inspecting the displacement of operating points in the σ–N_s plane, where each strategy is represented by “success” markers (points moved to the safe region) and “fail” markers (points that remain in the cavitation risk band);
- by assessing the corresponding displacement in the universal diagram (N_ED-Q_ED), highlighting how the successful candidates are reallocated in terms of non-dimensional speed and discharge.

The percentages reported below refer to the fraction of cavitating hours that are moved to the safe region for each strategy.

6.3.2.1. Zero power tolerance (ΔPmax = 0%)

With zero power tolerance the mitigation problem is strongly constrained, since the active power of UG2 must remain exactly equal to the historical value for every hour. Under this condition the success rates of the four strategies are:

- Q strategy: 0.0% of cavitating hours moved to the safe region;
- N strategy: 18.04% safe;
- NQ strategy: 18.04% safe;
- QN strategy: 13.73% safe.

Figure 62(a–d) summarizes the behavior of each strategy in the σ–Ns plane. In panel (a), the Q-only strategy is essentially inactive: any change in discharge immediately produces a power deviation and therefore violates the ΔPmax = 0% constraint, so all cavitating points remain inside the Arndt risk band. Panels (b)–(d) show that only the strategies that exploit speed variation are able to move points upwards in σ. The N strategy, Figure 62(b), uses the VSO band to search for alternative rotational speeds that keep power constant while increasing σ. This allows approximately 18% of the originally cavitating hours to cross the lower Arndt limit. Because no power margin is available for a subsequent discharge refinement, the NQ strategy effectively collapses to the N strategy, leading to the same success rate [Figure 62(c)]. The QN strategy, Figure 62(d), performs slightly worse (≈14% safe): its first Q-search is heavily penalized by the zero-tolerance constraint, which limits the number of feasible candidates that can later be improved by a speed adjustment.

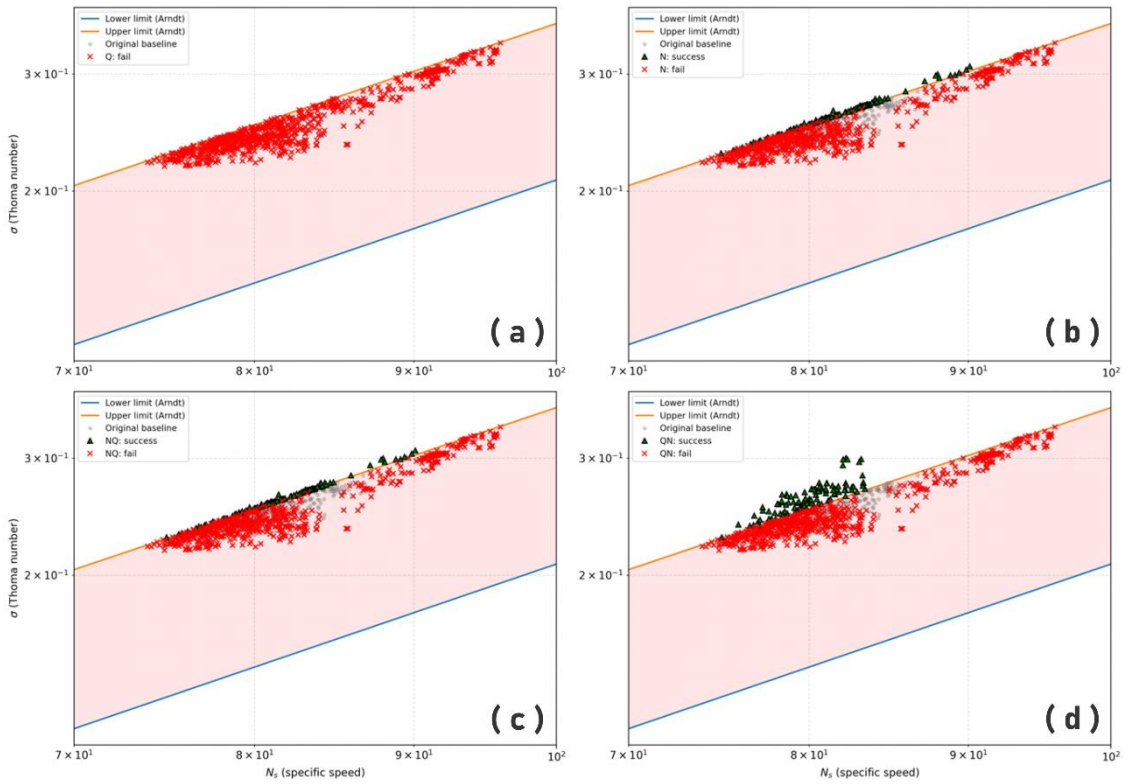

Figure 62 - Cavitation-mitigation results for ΔPmax = 0% in the σ–N_s plane: (a) Q strategy; (b) N strategy; (c) NQ strategy; (d) QN strategy.

The overall performance of the Best-of-all strategy for ΔPmax = 0% is depicted in Figure 63. In the σ–Ns diagram [Figure 63(a)], all successful points (green triangles) lie just above the Arndt lower boundary, indicating modest but effective increases in σ with negligible distortion of the original operating pattern. The corresponding universal diagram in terms of Ned and Qed [Figure 63(b)] confirms that the adjustments in speed factor and discharge factor are small and remain close to the historical trajectories. These results show that, even without any flexibility in active power, variable-speed operation alone can already mitigate cavitation for a non-negligible fraction of hours; however, the achievable reduction is intrinsically limited when ΔPmax = 0%.

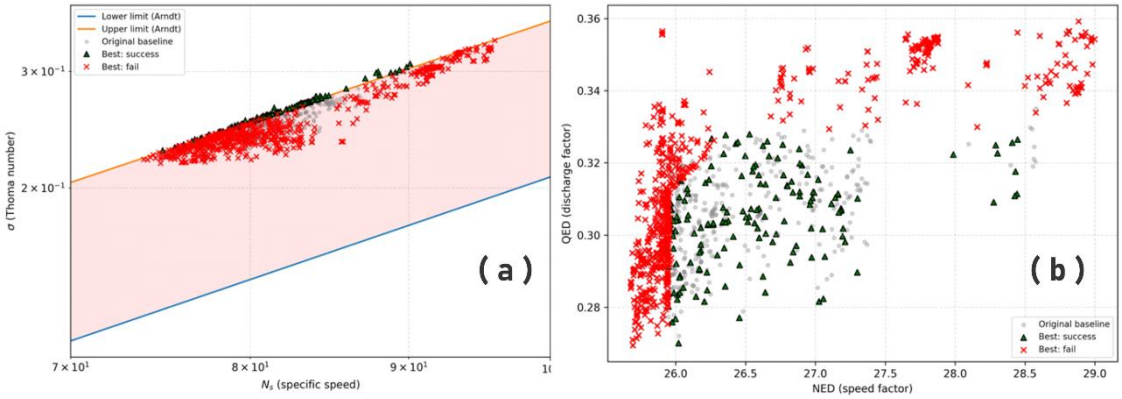

Figure 63 - Best-of-all solution for ΔPmax = 0%: (a) σ–Ns diagram; (b) corresponding operating points in the universal Ned x Qed diagram.

6.3.2.2. Moderate power tolerance (ΔPmax = 2%)

Allowing a ±2% deviation in active power relaxes the optimization problem and enables the strategies to explore a larger neighborhood around each historical operating point. Under this moderate tolerance the fraction of initially cavitating hours that can be moved to the safe region increases markedly:

- Q strategy: **34.50% safe**
- N strategy: **25.65% safe**
- NQ strategy: **45.17% safe**
- QN strategy: **39.04% safe**
- Best-of-all strategy: **64.81% safe**

Compared with the zero-tolerance case, the Q-only strategy becomes effective: small changes in discharge are now admissible without violating the power constraint, so that roughly one third of the cavitating hours can be pushed above the Arndt lower limit. The N-only strategy still relies exclusively on speed adjustments and achieves a more modest improvement (≈26% safe), confirming that discharge has a stronger leverage on σ than speed when a limited power margin is available.

The combined strategies NQ and QN provide the best individual performance. In NQ, the first step in N relocates the operating point towards a region more favorable to cavitation, and the subsequent Q refinement exploits the remaining power margin to further increase σ; this yields **45.17%** safe hours. In QN, the sequence is reversed: a primary adjustment in discharge is followed by a secondary tuning in speed, resulting in

39.04% safe hours. The slightly superior performance of NQ indicates that pre-positioning the point in σ–Ns through speed may facilitate a more efficient discharge correction. Figure 64(a–d) summarizes these results in the σ–Ns plane for ΔPmax = 2%. Each panel shows the Arndt envelope, the original cavitating baseline, and the outcome of one mitigation strategy: (a) Q-only; (b) N-only; (c) NQ; (d) QN.

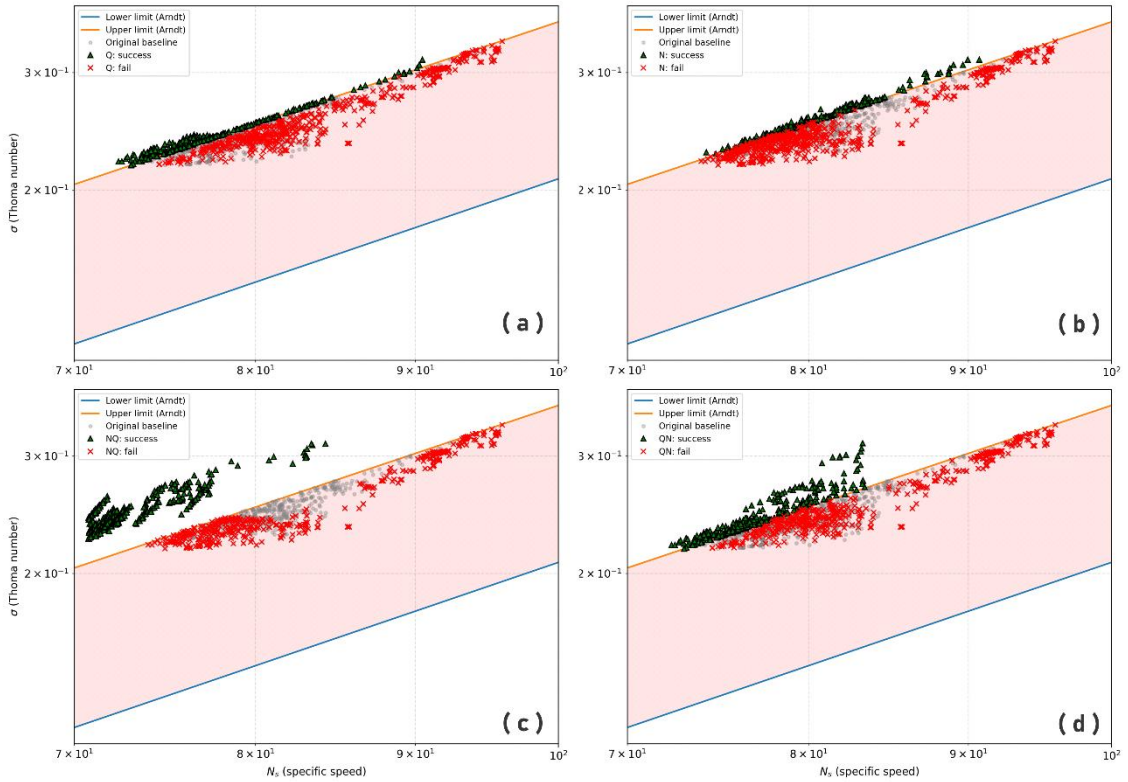

Figure 64 - Cavitation-mitigation results for ΔPmax = 2% in the σ–N_s plane: (a) Q strategy; (b) N strategy; (c) NQ strategy; (d) QN strategy.

Green triangles denote successful mitigations (points moved to the safe region), while red crosses correspond to residual cavitating hours. One can see that the Q and QN strategies mainly act along the upper branch of the envelope, adjusting Q at nearly constant Ns, whereas N and NQ redistribute points more broadly in Ns, especially in the mid-range of the diagram.

When all strategies are combined, the Best-of-all solution exploits the most advantageous adjustment for each hour, reaching **64.81%** of cavitating hours mitigated. Figure 65(a–b) illustrates this final outcome. Panel (a) shows the σ–Ns diagram, where most of the originally cavitating points are replaced by green markers located well above

the lower Arndt limit, leaving only a relatively small cluster of red crosses close to the boundary. Panel (b) displays the corresponding positions in the universal diagram (Ned-Qed): the successful points concentrate along narrow bands that remain close to the original operating trajectories, indicating that the mitigation can be achieved with moderate adjustments in both discharge and speed, without pushing the unit to extreme regions of the hill chart.

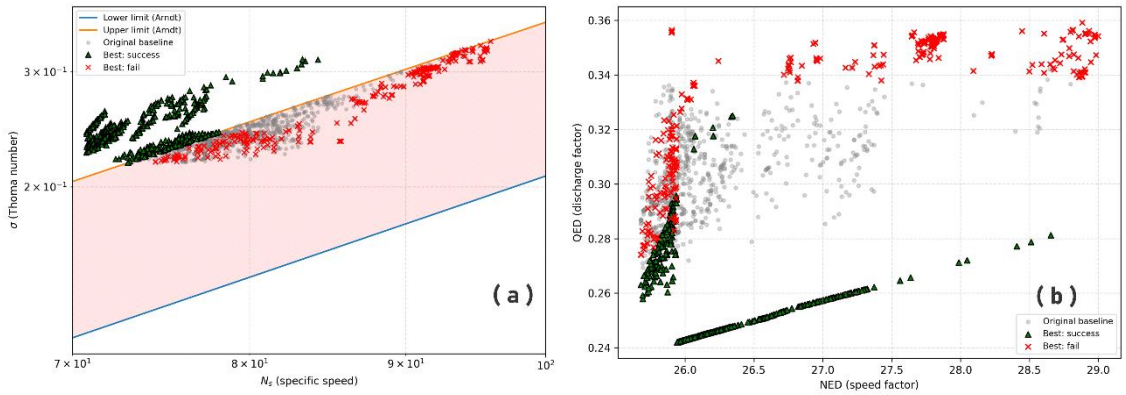

Figure 65 - Best-of-all solution for ΔPmax = 2%: (a) σ–Ns diagram; (b) corresponding operating points in the universal Ned x Qed diagram.

6.3.2.3. High power tolerance (ΔPmax = 4%)

Allowing a 4% deviation in active power gives the mitigation algorithm considerably more freedom to move each historical point in the σ–Ns plane. Under this condition, the performance of the strategies is:

- **Q strategy:** 55.50% of the cavitating hours moved to the safe region;
- **N strategy:** 37.91% safe;
- **NQ strategy:** 53.46% safe;
- **QN strategy:** 56.75% safe;
- **Best-of-all strategy:** 74.77% safe.

The σ–Ns diagrams in Figure 66**(a–d)** illustrate the behavior of the four individual strategies for ΔPmax = 4%.

- In Figure 66(a), the Q strategy now becomes highly effective: by moving the operating point along the discharge direction, while respecting the 4% power band, more than half of the originally cavitating hours are shifted above the Arndt

lower limit. The successful points (green triangles) accumulate just above the lower boundary, following the historical cloud.

- Figure 66(b) shows the N strategy, which relies exclusively on speed adjustment. Even with the enlarged power margin, its effect remains more modest (≈38% safe), because at high specific speeds the σ–Ns envelope is relatively steep and the available VSO band is limited.
- In Figure 66(c), the NQ strategy first moves points in speed (N) and then refines discharge (Q). This combination generates a dense cluster of successful points well above the lower σ-limit, but some operating hours remain trapped in the risk band due to simultaneous cavitation and power constraints.
- Figure 66(d) presents the QN strategy, which starts from a Q-adjustment and then exploits the speed degree of freedom. This ordering proves slightly more efficient, yielding 56.75% safe hours and pushing successful points farther away from the cavitation boundary.

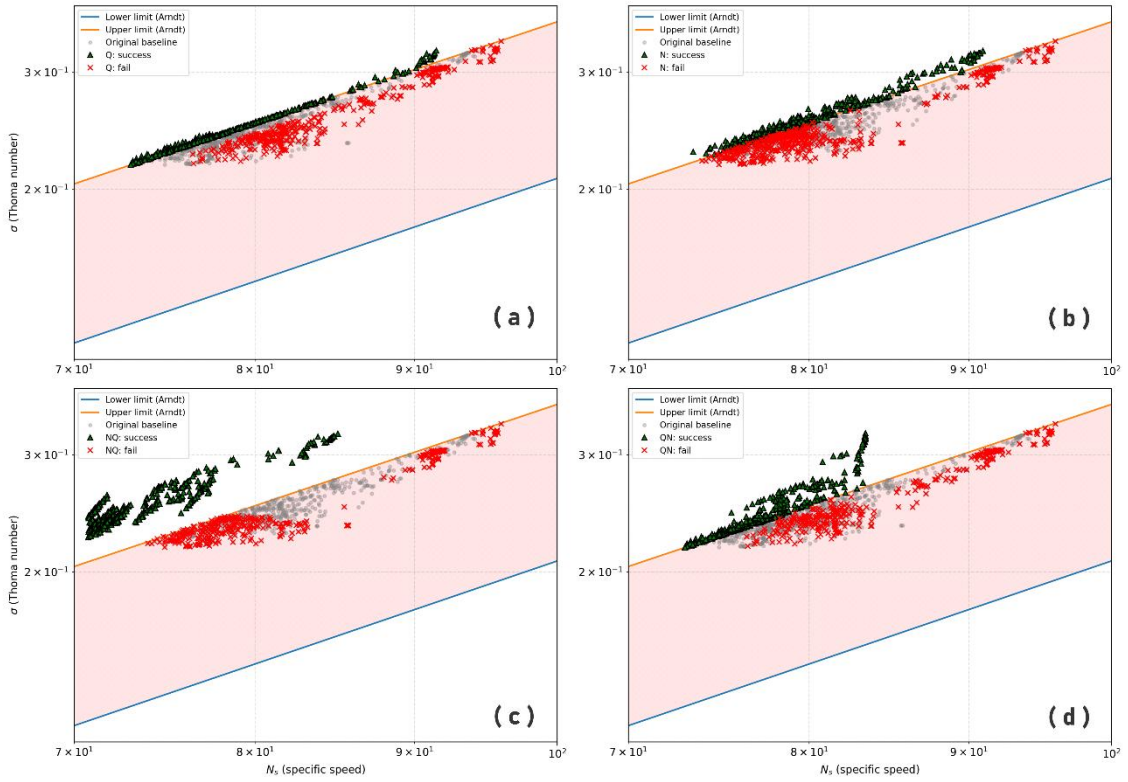

Figure 66 - Cavitation-mitigation results for ΔPmax = 4% in the σ–N_s plane: (a) Q strategy; (b) N strategy; (c) NQ strategy; (d) QN strategy.

The global outcome of the optimization for ΔPmax = 4% is summarized in Figure 67(a–b) for the Best-of-all strategy.

- Figure 67(a) shows the σ–Ns distribution after selecting, for each hour, the best candidate among Q, N, NQ and QN. Approximately 75% of the initially cavitating hours are now relocated to the safe region, forming a clear band of green triangles above the Arndt lower limit, while only a small fraction of red crosses remains in the transition zone.
- Figure 67(b) displays the same Best solution in the universal diagram (Ned x Qed). The optimized points concentrate along two main operating branches, indicating that the mitigation algorithm preserves realistic dispatch patterns while slightly reducing discharge and/or speed in the most critical regions.

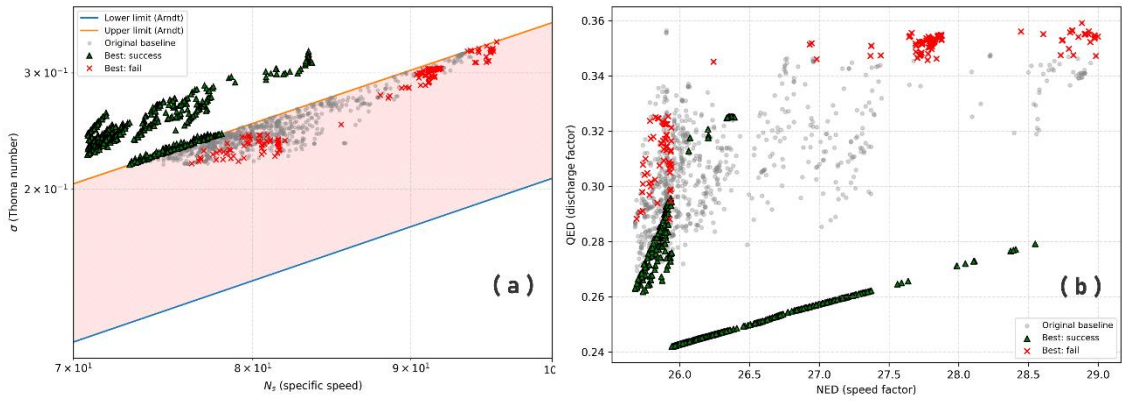

Figure 67 - Best-of-all solution for ΔPmax = 4%: (a) σ–Ns diagram; (b) corresponding operating points in the universal Ned x Qed diagram.

Overall, the 4% power tolerance nearly doubles the cavitation mitigation achieved with ΔPmax = 2%, and brings the Best-of-all strategy close to the practical saturation point: additional increases in ΔPmax would yield diminishing returns compared with the extra flexibility required from the remaining units in the plant.

6.3.2.4. Global influence of power tolerance on cavitation mitigation

The previous subsections analyzed in detail the behavior of each mitigation strategy for selected power-tolerance levels (0, 2 and 4%). To complete the assessment, Figure 68 summarizes the overall performance of the strategies as a function of the admissible power deviation ΔPmax, varying from 0 to 10%. The vertical axis represents the

percentage of originally cavitating hours that are successfully moved to the safe region of the σ–Ns diagram.

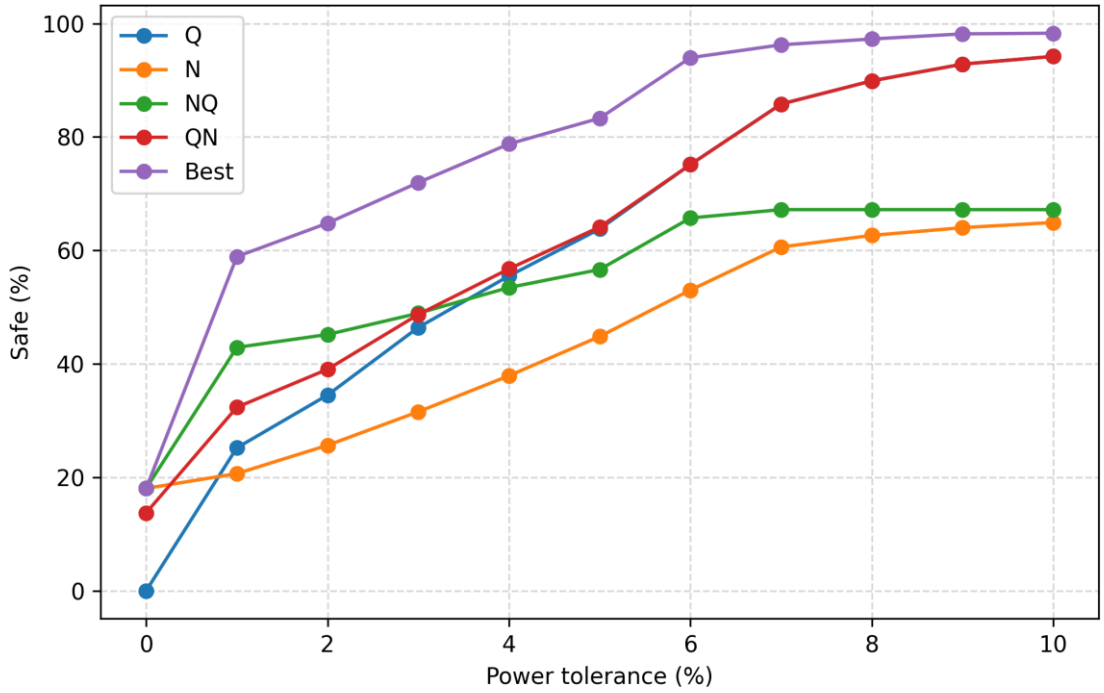

Figure 68 - Cavitation-mitigation results for ΔPmax = 2% in the σ–N_s plane: (a) Q strategy; (b) N strategy; (c) NQ strategy; (d) QN strategy.

At ΔPmax = 0%, the curves reproduce the behavior discussed in Section 6.3.2.1: the Q strategy is inactive, whereas the N and NQ strategies mitigate cavitation for about 18% of the hours and QN reaches roughly 14%. As soon as a small tolerance of 1% is allowed, all strategies exhibit a marked improvement. The Q strategy rises to about 25% safe hours, N and QN reach values close to 20–35%, and NQ approaches 45%. The Best-of-all curve responds even more sharply, jumping to almost 60% reduction with only 1% deviation in power, confirming that a modest degree of operational flexibility already enables significant mitigation.

Between ΔPmax = 2% and 4%, the individual strategies continue to improve almost linearly with the tolerance. The Q and NQ curves converge to values slightly above 50% at 4%, while QN becomes the most effective among the single strategies, exceeding 55%. In this same range, the Best-of-all solution climbs from about 65% to nearly 80% safe hours, corroborating the detailed analysis of Section 6.3.2.3 and indicating that a 3–4%

tolerance represents a particularly efficient operating point in terms of cavitation reduction versus power deviation.

For tolerances above 5–6%, the curves start to show diminishing returns. The N strategy remains the least effective, saturating around 65% safe hours. Q and NQ approach values close to 67–68%, with limited gains beyond 7–8%. The QN strategy, on the other hand, continues to benefit from the extra flexibility, reaching more than 90% safe hours at ΔPmax = 10%. The Best-of-all curve, which always envelops the others, increases rapidly up to about 95–96% at 6–7% and then asymptotically approaches ~98% for the largest tolerances, indicating that almost all cavitating hours can be eliminated if the plant is willing to accept larger redistributions of power among units.

From a practical point of view, Figure 68 highlights three main insights:

- **Variable speed is effective even with tight dispatch**: at ΔPmax = 0–1%, the combination of speed and discharge adjustments already removes 60% of cavitating hours in the best configuration, with minimal impact on the power schedule.
- **There is a favorable compromise region**: tolerances around **3–4%** allow 70–80% mitigation with relatively small deviations in unit power, which are generally manageable at plant level.
- **Beyond 6–7% tolerance, the marginal benefit decreases**: although QN and Best still improve, the incremental reduction in cavitation becomes small compared with the additional flexibility required from the remaining units.

Overall, the power-tolerance study confirms that **VSO combined with modest discharge adjustments can substantially reduce cavitating operation**, and that the proposed optimization framework offers a tunable compromise between cavitation mitigation and adherence to the original generation schedule.

6.4. ANALYSIS ON INCREASE IN ENERGY GENERATION

This subsection quantifies the potential gains in annual energy production associated with the introduction of VSO in the 200 MW case-study plant. Building on the new operational ranges presented in Section 6.1.2, two distinct operating strategies are evaluated. In both cases, the historical hydraulic conditions of 2021 are preserved, so that

any change in energy production can be attributed solely to the enlarged operating region provided by VSO and to the adopted dispatch policy.

Before introducing the VSO-based scenarios, it is useful to characterize the historical reference against which all gains are measured. Figure 69 presents the monthly total generation of the plant in 2021 for the BASE case. without VSO and without any modification of the original dispatch strategy. The plot highlights the seasonal pattern of the plant, with moderate production in the first half of the year and a marked increase in August and September, followed by a return to intermediate levels towards the end of the year.

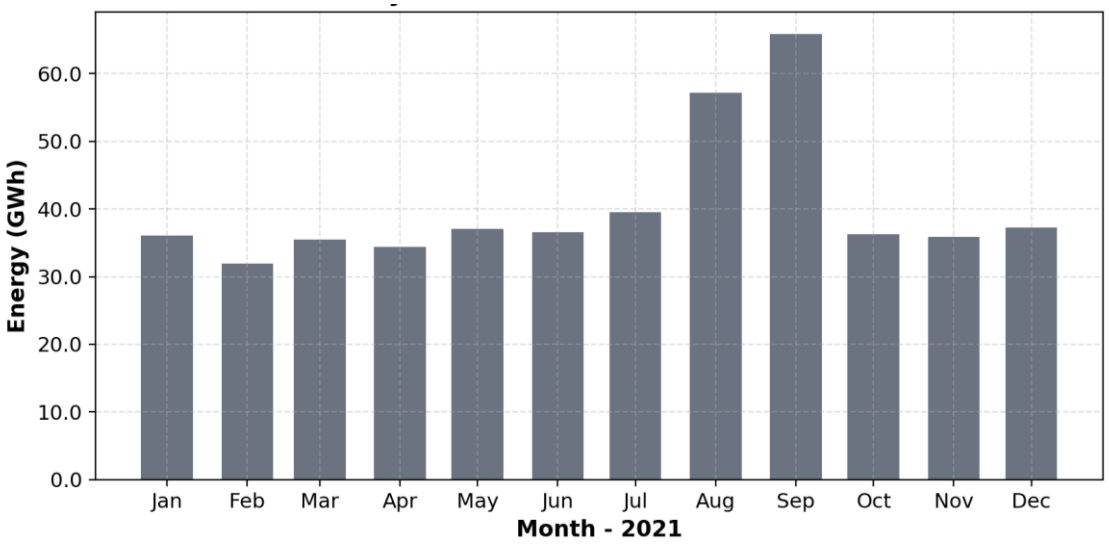

Figure 69 - Monthly total historical generation in 2021 (BASE case).

Figure 70 decomposes the same historical generation into the contributions of UG1 and UG2. The monthly profiles of the two units are broadly similar, but with noticeable differences in specific months that reflect the original unit-commitment decisions and maintenance outages. These two plots define the baseline energy production against which the incremental gains of the subsequent VSO scenarios are computed.

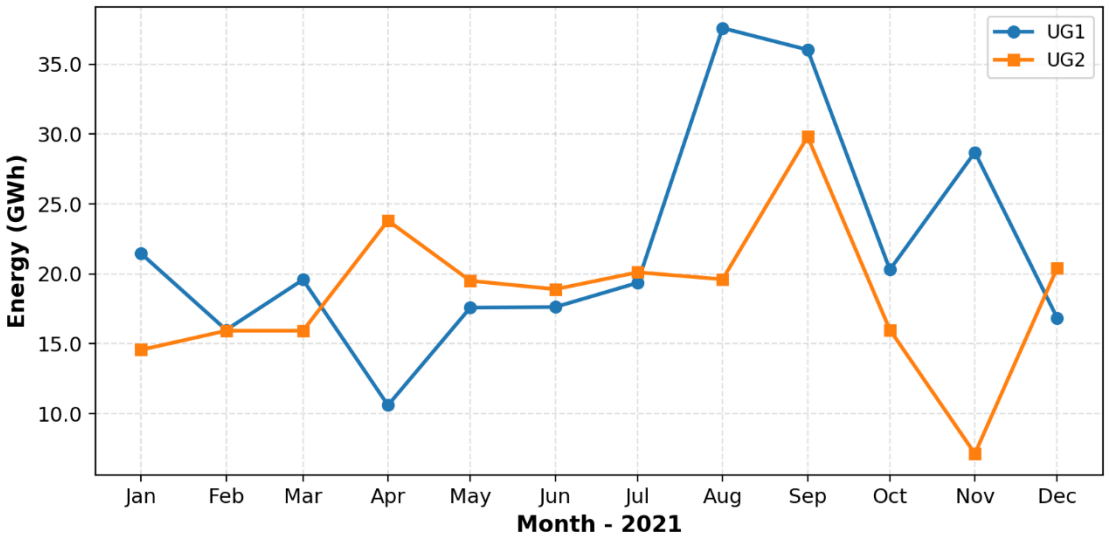

Figure 70 - Monthly historical unit generation in 2021 (BASE case).

In Scenario 1, the plant is virtually retrofitted to VSO while keeping the original fixed-speed dispatch strategy: the same unit commitment and the same hourly discharge schedule are maintained, and only the efficiency improvement provided by VSO is exploited. In Scenario 2, the additional flexibility offered by the VSO region is combined with an optimized redistribution of power between the units, aiming at maximizing energy production within the admissible H-Q envelope. For each scenario, the following subsections present graphical analyses and summary tables of annual and seasonal energy gains, highlighting the contribution of VSO alone and of the combined VSO-plus-redispatch strategy.

6.4.1. VSO with Original Dispatch Strategy

In the first scenario, the 200 MW case-study plant is virtually retrofitted to operate under VSO while preserving the historical dispatch adopted in 2021. The hourly sequence of total discharge, net head and unit commitment is kept exactly as in the base case, and only the rotational speed and efficiency are modified according to the VSO hill charts derived in Section 5.2. In other words, for each operating point the same net head and the same unit discharge are imposed, but the turbine-generator set is allowed to move along the VSO efficiency map in order to extract the maximum power compatible with the new H-Q operating region. This configuration isolates the intrinsic contribution of VSO to

energy production, without the additional effects of changes in dispatch rules or power redistribution between units.

Within this framework, three partial-conversion configurations are examined before the full VSO case: conversion of only unit UG1, conversion of only unit UG2, and conversion of both units simultaneously. For each configuration, the hourly power output in 2021 is recomputed under VSO, enforcing all operational constraints (VSO envelope, cavitation limits and electrical and mechanical ratings) and ensuring that the total discharge released by the plant matches the historical fixed-speed series. Converter losses are not explicitly modelled at this stage, so the frequency converters are assumed ideal and the resulting power and energy gains should be interpreted as upper-bound values. The results are then compared with the original 2021 records, allowing a direct quantification of the additional energy that could have been produced solely due to the efficiency improvement brought by VSO.

Before presenting annual indicators, the methodology is illustrated at a more detailed time scale using a representative operating day. Figure 71 shows the simulated behaviour on 28 September 2021 for the full-conversion case (UG1 + UG2 under VSO), plotted together with the corresponding historical FSO from 07:00 to 19:00. The upper subplot compares the total plant discharge in both situations. As expected from the scenario definition, the FSO and VSO curves are practically coincident: each change in discharge during the day is reproduced exactly by the VSO simulation, confirming that the procedure preserves the original water usage and that any difference in energy production stems only from efficiency effects.

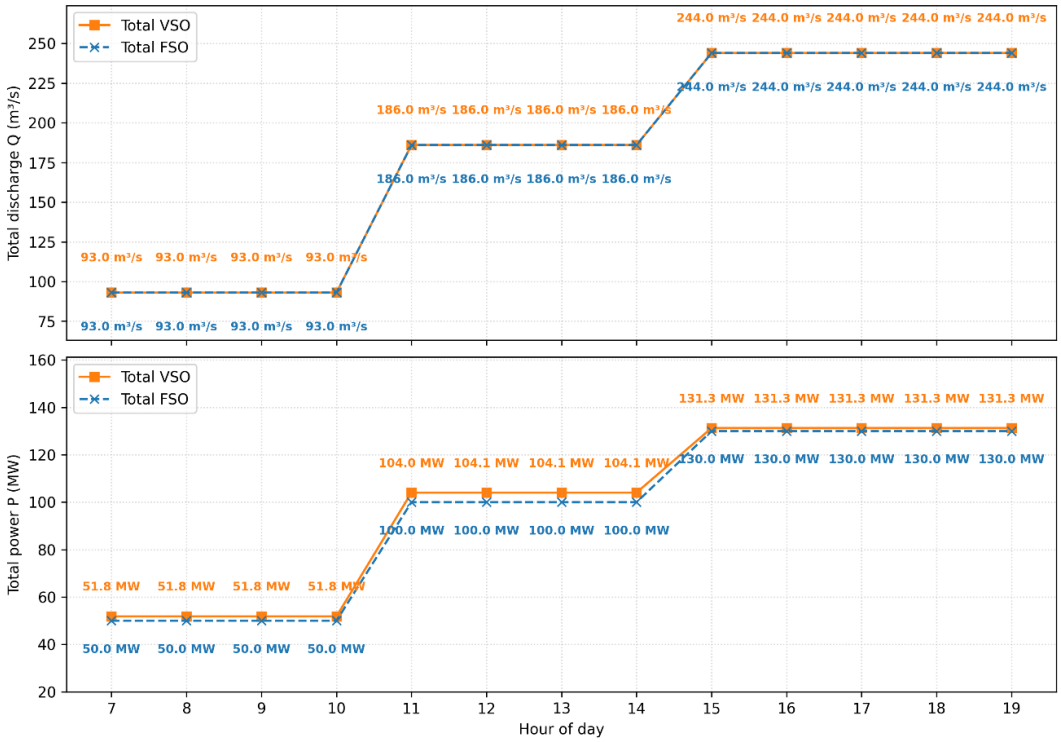

Figure 71 - Plant discharge and power on 28 September 2021 for FSO and VSO.

The lower subplot of Figure 71 presents the corresponding evolution of total active power. In this case, clear differences appear between the FSO and VSO curves, especially during periods when the plant operates at partial load. For the same discharge levels used historically, the variable-speed simulation yields a systematically higher power output, with more pronounced gains in the morning and early afternoon, when the units are further away from their best-efficiency region under fixed speed. As an illustrative example, at 14:00 the FSO delivers 100 MW whereas the VSO case reaches 104.1 MW, corresponding to an instantaneous power gain of 4.1%. When the plant approaches higher load levels the relative gain decreases but remains positive, reflecting the fact that VSO enables operation closer to the optimal regions of the η(H,Q) and η(H,P) maps.

To better understand the origin of the plant-level gains observed in the previous figure, Figure 72 zooms into the behavior of unit UG1 for the same operating day (28 September 2021). The upper subplot compares the unit active power under FS and VS operation and reports the corresponding rotational speed at each hour. Under FSO the unit remains essentially flat at 50 MW for most of the period, with a step to 65 MW in the late afternoon, always at synchronous speed (171.4 rpm). When VSO is enabled, the unit

operates at reduced speed in the morning and early afternoon (around 148–149 rpm), producing between 51.8 and 52.0 MW for the same discharge and head conditions. After 15:00, when the plant approaches higher load, the unit moves to a new operating point around 65.6 MW at approximately 163 rpm, still delivering slightly more power than the FS case.

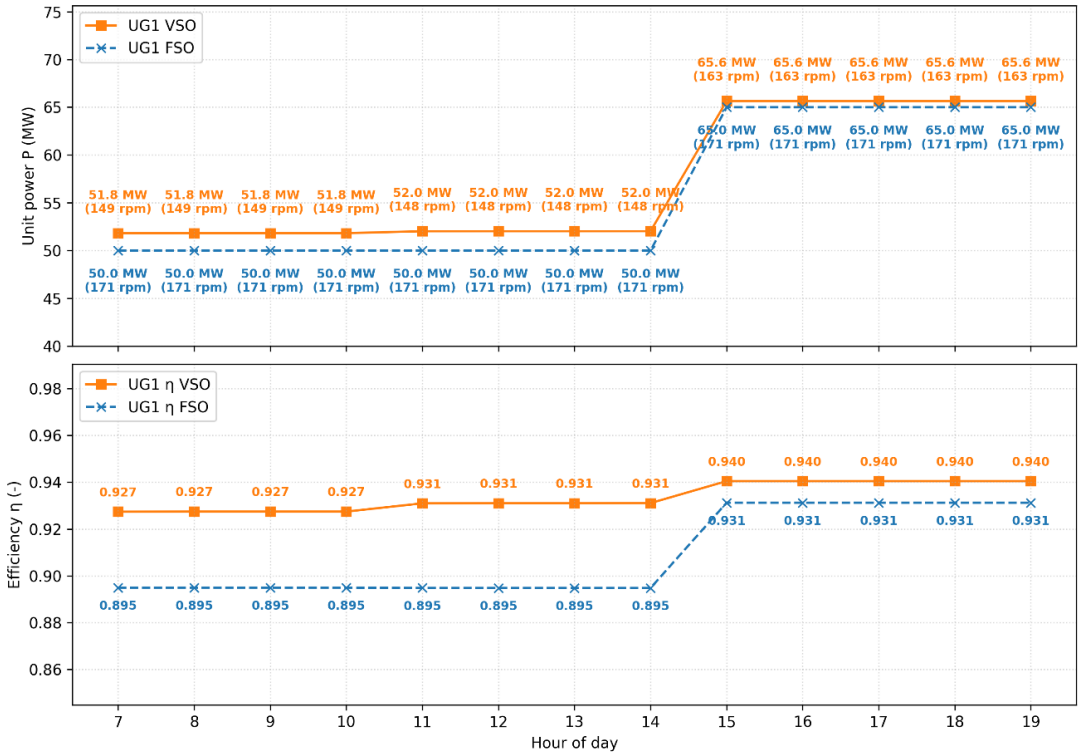

Figure 72 - UG1 power, speed and efficiency on 28 September 2021 for FSO and VSO.

The lower subplot of Figure 72 shows the corresponding evolution of hydraulic efficiency, which reveals the physical mechanism behind these power gains. While FSO operation keeps UG1 at about 89.5% efficiency during most of the day, VSO allows the unit to move to points on the hill chart where the efficiency increases to around 92.7–94.0% for the same discharge. At 14:00, for example, efficiency rises from 89.5% to 93.1%, an increase of 3.6 percentage points that directly translates into an additional unit power of roughly 4% at that instant. In the late afternoon, both strategies converge to higher efficiencies, but VSO still attains about 94%, remaining closer to the best-efficiency region. This detailed view confirms that the extra energy obtained in the plant-level simulation arises from the systematic improvement in unit efficiency enabled by speed variation.

To further detail how the similarity-based search identifies the new operating points, Figure 73 and Figure 74 superimpose the similarity curve on the η(H,Q) hill chart for unit UG1. In both panels the dashed line represents the locus of points that preserve the reduced variables (n_{11}, Q_{11}) associated with the historical operating condition at fixed speed. The blue marker indicates the original FSO point, while the red star corresponds to the VSO solution selected by the methodology, the point along the similarity curve that satisfies all VSO constraints and maximizes efficiency on the hill chart.

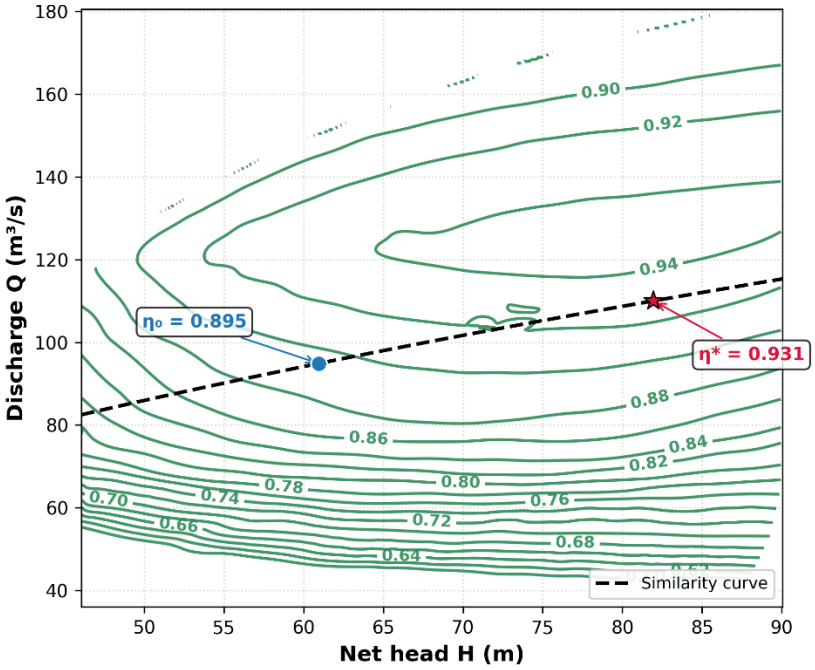

Figure 73 - Efficiency along the similarity curve at 2 PM on 28 September 2021.

Figure 73 refers to 14:00 on 28 September 2021, when the plant operates at relatively low head and intermediate discharge. The original UG1 point lies on the η_0 = 0.895 isoline, clearly away from the best-efficiency zone. By moving along the similarity curve, the VSO search identifies an alternative point on the η^* = 0.931 isoline, yielding a gain of 3.6 percentage points in efficiency for the same operating day. This illustrates that, under partial-load and low-head conditions, VS has substantial freedom to reposition the operating point inside the η(H,Q) map and recover efficiency that is lost under fixed speed.

Figure 74 shows the same procedure applied to the subsequent hour (15:00), when both head and discharge are higher and the historical operating point is already closer to the high-efficiency region (η_0 = 0.931). In this case the similarity-based search still finds

a better point, now on the η* = 0.940 isoline, but the relative improvement is smaller (0.9 percentage points).

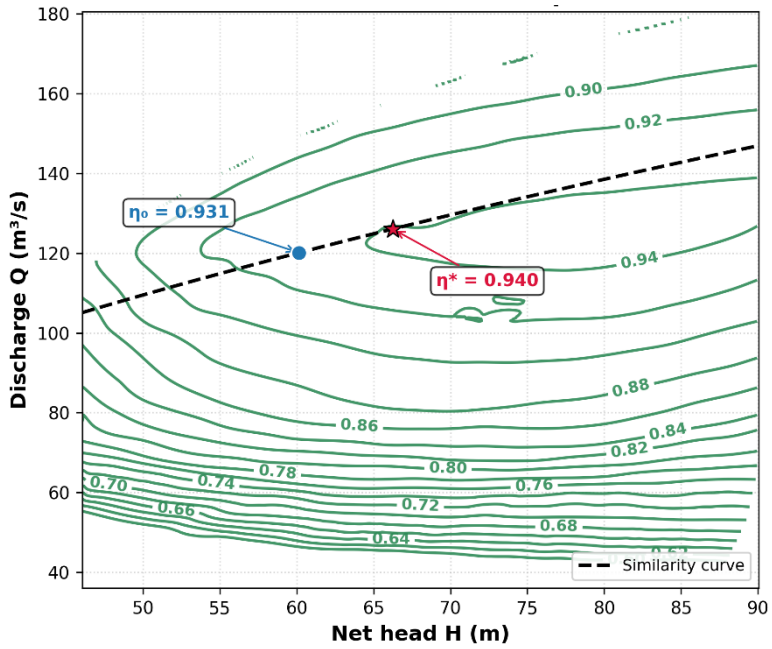

Figure 74 - Efficiency along the similarity curve at 3 PM on 28 September 2021.

The comparison between Figure 73 and Figure 74 confirms that the largest benefits of VSO occur when the FSO point is far from the optimal region of the hill chart, whereas at higher loads the available efficiency margin becomes more limited.

The previous figures illustrated, on an hourly basis, how VSO increases unit efficiency and power for the same discharge. In order to quantify the impact over the whole year, the hourly power gains obtained with VSO were integrated to compute monthly and annual energy gains for the three conversion configurations: partial conversion of UG1 (Partial-UG1VSO), partial conversion of UG2 (Partial-UG2VSO) and full conversion of both units (Full-2VSO). In all cases the original discharge series of 2021 was preserved, and converter losses were not included, so that the reported values reflect solely the improvement in hydraulic efficiency.

The monthly behavior of the energy gains obtained with VSO is summarized in Figure 75, which presents the additional energy ΔE for each month of 2021 under the three configurations analyzed. For every month the bars are strictly positive, confirming that, even when the original dispatch strategy is preserved, the application of VSO always leads to an increase in annual energy production with respect to the historical FSO. As

expected, the Full-2VSO case systematically yields the largest monthly gains, whereas the partial-conversion cases provide intermediate improvement that scale with the number of units operating under VS.

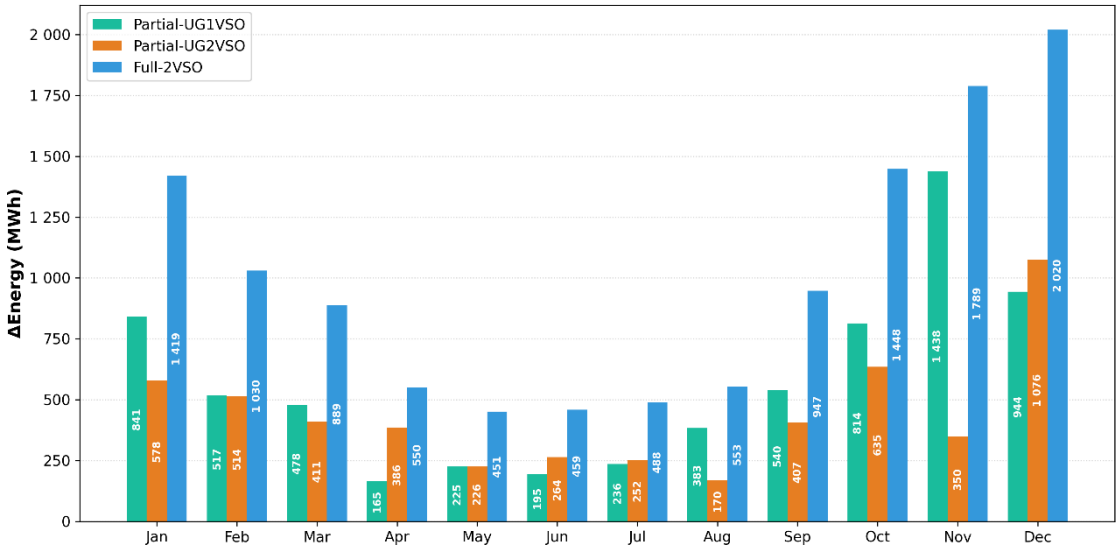

Figure 75 - Monthly additional energy in 2021 for VSO scenarios (relative to historical FSO).

These trends are quantified in Table 5, which reports the monthly gains both in absolute terms (GWh) and as a percentage of the original monthly energy. In the Full-2VSO configuration, the largest relative gains occur in December (2.020 GWh, 5.42%), November (1.789 GWh, 4.99%), October (1.448 GWh, 3.99%) and January (1.419 GWh, 3.94%), indicating that the benefits of VSO are particularly significant during periods with higher average loading and more frequent operation away from the fixed-speed best-efficiency region.

Conversely, the smallest relative gains are observed around mid-year, with a minimum of 0.97% in August (0.553 GWh) and values close to 1.2–1.3% between May and July. The partial-conversion scenarios exhibit the same seasonal pattern: monthly gains for Partial-UG1VSO range from 0.165 GWh (0.48%) in April up to 1.438 GWh (4.01%) in November, while Partial-UG2VSO varies between 0.170 GWh (0.30%) in August and 1.076 GWh (2.89%) in December. These results show that even the conversion of a single unit can produce monthly gains in the order of 0.5–1.5 GWh during the most favorable periods.

Table 5 - Monthly energy gains for VSO scenarios.

Month	dE_UG1VSO (GWh)	dE_UG1VSO (%)	dE_UG2VSO (GWh)	dE_UG2VSO (%)	dE_Full (GWh)	dE_Full (%)
Jan	0,841	2,34	0,578	1,60	1,419	3,94
Feb	0,517	1,62	0,514	1,61	1,030	3,23
Mar	0,478	1,35	0,411	1,16	0,889	2,50
Apr	0,165	0,48	0,386	1,12	0,550	1,60
May	0,225	0,61	0,226	0,61	0,451	1,22
Jun	0,195	0,53	0,264	0,72	0,459	1,26
Jul	0,236	0,60	0,252	0,64	0,488	1,24
Aug	0,383	0,67	0,170	0,30	0,553	0,97
Sep	0,540	0,82	0,407	0,62	0,947	1,44
Oct	0,814	2,24	0,635	1,75	1,448	3,99
Nov	1,438	4,01	0,350	0,98	1,789	4,99
Dec	0,944	2,53	1,076	2,89	2,020	5,42

The integrated annual effect of these gains is illustrated in Figure 76, which compares the total additional energy in 2021 for the three VSO configurations relative to the historical FS baseline. Starting from the same reference annual energy of 483.44 GWh for the base case, the Partial-UG1VSO and Partial-UG2VSO scenarios yield total annual gains of 6.78 GWh and 5.27 GWh, respectively, whereas the Full-2VSO configuration reaches 12.04 GWh of additional energy in the same hydrological year. The monotonic increase from the partial to the full-conversion case shows that, under the same historical dispatch, VSO benefits systematically increase with the number of converted units, although the gains are not strictly proportional, in line with the local power and efficiency analyses.

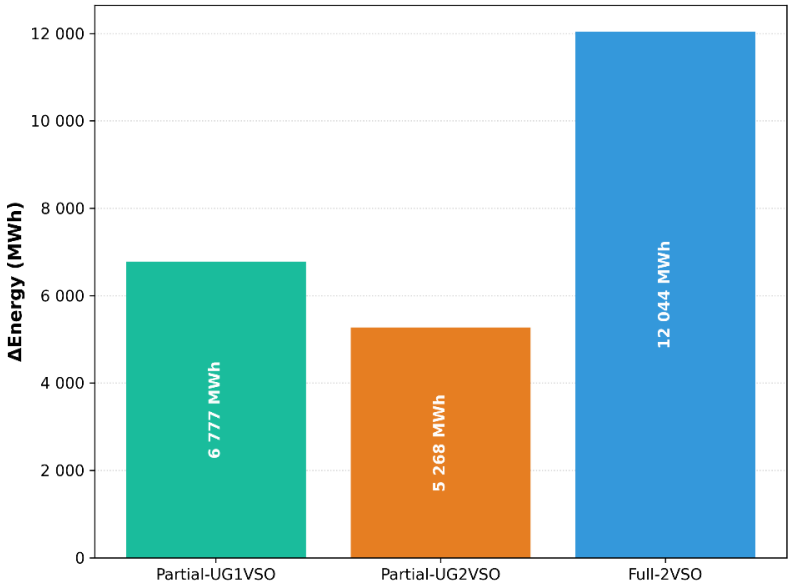

Figure 76 - Total additional energy in 2021 for VSO scenarios (relative to historical FSO).

These aggregated values are summarized in Table 6, which reports both the original and the recomputed annual energies for each scenario. In relative terms, the annual gains correspond to 1.40% for Partial-UG1VSO (from 483.44 to 490.22 GWh), 1.09% for Partial-UG2VSO (from 483.44 to 488.71 GWh) and 2.49% for Full-2VSO (from 483.44 to 495.49 GWh). The fact that the two partial-conversion alternatives provide gains of comparable magnitude indicates that both units operate under broadly similar hydraulic and electrical conditions along the year, so that converting either UG1 or UG2 leads to improvements of the same order. For the full-conversion case, the additional 12.04 GWh obtained in 2021 are equivalent to an average increase of approximately 1.4 MW of firm power over the entire year, achieved without any change in the plant dispatch strategy and neglecting converter losses. Therefore, these results can be interpreted as an upper bound for the energy benefit of VSO under the original operating policy; in practice, they still represent a substantial gain for a medium-sized plant in analysis.

Table 6 - Annual energy gains for VSO scenarios.

Scenario	E_base (GWh)	E_new (GWh)	E_gain (GWh)	E_gain (%)
Partial-UG1VSO	483,44	490,22	6,78	1,40
Partial-UG2VSO	483,44	488,71	5,27	1,09
Full-2VSO	483,44	495,49	12,04	2,49

6.4.2. VSO with Optimized Flow Allocation

In this subsection, the impact of combining VSO with an optimized flow allocation is evaluated for the year 2021. As detailed in Section 4.5.4, the optimization problem is formulated on an hourly basis, keeping the same total discharge and net head as in the historical operation. For each hour, the algorithm selects the operating points of the two units, either at synchronous speed or in VSO, that maximize the total active power while satisfying the individual limits of discharge and speed. All results presented here are therefore expressed as additional energy (ΔEnergy) with respect to the historical base case.

Four scenarios are compared. The Base-2FSO scenario represents the historical operating regime with both units at fixed speed, but subjected to the optimized flow allocation. The Partial-UG1VSO and Partial-UG2VSO scenarios introduce VSO in only one of the units (UG1 or UG2, respectively), while the other remains at synchronous speed; in both cases, the hourly optimal dispatch is recalculated considering the extended operating range of the converted unit. Finally, the Full-2VSO scenario assumes that both units operate at variable speed, again with the same optimization strategy and the same hourly discharge as in the historical record.

The monthly behavior of the additional energy obtained in each scenario is shown in Figure 77. The curves reveal that the seasonal pattern of ΔEnergy follows the underlying hydrology: the largest gains occur in the months with higher inflows, while during the drier period (roughly May to September) the absolute values of additional energy are smaller. The Base-2FSO curve remains almost flat at the bottom of the plot, with monthly gains between 0.000 and 0.042 GWh (0.00-0.07% of the historical monthly energy), indicating that the optimization alone, when both units are constrained to synchronous speed, has a negligible effect on the annual energy production. In contrast, the three scenarios with VSO show consistent gains throughout the year. The two partial-conversion cases (UG1VSO and UG2VSO) are practically indistinguishable in the figure, confirming that the benefit of VSO does not depend on which unit is converted when both have similar characteristics. The Full-2VSO scenario lies slightly above the partial cases, especially in months such as August, September and December, but the visual difference is small.

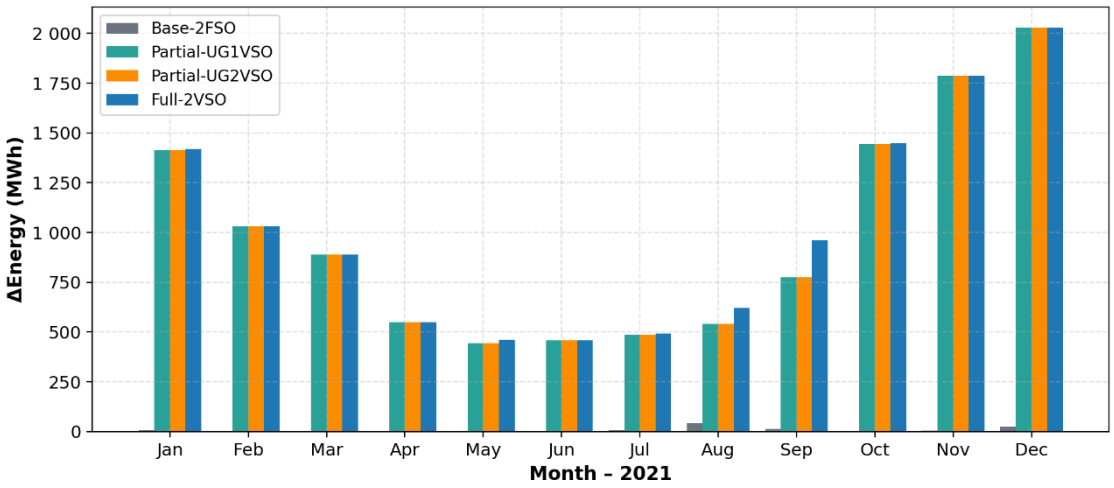

Figure 77 - Monthly additional energy for VSO scenarios with optimized flow allocation.

These trends are quantified in Table 7, which summarizes the monthly values of ΔEnergy and the corresponding percentage increase relative to the historical generation. In the partial-conversion scenarios, the largest relative gains occur in the wet-season months: December reaches about 2.03 GWh, corresponding to 5.45% of the historical energy, while November and October reach 1.79 GWh (4.99%) and 1.45 GWh (3.98%), respectively. Significant increases also appear in January (1.41 GWh; 3.92%) and February (1.03 GWh; 3.23%). During the drier months, the relative gains remain positive but more modest, typically between 0.95% and 1.26%. The Full-2VSO scenario systematically adds a small margin on top of these values – for example, raising the August gain from 0.54 GWh (0.95%) to 0.62 GWh (1.09%), and the September gain from 0.78 GWh (1.18%) to 0.96 GWh (1.46%) – but the incremental benefit of converting the second unit is clearly limited when compared to the step change obtained with the first conversion.

Table 7 - Monthly additional energy and gains for VSO scenarios with optimized flow allocation.

Month	dE_2FSO (GWh)	dE_2FSO (%)	dE_UG1 VSO (GWh)	dE_UG1 VSO (%)	dE_UG2 VSO (GWh)	dE_UG2 VSO (%)	dE_Full (GWh)	dE_Full (%)
Jan	0,007	0,02	1,414	3,92	1,414	3,92	1,420	3,94
Feb	0,000	0,00	1,030	3,23	1,030	3,23	1,030	3,23
Mar	0,000	0,00	0,889	2,50	0,889	2,50	0,889	2,50
Apr	0,000	0,00	0,550	1,60	0,550	1,60	0,550	1,60
May	0,000	0,00	0,443	1,20	0,444	1,20	0,460	1,24
Jun	0,001	0,00	0,459	1,26	0,459	1,26	0,460	1,26
Jul	0,007	0,02	0,487	1,23	0,487	1,23	0,494	1,25

Aug	0,042	0,07	0,541	0,95	0,541	0,95	0,621	1,09
Sep	0,013	0,02	0,776	1,18	0,776	1,18	0,960	1,46
Oct	0,000	0,00	1,446	3,98	1,446	3,98	1,448	3,99
Nov	0,005	0,01	1,788	4,99	1,788	4,99	1,788	4,99
Dec	0,025	0,07	2,030	5,45	2,030	5,45	2,031	5,45

The annual impact of each configuration is illustrated in Figure 78, which presents the total additional energy in 2021 for the four scenarios, and summarized in Table 6.xy. The historical case produces 483.44 GWh in 2021. When only the optimized flow allocation is applied with both units at fixed speed (Base-2FSO), the annual gain is merely 0.10 GWh, corresponding to 0.02% of the historical energy, confirming that the optimization alone does not materially change the energy output. Introducing VSO in a single unit leads to a substantial increase: both Partial-UG1VSO and Partial-UG2VSO reach an annual gain of approximately 11.85 GWh, or 2.45% above the historical value. This means that almost the entire potential benefit of the "VSO + optimization" strategy is captured once one unit operates in variable speed and the dispatch algorithm can systematically allocate more flow to the high-efficiency region of that machine.

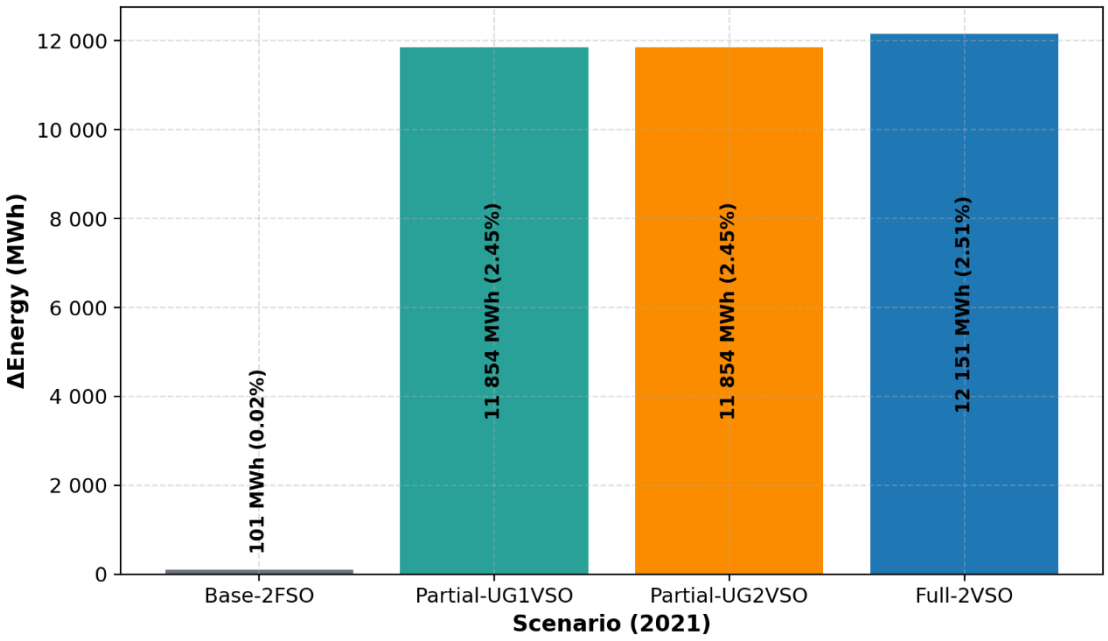

Figure 78 - Annual additional energy for VSO scenarios with optimized flow allocation.

The Full-2VSO scenario yields an annual additional energy of 12.15 GWh, 2.51% above the historical case. The incremental gain with respect to the partial-conversion

scenarios is therefore about 0.30 GWh, which represents only 0.06% of the historical annual generation. From a planning perspective, this result is crucial: converting the second unit to VSO provides only a marginal increase in energy when compared to the first conversion, while it would entail additional investment, outages and technological risk. Consequently, for the hydrological conditions and operating constraints analyzed in 2021, a single unit converted to VSO, combined with an optimized flow allocation, is sufficient to capture almost all the available energy gains, suggesting a shorter payback time and a more favorable cost-benefit ratio for partial conversion projects.

7. CONCLUSIONS

This work presented a comprehensive study on the feasibility and benefits of converting the Tucuruí Hydropower Plant to variable-speed operation under both partial and full-conversion scenarios. The central hypothesis was that VSO would reduce machine starts and stops, alleviate mechanical stress, increase the operational flexibility of the plant and contribute to system-wide stability in an electric grid with growing penetration of intermittent renewable sources. The results obtained in this study strongly support this hypothesis, showing that VSO is not only technically feasible for large hydropower plants, but can also play a key role in their modernization for a renewable-dominated future.

From the standpoint of dynamic operation, all conversion scenarios led to a reduction in the number of starts and stops when compared with the fixed-speed baseline. The reductions ranged from about 19% for the most modest scenario in CFII up to approximately 32% for the fully converted 23-unit case. Fewer starts and stops are directly associated with lower mechanical and thermal cycling, which in turn translates into reduced wear of critical components, extended equipment lifetime and lower maintenance needs. In addition, the increased ability to modulate power smoothly improves the participation of the plant in primary frequency control and in the provision of ancillary services to the grid, in line with the conclusions of previous studies that highlight VSO as a key enabler of flexibility for large hydropower plants.

A second important contribution of this work is the detailed assessment of energy gains made possible by VSO. Using turbine hill charts, universal diagrams and similarity relations, new operational limits were derived for the plant under variable speed, significantly expanding the feasible operating domain in the head–discharge–power space. Based on these extended limits, an optimization-based power-redispatch algorithm was developed and applied to different conversion scenarios. The results show consistent monthly and annual energy gains with respect to the fixed-speed reference, particularly in operating regimes where conventional units are forced to run away from their best-efficiency region. A key finding is that full conversion of all units is not strictly necessary to capture most of the energy-gain potential. Optimized scenarios with partial conversion, in which only a subset of units is equipped with VSO and used as “flexible anchors” in

the dispatch, were able to recover a large share of the total energy gain and of the start-stop reduction observed in the fully converted case. This indicates that, from a practical standpoint, staged or selective conversion can offer a technically robust and economically attractive pathway, since it avoids the need to retrofit the entire powerhouse at once.

The study also advanced a detailed methodology for cavitation minimization under VSO, moving beyond the preliminary indications of earlier work and treating cavitation as a central design objective. Cavitation risk was quantified by combining the Thoma coefficient with an empirical σ–Ns envelope adapted from Arndt's diagram, applied to hourly operating data and to the same hydraulic model used in the energy-gain analysis. For each cavitating operating point, four mitigation strategies were implemented, Q, N, NQ and QN-based on local adjustments in discharge and rotational speed, complemented by a Best-of-all strategy that selects, for each hour, the most effective feasible candidate. The results for UG2 in CFI show that even with zero power tolerance (ΔPmax = 0%), variable speed alone can move about 18% of cavitating hours into the safe region. When a modest power tolerance is allowed, representing local deviations that can be compensated by power redistribution among the remaining units, the benefits become much more pronounced: with ΔPmax = 2%, the Best-of-all strategy mitigates about 65% of cavitating hours, and with ΔPmax = 4% this figure rises to nearly 75%. In operational terms, this means that small adjustments in unit power, redistributed at plant level, can be used to displace a large portion of the historical operating points from the cavitation-risk band to the safe region, with limited impact on the global generation schedule.

These cavitation-mitigation results are also consistent with the analysis in the universal diagram: the successful candidates cluster along trajectories of increased σ and slightly modified specific speed, while remaining within realistic bands of discharge factor. This confirms that the proposed methodology does not rely on unrealistic operating points, but rather on combinations of rotational speed and discharge that are compatible with the manufacturer's hill chart and with the physical limits of the plant. Taken together, the energy-gain and cavitation analyses show that VSO, when combined with optimized dispatch and coordinated multi-unit operation, can simultaneously increase energy production, reduce damaging operating regimes and enhance the overall robustness of the plant.

From a technological perspective, the work also reinforces that a practical route for implementing VSO in large existing plants lies in advanced power-converter solutions, particularly modular multilevel converters (MMC). The modular and scalable structure of MMCs allows them to interface high-power synchronous generators with the grid without the need to replace the existing machines, thus preserving the hydraulic and electromechanical assets while enabling variable-speed operation. This makes VSO a technically sound and potentially cost-effective strategy for the long-term modernization of large hydropower schemes such as Tucuruí.

Despite these positive findings, some important limitations must be highlighted. The present study focused on hydraulic, electrical and operational aspects, without carrying out a detailed techno-economic assessment of the conversion. In particular, the costs associated with MMC-based retrofit, auxiliary systems, civil works, control upgrades and plant outages were not explicitly quantified. Experience with real large-scale conversion projects is still limited, and obtaining reliable cost benchmarks for plants the size of Tucuruí remains challenging, which complicates the task of pricing a full or partial conversion. Furthermore, the simulations were performed using a single historical year as reference; extending the analysis to multi-year hydrological series and to different system-level conditions would provide a broader view of the long-term benefits and risks.

In view of this, future work should include a comprehensive financial analysis that monetizes the main gains identified here: additional annual energy, reduction in starts and stops, mitigation of cavitation-related damage and improvement in reliability and availability. Such an assessment should weigh these benefits against the capital and implementation costs of partial and full-conversion scenarios, explicitly considering the uncertainties in converter pricing and in large-project engineering. Additional research is also recommended to refine the cavitation model, using more detailed three-dimensional hydraulic simulations and field measurements ,and to couple the VSO plant model with system-level studies that account for ancillary services, virtual inertia and fast-frequency-response requirements in high-renewable grids.

In conclusion, this study has shown that VSO is a promising and technically sound option for the Tucuruí Hydropower Plant and, by extension, for other large hydropower schemes. By reducing starts and stops, expanding the safe operating range, enabling measurable energy gains and mitigating cavitation through coordinated adjustments of

speed and discharge, VSO can substantially enhance the role of hydropower in a low-carbon energy system. The evidence that a carefully optimized partial conversion can capture most of these benefits is particularly relevant for practical implementation, as it opens a realistic and potentially more economical path for staged modernization. While detailed economic evaluations remain to be completed, the technical results obtained here indicate that VSO has the potential to become a central pillar in the long-term strategy for upgrading existing hydropower assets and securing their contribution to a renewable-dominated electricity supply.

REFERENCES

[1] Chen Y, Liu J, Yu D. Balancing the output and quality of variable renewable energy generation in wide area based on multi-objective optimization. Energy Convers Manag 2025;328. https://doi.org/10.1016/j.enconman.2025.119632.

[2] Christe A, Faulstich A, Vasiladiotis M, Steinmann P. World's First Fully Rated Direct ac/ac MMC for Variable-Speed Pumped-Storage Hydropower Plants. IEEE Transactions on Industrial Electronics 2023;70:6898–907. https://doi.org/10.1109/TIE.2022.3204858.

[3] Wang Z, Fang G, Wen X, Tan Q, Zhang P, Liu Z. Coordinated operation of conventional hydropower plants as hybrid pumped storage hydropower with wind and photovoltaic plants. Energy Convers Manag 2023;277. https://doi.org/10.1016/j.enconman.2022.116654.

[4] Valavi M, Nysveen A. Variable-Speed Operation of Hydropower Plants: A Look at the Past, Present, and Future. IEEE Industry Applications Magazine 2018;24:18–27. https://doi.org/10.1109/MIAS.2017.2740467.

[5] Koritarov V, Kwon J, Ploussard Q, Balducci P. A Review of Technology Innovations for Pumped Storage Hydropower. 2022.

[6] Alizadeh Bidgoli M, Yang W, Ahmadian A. DFIM Versus Synchronous Machine for Variable Speed Pumped Storage Hydropower Plants: A Comparative Evaluation of Technical Performance. Renew Energy 2020;159:72–86. https://doi.org/10.1016/j.renene.2020.05.163.

[7] Mohanpurkar M, Ouroua A, Hovsapian R, Luo Y, Singh M, Muljadi E, et al. Real-Time Co-simulation of Adjustable-Speed Pumped Storage Hydro for Transient Stability Analysis. Electric Power Systems Research 2018;154:276–86. https://doi.org/10.1016/j.epsr.2017.08.010.

[8] Presas A, Valero C, Valentín D, Egusquiza M, Diogo Pinto P, Gonçalves de Carvalho A, et al. Water saving options in hydropower by means of variable speed operation: A prototype study in a mid-head Francis turbine. Energy Convers Manag 2023;291. https://doi.org/10.1016/j.enconman.2023.117296.

[9] Xu J, Ni T, Zheng B. Hydropower development trends from a technological paradigm perspective. Energy Convers Manag 2015;90:195–206. https://doi.org/10.1016/j.enconman.2014.11.016.

[10] Antunes Campos R, Rafael do Nascimento L, Rüther R. The complementary nature between wind and photovoltaic generation in Brazil and the role of energy storage in utility-scale hybrid power plants. Energy Convers Manag 2020;221. https://doi.org/10.1016/j.enconman.2020.113160.

[11] Wang X, Virguez E, Kern J, Chen L, Mei Y, Patiño-Echeverri D, et al. Integrating wind, photovoltaic, and large hydropower during the reservoir refilling period. Energy Convers Manag 2019;198. https://doi.org/10.1016/j.enconman.2019.111778.

[12] Shi Y, Shi X, Yi C, Song X, Chen X. Control of the Variable-Speed Pumped Storage Unit-Wind Integrated System. Math Probl Eng 2020;2020. https://doi.org/10.1155/2020/3816752.

[13] Yang W, Yang J. Advantage of Variable-Speed Pumped Storage Plants for Mitigating Wind Power Variations: Integrated Modelling and Performance Assessment. Appl Energy 2019;237:720–32. https://doi.org/10.1016/j.apenergy.2018.12.090.

[14] Iliev I, Trivedi C, Dahlhaug OG. Variable-Speed Operation of Francis Turbines: A Review of the Perspectives and Challenges. Renewable and Sustainable Energy Reviews 2019;103:109–21. https://doi.org/10.1016/j.rser.2018.12.033.

[15] Cebeci C, Parker M, Recalde-Camacho L, Campos-Gaona D, Anaya-Lara O. Variable-Speed Hydropower Control and Ancillary Services: A Remedy for Enhancing Grid Stability and Flexibility. Energies (Basel) 2025;18. https://doi.org/10.3390/en18030642.

[16] Yang W, Yang J. Evaluating Fast Power Response of Variable Speed Pumped Storage Plants to Balance Wind Power Variations. Energy Procedia, vol. 158, Elsevier Ltd; 2019, p. 6341–6. https://doi.org/10.1016/j.egypro.2019.01.274.

[17] Bortoni E da C, Luz DRMR da, Souza OH de, Siniscalchi RT, Jardini JA. Feasibility of Variable-Speed in Hydropower Plants Connected to DC Transmission Systems 2025. https://doi.org/10.36227/techrxiv.173626913.30210587/v1.

[18] Engevik EL. Thesis for the Degree of Philosophiae Doctor Design and Operation Investigations for Large Converter-Fed Synchronous Machines in Hydropower Applications, 2019.

[19] Polster S, Power H, Aubert S, Häderli C, Ladreiter-Knauss C, Polster S, et al. Malta Oberstufe Overhaul Project Variable Speed Operation with MMC Full Converter. 2022.

[20] Tiwari R, Nilsen R, Nysveen A. Modular Multilevel Converter for Variable Speed Operation of Pumped Storage Hydropower Plants 2021.

[21] Polster S, Deschler J, Renner H, Bocquel A, Janssen M. Challenges of Large Converter-Fed Synchronous Machines for Variable-Speed Pumped Hydro Storage. Energies (Basel) 2023;16. https://doi.org/10.3390/en16227506.

[22] Ye H, Zhang L, Yang M, Liang G, Liu S, Li G, et al. Variable-speed Pumped Hydro Storage Technology: Overview, Solutions and Case Studies. 2021 6th International Conference on Power and Renewable Energy, ICPRE 2021, Institute of Electrical and Electronics Engineers Inc.; 2021, p. 1273–8. https://doi.org/10.1109/ICPRE52634.2021.9635226.

[23] Bortoni E, de Souza Z, Viana A, Villa-Nova H, Rezek Â, Pinto L, et al. The Benefits of Variable Speed Operation in Hydropower Plants Driven by Francis Turbines. Energies (Basel) 2019;12. https://doi.org/10.3390/en12193719.

[24] Basic M, Schwery A, Dujic D. Highly Flexible Indirect Modular Multilevel Converter for High Power Pumped Hydro Storage Plants. IECON 2020 The 46th Annual Conference of the IEEE Industrial Electronics Society, IEEE; 2020, p. 5290–5. https://doi.org/10.1109/IECON43393.2020.9254657.

[25] Vasudevan KR, Ramachandaramurthy VK, Venugopal G, Ekanayake JB, Tiong SK. Variable speed pumped hydro storage: A review of converters, controls and energy management strategies. Renewable and Sustainable Energy Reviews 2021;135. https://doi.org/10.1016/j.rser.2020.110156.

[26] Mesquita ALA, Da Silva LJS, Almir J, Pereira R, Abrahim Júnior O. Utilização de Bombas Centrífugas em Velocidade Variável para a Redução do Consumo de Energia, 2024.

[27] Ciocan GD, Teller O, Czerwinski F. VARIABLE SPEED PUMP-TURBINES TECHNOLOGY. UPB Sci Bull, Series D 2012;74.

[28] Deng Y, Wang P, Morabito A, Feng W, Mahmud A, Chen D, et al. Dynamic analysis of variable-speed pumped storage plants for mitigating effects of excess wind power generation. International Journal of Electrical Power and Energy Systems 2022;135. https://doi.org/10.1016/j.ijepes.2021.107453.

[29] Muljadi E, Singh M, Gevorgian V, Mohanpurkar M, Hovsapian R, Koritarov V. Dynamic modeling of adjustable-speed pumped storage hydropower plant. IEEE Power and Energy Society General Meeting, vol. 2015- September, IEEE Computer Society; 2015. https://doi.org/10.1109/PESGM.2015.7286214.

[30] Padoan AC, Kawkabani B, Schwery A, Ramirez C, Nicolet C, Simond JJ, et al. Dynamical behavior comparison between variable speed and synchronous machines with PSS. IEEE Transactions on Power Systems 2010;25:1555–65. https://doi.org/10.1109/TPWRS.2009.2039586.

[31] Li S, Xie H, Yan Y, Wu T, Huang T, Liu Y, et al. Excitation control of variable speed pumped storage unit for electromechanical transient modeling. Energy Reports 2022;8:818–25. https://doi.org/10.1016/j.egyr.2022.10.030.

[32] Wegiel T, Borkowski D, Liszka D. Efficiency analysis of an energy conversion system for a variable speed small hydropower plant; Efficiency analysis of an energy conversion system for a variable speed small hydropower plant 2016. https://doi.org/10.1051/2016.

[33] Pannatier Y, Kawkabani B, Nicolet C, Simond JJ, Schwery A, Allenbach P. Investigation of control strategies for variable-speed pump-turbine units by using a simplified model of the converters. IEEE Transactions on Industrial Electronics 2010;57:3039–49. https://doi.org/10.1109/TIE.2009.2037101.

[34] Gonzales-Longatt F, Torres J. Modelling and Simulation of Power Electronic Converter Dominated Power Systems in PowerFactory. Cham: Springer International Publishing; 2021. https://doi.org/10.1007/978-3-030-54124-8.

[35] Nicolet C, Pannatier Y, Kawkabanu B, Schwery A, Avellan F, Simond JJ. Benefits of Variable Speed Pumped Storage Units in Mixed Islanded Power Network during Transient Operation 2009.

[36] Acosta MN, Pettersen D, Gonzalez-Longatt F, Argos JP, Andrade MA. Optimal frequency support of variable-speed hydropower plants at telemark and vestfold,

norway: Future scenarios of nordic power system. Energies (Basel) 2020;13. https://doi.org/10.3390/en13133377.

[37] Huang Y, Yang W, Zhao Z, Han W, Li Y, Yang J. Dynamic modeling and favorable speed command of variable-speed pumped-storage unit during power regulation. Renew Energy 2023;206:769–83. https://doi.org/10.1016/j.renene.2023.02.112.

[38] Zuo Z, Fan H, Liu S, Wu Y. S-shaped characteristics on the performance curves of pump-turbines in turbine mode - A review. Renewable and Sustainable Energy Reviews 2016;60:836–51. https://doi.org/10.1016/j.rser.2015.12.312.

[39] Feng C, Li C, Chang L, Ding T, Mai Z. Advantage analysis of variable-speed pumped storage units in renewable energy power grid: Mechanism of avoiding S-shaped region. International Journal of Electrical Power and Energy Systems 2020;120. https://doi.org/10.1016/j.ijepes.2020.105976.

[40] Sivakumar N, Das D, Padhy NP. Variable speed operation of reversible pump-turbines at Kadamparai pumped storage plant - A case study. Energy Convers Manag 2014;78:96–104. https://doi.org/10.1016/j.enconman.2013.10.048.

[41] Basic M, Silva P, Dujic D, Basić M, Silva PCO, Dujić D. High Power Electronics Innovation Perspectives for Pumped Storage Power Plants. 2018.

[42] Tiwari R, Nilsen R, Mo O. Control Strategies for Variable Speed Operation of Pumped Storage Plants with Full-size Converter Fed Synchronous Machines. 2021 IEEE Energy Conversion Congress and Exposition, ECCE 2021 - Proceedings, Institute of Electrical and Electronics Engineers Inc.; 2021, p. 61–8. https://doi.org/10.1109/ECCE47101.2021.9595041.

[43] Madureira AT. Stability of Energy Generation at Hydroelectric Plants with Reversible Francis Turbines: Case Study of Tucuruí Hydropower Plant [In Portuguese]. Dissertação de Mestrado. UFPA, 2023.

[44] Schlunegger H, Oberhasli AT. 100 MW Full-Size Converter in the Grimsel 2 Pumped Storage Plant. 2014.

[45] Nicolet C, Braun O, Ruchonnet N, Beguin A, Avellan F. Full Size Frequency Converter for Fast Francis Pump-Turbine Operating Mode Transition Christophe NICOLET Power Vision Engineering Sàrl, Ecublens, Switzerland. 2016.

[46] Steimer PK, Senturk O, Aubert S, Linder S. Converter-Fed Synchronous Machine for Pumped Hydro Storage Plants. 2014 IEEE Energy Conversion Congress and Exposition (ECCE), IEEE; 2014, p. 4561–7. https://doi.org/10.1109/ECCE.2014.6954025.

[47] Dekka A, Wu B, Fuentes RL, Perez M, Zargari NR. Evolution of Topologies, Modeling, Control Schemes, and Applications of Modular Multilevel Converters. IEEE J Emerg Sel Top Power Electron 2017;5:1631–56. https://doi.org/10.1109/JESTPE.2017.2742938.

[48] Holzer T, Muetze A. Full-size converter operation of hydro power generators: a state-of-the-art review of motivations, solutions, and design implications. Elektrotechnik Und Informationstechnik 2019;136:209–15. https://doi.org/10.1007/s00502-019-0710-3.

[49] Tiwari R, Nilsen R, Nysveen A. Evaluation and Comparison between Multilevel Converters for Variable Speed Operation of Pumped Storage Power Plants with Full-size Converters. Conference Record - IAS Annual Meeting (IEEE Industry Applications Society), vol. 2021- October, Institute of Electrical and Electronics Engineers Inc.; 2021. https://doi.org/10.1109/IAS48185.2021.9677283.

[50] Electrics G. MM7 Modular multilevel converter (MMC) for various applications. 2021.

[51] Gontijo G. Novel Converter Solutions with a Modular Multilevel Structure for High-Power Medium-Voltage Electrical Machine Drive Applications. Aalborg University, 2022. https://doi.org/10.54337/aau504491302.

[52] Sadowski P. The Advantages of Modular Multilevel Converter Topologies for Medium-Voltage, High-Power Applications. 2023.

[53] Nicolet C, Beguin A, Alligne S, Beguin A, Jung A, Cordeiro D, et al. Inertia Emulation Contribution of Frades 2 Variable Speed Pump-Turbine to Power Network Stability 2022.

[54] Savin O, Baroth J, Badina C, Charbonnier S, Bérenguer C. Damage due to start-stop cycles of turbine runners under high-cycle fatigue. Int J Fatigue 2021;153. https://doi.org/10.1016/j.ijfatigue.2021.106458.

[55] Savin O, Badina C, Drommi J-L, Baroth J, Charbonnier S, Bérenguer C. Influence of Starts and Stops on the Aging of Hydroelectric Generator Stators by

Thermal Cycling: Empirical Study and Accelerated Lifetime Model 2021:0–9. https://doi.org/10.3850/978-981-18-2016-8_315-cdï.

[56] Savin O, Badina C, Pollier R, Drommi JL, Baroth J, Charbonnier S, et al. Effect of start and stop cycles on hydropower plants: modelling the deterioration of the equipment to evaluate the cycling cost. IOP Conf Ser Earth Environ Sci, vol. 1136, Institute of Physics; 2023. https://doi.org/10.1088/1755-1315/1136/1/012057.

[57] Goyal R, Gandhi BK, Cervantes MJ. Measurements on a model Francis turbine during start-stop. International Journal of Fluid Machinery and Systems 2019;12:217–27. https://doi.org/10.5293/IJFMS.2019.12.3.217.

[58] Eggen AO, Belsnes M. Operation related maintenance and reinvestment costs for hydropower scheduling. Energy Systems 2023. https://doi.org/10.1007/s12667-023-00589-w.

[59] Vieira DP, Tadeu C, Josué S, Betemps Vaz Da Silva C, Gonçalves De Oliveira J, Carolina A, et al. Modeling Costs of Stopping and Startup of Generating Units and Operation as Synchronous Compensator - Copel's Experience (In Portuguese), Recife-PE: XX SNPTEE; 2009, p. 1.

[60] Savin O, Badina C, Baroth J, Charbonnier S, Bérenguer C. Start and stop costs for hydro power plants: A critical literature review. Proceedings of the 30th European Safety and Reliability Conference and the 15th Probabilistic Safety Assessment and Management Conference, Research Publishing, Singapore; 2020, p. 342–9. https://doi.org/10.3850/978-981-14-8593-0_4102-cd.

[61] Osburn G. Hydrogenerator Start and Stop Costs 2014.

[62] DeHaan J. Determining Hydro Generation Start/Stop and Cycling Costs Science and Technology Program Research and Development Office. 2020.

[63] Kumar N, Besuner P, Lefton S, Agan D, Hilleman D. Power Plant Cycling Costs. 2012.

[64] Arndt REA. Cavitation in Fluid Machinery and Hydraulic Structure. vol. 13. 1981.

[65] Avellan F. Introduction to Cavitation in Hydraulic Machinery. 2004.

[66] Luo XW, Ji B, Tsujimoto Y. A review of cavitation in hydraulic machinery. Journal of Hydrodynamics 2016;28:335–58. https://doi.org/10.1016/S1001-6058(16)60638-8.

[67] Kumar P, Saini RP. Study of cavitation in hydro turbines-A review. Renewable and Sustainable Energy Reviews 2010;14:374–83. https://doi.org/10.1016/j.rser.2009.07.024.

[68] Brijkishore, Khare R, Prasad V. Prediction of cavitation and its mitigation techniques in hydraulic turbines - A review. Ocean Engineering 2021;221. https://doi.org/10.1016/j.oceaneng.2020.108512.

[69] Trivedi C, Iliev I, Dahlhaug OG, Markov Z, Engstrom F, Lysaker H. Investigation of a Francis turbine during speed variation: Inception of cavitation. Renew Energy 2020;166:147–62. https://doi.org/10.1016/j.renene.2020.11.108.

[70] Celebioglu K, Altintas B, Aradag S, Tascioglu Y. Numerical research of cavitation on Francis turbine runners. Int J Hydrogen Energy 2017;42:17771–81. https://doi.org/10.1016/j.ijhydene.2017.03.180.

[71] Ayli E. Cavitation in hydraulic turbines. International Journal of Heat and Technology 2019;37:334–44. https://doi.org/10.18280/ijht.370140.

[72] Westin LGF, Conceição LR, Bortoni EC, Marcato ALM, Ribeiro CB de M, Honório L de M. Evaluating the impact of streamflow rating curve precision on firm energy of hydropower plants. Water (Switzerland) 2021;13. https://doi.org/10.3390/w13081016.

[73] Vieira D. MODELO ECONÔMICO DE PROGRAMAÇÃO DIÁRIA DA GERAÇÃO CONSIDERANDO OS CUSTOS DE PARADA E PARTIDA E OPERAÇÃO COMO COMPENSADOR SÍNCRONO. Dissertação de Mestrado. Universidade Federal do Paraná, 2007.

[74] Vieira DP, Tadeu C, Josué S, Betemps Vaz Da Silva C, Gonçalves De Oliveira J, Carolina A, et al. MODELAGEM DOS CUSTOS DE PARADA E PARTIDA DE UNIDADES GERADORAS E DA OPERAÇÃO COMO COMPENSADOR SÍNCRONO - A EXPERIÊNCIA DA COPEL 2009:1–8.

[75] Savin O. Effet des cycles de démarrages et d'arrêts pour les centrales hydrauliques : modélisation de la détérioration des matériels pour l'évaluation des coûts de cyclage. 2022.

[76] Vieira DAG, Guedes LSM, Lisboa AC, Saldanha RR. Formulations for hydroelectric energy production with optimality conditions. Energy Convers Manag 2015;89:781–8. https://doi.org/10.1016/j.enconman.2014.10.048.

[77] MATAIX C. Hydraulic Turbomachines: Hydraulic Turbines, Pumps, Fans [In Portuguese]. vol. 2. 2nd ed. Barcelona: Ediciones del Castillo; 1975.

[78] Machado J. Starts and Stops at Hydroelectric Plants: ONS Service and Operating Costs [In Portuguese]. Dissertação de Mestrado. UFPA, 2023.

[79] Tang Y, Fang G, Tan Q, Wen X, Lei X, Ding Z. Optimizing the sizes of wind and photovoltaic power plants integrated into a hydropower station based on power output complementarity. Energy Convers Manag 2020;206. https://doi.org/10.1016/j.enconman.2020.112465.

[80] EPE. Calculation of Physical Energy Guarantee Amount - Centrally Dispatched Eletrobras Hydroelectric Plants Achieved by Law 14,182/2021 [In Portuguese]. 2021.